Doctoral Thesis

Data-driven neural mass modelling

Lara Escuain-Poole

Supervised by:
Antonio J. Pons
Jordi Garcia-Ojalvo

A thesis submitted in partial fulfillment of the requirements for the degree of Doctor of Philosophy

Terrassa, Tuesday 15th January, 2019

Departament de Física
Universitat Politècnica de Catalunya

UNIVERSITAT POLITÈCNICA
DE CATALUNYA
BARCELONATECH

Data-driven neural mass modelling

Lara Escuain-Poole

To my husband. To my son.

To my parents and my brothers and sister.

To my friends.

And to the anonymous taxpayer.

Acknowledgements

This is the best bit. This is basically where I explain how I managed to write this. This Thesis started when my parents gave me a little transparent pot with a magnifying lid to observe bugs in, when I was about six or seven. I decided then and there, with my first observed critter, that knowing things seemed a great way of life, and that one day I was going to be a scientist.

Toni Pons signed to accept me as a doctorate student at full blast with a 39 Celsius degree fever, and since then everything's been an absolute whirlwind, during which I've had the privilege to learn from and with one of the greatest people I know. Toni, una de les coses més grans que m'emporto de tot això és la teva amistat, sense cap mena de dubte. And Jordi. While a student of Engineering in Terrassa, little did I imagine that those eternal (but captivating) Physics lessons on Mondays from 5 to 8 pm with you would wind up, ten years later, in the writing of these words. La teva energia, la teva passió i el teu "optimisme irresponsable" (sic) són increïblement contagiosos. Ha estat un honor i un immens plaer.

I would like to thank all the teachers who, in one way or another, challenged me and encouraged me during all the years previous to University. In a

chronological order of sorts, Maria Rovirosa, Ramón Tobarra, Isabel Pahissa, Montse Borrell, Eli Rafecas, Núria Ventosa, Romà Pujol, Raimon Páez, and Pep Calero. As to university, I would like to thank ALL my professors—I will mention especially Vicenç Sales, Antoni Magaña, Dolors Llongueras, Crina Cojocaru, Maria Albareda, Inés Algaba, David Arencón, Juozas Gudžinskas, Linas Kliučininkas, and very especially Josep Lluís Font, Montserrat Pepió and David Arencón, whom I have the honour of counting among my friends. I would like to remember Manuel Ochoa and Juan Carlos Palacín here: their early passing was a shock and a great loss, and their valuable teachings have stayed with me through the years.

This Thesis has been sort of a lonely job, living so far away from civilisation and all. However, I am grateful especially to Daniel Malagarriga and Maciek Jedynak, my "scientific brothers", with whom I've had enriching discussions and interesting conversations. I would also like to mention the people at the Dynamical Systems Biology group in Barcelona: in no particular order, Rosa, Letícia, Carlos, Pablo Ruiz, Marçal, and Grace. And from the Nonlinear Dynamics, Nonlinear Optics and Lasers group in Terrassa: Ignacio, Carlos, Maria, Judith, José María, and Jordi Tiana.

I would also like to thank my students, from whom I've learnt a great deal and with (some of) whom I've had good fun over my fifteen-year teaching career; especially, Albert Garcia, Laia Fontelles and Alberto Hernández.

My friends! Golfillus! Marc Pau, Albert, Marc Freixas, Eric, Alex, Abel: we made it through thick and thin together at uni and here we are, all grown up, with jobs and significant others, some with children, what on Earth is the world coming to? Here's to the next ten years! My old friends while

growing up: Komal, Roser, Ouanissa, Marta. And my new friends: David and Petra, Jean-Marc and Rachel.

I also wish to thank my neighbours and all the people who make my life in the village so much more interesting: els senyors amb qui parlo de gallines i d'horts, les senyores del banc a la Plaça del Firal amb qui parlo de nens i de la vida, i sobretot del meu nen. Els veïns de casa, persones amables i generoses com poques, i especialment el Pau Maré per la correcció del resum en català.

My dear family all over the world, cousins, uncles and aunts, and Iaia: I love you, I miss you, and I wish you were closer. My in-laws: thank you for all you've done for us, for taking me into your family like you have, and for all your help with practical matters. And Gisela, my lovely sister-in-law, and my beautiful nieces!

Papa and Mama, what can I say? My gratitude knows no bounds. Your loving care, your teachings and all you've given me over the years... I am sure I'm not even able to fully appreciate it all, but know that I love you and I hope I've made you proud. Thank you for being there for me now I'm a Mama myself, too! My siblings, such concentration of awesomeness per person the world has never seen before: Robert; Anna and Daniel and their beautiful babies Abigail and Natanael; Samuel; and Martí. I love you so, so much, and I am so proud to be your sister.

And Roger, my one and only, the noblest, most generous and loving husband I could have ever wished for. You give me wings when I want to fly, every single time; even when it involves a sacrifice for you. Being your wife is one of the best three things that have happened to me in my whole life. Other

things I have to say to you are nobody else's business—sorry, folks. And my precious baby Timoteu: life with you is a blast. You've no idea how happy you've made me! I love you and am fiercely proud of you.

And finally, last but certainly not least, all the glory be to God, Who "hath made everything beautiful in its time", and from Whom all good things come!

Resum

El cervell humà és un òrgan de gran complexitat l'activitat del qual es desenvolupa en múltiples escales, tant espacials com temporals. Es creu que la unitat computacional del cervell és la neurona, una cèl·lula altament especialitzada que té com a funció rebre, processar i transmetre informació. A nivell microscòpic, les neurones es comuniquen les unes amb les altres per potencials d'acció. Aquests es poden observar experimentalment *in vivo* per mitjà de tècniques de gran precisió que només poden tenir en compte un nombre relativament reduït de cèl·lules i interaccions, i que es poden modelar matemàticament de diverses maneres. Altres tècniques tracten amb grans grups de neurones a escala mesoscòpica, o columnes corticals, i detecten l'activitat mitjana de la població neuronal; en aquest cas també abunden els models teòrics que intenten reproduir aquests senyals.

Malgrat que està ben establert que hi ha una intercomunicació entre les escales microscòpica i mesoscòpica, relacionar una escala amb una altra no és gens trivial. Les derivacions analítiques de models mesoscòpics a partir de xarxes microscòpiques es basen en suposicions que no sempre es poden justificar. A part, tradicionalment hi ha hagut una frontera de

separació entre els analistes clínics que processen senyals neuronals amb fins mèdics (i que sovint usen tècniques molt invasives i/o costoses), i la comunitat teòrica que modelitza aquests senyals, per a qui el repte més gran és caracteritzar els paràmetres que governen els models perquè aquests s'acostin el més possible a la realitat.

Aquesta Tesi té com a objectiu, per una banda, fer un pas més a caracteritzar la relació entre les escales microscòpica i mesoscòpica d'activitat cerebral, i, per l'altra, establir ponts entre els punts de vista experimental i teòric del seu estudi. Ho aconseguim amb un algoritme d'assimilació de dades, el filtre de Kalman desodorat (UKF, de les sigles en anglès), que ens permet combinar informació de diverses procedències (microscòpica/mesoscòpica o experimental/teòrica). El resultat és una comprensió més àmplia del sistema estudiat que la que haurien permès les fonts d'informació per separat.

La Tesi està organitzada de la següent manera. El capítol 1 comença amb una breu reflexió sobre la metodologia científica actual i les seves motivacions subjacents (segons l'autora). El segueixen els capítols del 2 al 4, que introdueixen i posen en context els conceptes que s'exposen a la resta del treball.

El capítol 5 aborda el problema de la relació entre l'escala microscòpica i la mesoscòpica. Tot i que existeixen diverses derivacions d'equacions mesoscòpiques partint de models de xarxes neuronals, sovint es basen en suposicions fràgils que no es compleixen en situacions més complicades. Aquí utilitzem l'UKF per assimilar la sortida de xarxes microscòpiques en un model mesoscòpic simple i estudiar diverses situacions dinàmiques. Els resultats mostren que la manera que el filtre de Kalman gestiona les incerteses del model compensa les pèrdues d'informació pròpies de les derivacions analítiques de models mesoscòpics.

Els capítols 6 i 7 tracten la combinació de dades experimentals del cervell amb models de masses neurals que descriuen la dinàmica de grups de neurones. Concretament, estenem el model de Jansen i Rit d'una columna cortical amb un model del cap, el qual ens permet fer servir dades extracranials no invasives. Amb això estimem l'estat del sistema i un paràmetre d'interès de possible rellevància en l'estudi clínic d'afeccions com l'epilèpsia.

En el capítol 6 fem servir dades *in silico* per provar l'UKF en diversos escenaris dinàmics: conjunts de paràmetres que causen comportaments diferents en les columnes corticals, diferents nivells de soroll de mesura i dues modalitats de transmissió d'informació; tot això comparant dades intracranials simulades amb simulacions d'electroencefalogrames (EEG). En totes les situacions estudiades, l'estimació extracranial és sempre superior, en velocitat i precisió, a l'estimació intracortical, encara que els elèctrodes intracorticals són molt més propers a la font de l'activitat que els elèctrodes de la superfície cranial. Suggerim que això pot ser causat per la visió més completa del còrtex que es pot obtenir amb el conjunt d'elèctrodes extracranials. Aquesta idea ve reforçada pels resultats observats amb elèctrodes extracranials individuals treballant de manera independent, que apunten a la sensibilitat espacial de les mesures.

En el capítol 7 alimentem el model de Jansen i Rit amb dades experimentals de l'EEG d'un pacient epilèptic; l'objectiu és estimar un paràmetre significatiu que governa l'evolució dinàmica del sistema, de nou amb l'UKF. L'estimació de l'estat és precisa i el paràmetre es veu afectat pels canvis de règim, especialment (però no exclusivament) per les convulsions.

Aquests resultats són prometedors a l'hora d'utilitzar l'assimilació de dades per superar les diverses carències de les tècniques de modelització cerebral.

Per una banda, la influència mútua entre estructures a escala microscòpica i a escala mesoscòpica es pot caracteritzar millor, gràcies a tècniques de filtrat que permeten esquivar les habituals limitacions analítiques. Això dóna com a resultat una millor comprensió de l'estructura i funció cerebrals. Per una altra banda, fusionar dades experimentals d'EEG amb els models matemàtics del cervell existents ens pot permetre determinar les dinàmiques subjacents dels senyals fisiològics que tenim disponibles, a la vegada que millorem els nostres models amb informació individual de cada pacient. Aquests algoritmes augmentats tenen potencial per a un ampli espectre d'aplicacions en el camp de les neurociències, des d'interfícies cervell/ordinador fins a tota mena d'usos en medicina personalitzada com el diagnòstic precoç de malalties neurodegeneratives, la predicció de crisis convulsives o la monitorització de la rehabilitació postisquèmica o posttraumàtica, entre molts altres.

Abstract

The human brain is a highly complex organ whose activity spans multiple scales, both spatial and temporal. The computational unit of the brain is thought to be the neurone, a highly specialised cell whose purpose is to receive, integrate and transmit information. At the microscopic level, neurones communicate with each other via action potentials. These may be observed experimentally *in vivo* by means of highly precise techniques that can take into account only a small number of these cells and their interactions, and can also be modelled mathematically in a variety of ways. Other techniques consider large groupings of neurones in the mesoscale, or cortical columns, and detect the averaged activity of a cell population; theoretical models that aim to reproduce these signals also abound.

Although it is known that there is an interplay between the microscopic and mesoscopic scales, the problem of relating one scale to another is far from being trivial. Analytical derivations of mesoscopic models from microscopic networks are based on sets of assumptions that are not always justified. Also, traditionally there has been a separation between the clinically oriented analysts who process neural signals for medical purposes—and

who often use highly invasive and/or costly techniques—, and the theoretical modelling community, where it is often a challenge to characterise the parameters that govern the activity of a given model.

This Thesis aims to lay bridges both between the microscopic and mesoscopic scales of brain activity, and between the experimental and theoretical angles of its study. This is achieved via a data assimilation algorithm, namely, the unscented Kalman filter (UKF), which allows us to combine knowledge from different sources (microscopic/mesoscopic and experimental/theoretical). The outcome is a stronger understanding of the system under study than each of the sources of information could provide separately by themselves.

The Thesis is organised as follows. Chapter 1 starts with a brief reflection on the current methodology in Science and its underlying motivations, as perceived by the author. This is followed by chapters 2 to 4, which constitute an introduction to the concepts discussed in the remainder of the chapters and places them in their context.

Chapter 5 tackles the problem of the microscopic and mesoscopic scales and their interrelationship. Although several efforts have been made to derive mesoscopic equations from models of microscopic networks, they are based on assumptions that may not hold in more complicated scenarios. We use the UKF to assimilate the output of microscopic networks into a simple mesoscopic model and study a variety of dynamical situations. Our results show that the way the Kalman filter handles model uncertainties compensates for the loss of information that is common in analytical derivations of models in the mesoscale.

Chapters 6 and 7 address the combination of experimental data with neural mass models that describe the dynamics of neurone groupings. More specifically, we extend Jansen and Rit's model of a cortical column with a model of the head, which allows us to use non-invasive extracranial data. With this, we estimate the state of the system and a parameter of choice that may be relevant in the clinical study of conditions such as epilepsy.

In chapter 6 we use *in silico* data to test the UKF under a variety of dynamical conditions: different parameter sets that cause different behaviours in the cortical columns, different levels of measurement noise, and different modalities of information transmission, comparing simulated intracranial data with simulated EEG. In every situation, extracranial estimation is always superior in speed and quality to intracortical estimation, even though intracortical electrodes are much closer to the source of activity than electrodes placed on the skull. We suggest that this is due to the more complete picture of the cortex that is visible with the set of extracranial electrodes. This is reinforced by the results of single extracranial electrodes working independently, which point to the spatial sensitivity of the measurements.

Chapter 7 feeds experimental EEG data of an epileptic patient into Jansen and Rit's model; the goal is to estimate the parameters that govern the dynamical behaviour of the system, again with the UKF. The estimation of the state closely follows the experimental data, while the parameter shows sensitivity to the changes in brain regimes, especially (but not only) to seizures.

These results all show promise for using data assimilation to address the several shortcomings of brain modelling techniques. On the one hand, the mutual influence of neural structures at the microscopic and the mesoscopic

scales on each other may become better characterised, by means of filtering approaches that bypass common analytical limitations, resulting in improved modelling techniques that will enable us to further our understanding of brain structure and function. On the other hand, fusing experimental EEG data with the existing mathematical models of the brain may enable us to determine the underlying dynamics of observed physiological signals, and at the same time to improve our models with real, patient-specific information. The potential of these enhanced algorithms spans a wide range of brain-related applications, from brain-computer interfaces to all manner of uses in personalised medicine, including early diagnosing of neurodegenerative diseases, seizure prediction, and monitoring of rehabilitation from trauma and strokes, to name but a few.

Table of contents

List of figures

List of tables

It is more fun to talk with someone who doesn't use long, difficult words but rather short, easy words like "What about lunch?"

Winnie the Pooh

List of acronyms

ECoG electrocorticography. 16, 102

EEG electroencephalography. xix, xx, 12, 14, 15, 16, 27, 30, 53, 73, 74, 75, 82, 86, 89, 91, 92, 96, 100, 102, 104, 107, 108, 109, 115, 118, 119, 126, 128

EEG electroencephalogram. 11, 12, 14, 29, 74, 93, 115

EKF extended Kalman filter. 46

EnKF ensemble Kalman filter. 40

EPSP excitatory post-synaptic potential. 93, 115, 119

IPSP inhibitory post-synaptic potential. 115

PSP post-synaptic potential. 28, 57, 78, 120, 121

UKF unscented Kalman filter. xviii, 40, 41, 46, 47, 59, 62, 63, 64, 65, 68, 71, 91, 92, 93, 100, 101, 104, 108, 123

Part I

Introduction

Flower in the crannied wall,
I pluck you out of the crannies,
I hold you here, root and all, in my hand,
Little flower—but if I could understand
What you are, root and all, and all in all,
I should know what God and man is.

Alfred Lord Tennyson

1

A brief philosophical reflection

The above poem is among the densest passages in the English literature, as measured in depth per written line. Its main idea is that a detailed study of the parts that constitute a being would bring us closer to understanding a higher or transcendent entity. The poet stands in front of a dry dead wall and finds a flower growing in a perhaps unexpected place. He picks the flower and examines the whole entity, seeing for the first time the root as well as the flower, and hypothesises that understanding the flower would give him the knowledge of God. To me, this idea of understanding the

whole (and more) from the sum of its parts seems to be also the history of every major undertaking in human cognissance, and therefore also the backbone of Neuroscience.

When the poet plucks the flower from the nook where it was growing, he isolates it from its usual environment; the root becomes visible and with it, a better picture of the flower in its wholeness is obtained. Or is it? The roots are no longer in contact with the soil: we cannot observe the uptake of water and minerals, or the amazing process of photosynthesis; it is true, however, that we could not see these things before, while the flower was in the cranny, either. But then, the stem can no longer sway with the wind now; much less can a passerby enjoy the flower's scent, or the bees drink its nectar. Do not these things constitute the flower's being too? And its purpose, and the very reason for its existence? And we could see them, when the flower was still in its little crack.

> A recognized fact which goes back to the earliest times is that every living organism is not the sum of a multitude of unitary processes, but is, by virtue of interrelationships and of higher and lower levels of control, an unbroken unity. When research, in the efforts of bringing understanding, as a rule examines isolated processes and studies them, these must of necessity be removed from their context. In general, viewed biologically, this experimental separation involves a sacrifice. In fact, quantitative findings of any material and energy changes preserve their full context only through their being seen and understood as parts of a natural order.
> (Walter Hess)

I believe the same sacrifice is being made in the study of the brain, and indeed, in the whole of modern Medicine and Biology. The reductionist and materialistic views that have pervaded Science since the Age of Enlightment (*sic*?) have become the *status quo*, and I fear that this very view is behind some of today's greatest scientific failures. Indeed, it is probably not questioned that what we know, in the rational and scientific sense of the word, is

necessarily limited by the experimental techniques available (Stevenson and Kording, 2012; Yuste, 2015); but then, all we may actually experiment with is systems out of their context:

> A good physiological experiment like a good physical one requires that it should present anywhere, at any time, under identical conditions, the same certain and unequivocal phenomena that can always be confirmed.
> (Johannes Peter Müller)

Furthermore, much as we would like to deny it, I will venture that we readily accept experimental results only when they conform to an accepted theoretical framework—which also, in turn, shapes the very experiments!

> One only sees what one looks for. One only looks for what one knows.
> (Johann Wolfgang von Goethe)

Unfortunately, this makes us stuck in an intellectual rut of sorts. While we can be happy there are no more trephinations or lobotomies, no more seizure therapy or insulin shocks (Faria, Jr., 2013), we don't think twice about flooding brains with weird chemicals that wreak havoc (Albrecht et al., 2014; Bahrick, 2008; Fergusson et al., 2005; Hibel et al., 2007; Miele et al., 2017; Moore et al., 2010; Nasrallah et al., 1986), playing with things we do not fully understand (Bushara, 2005; de la Monte and Wands, 2008; Fisher and Fisher, 1996; Lacasse and Leo, 2005; Molina et al., 2009; Moreno et al., 2007), and seeking cures without reflecting on causes. (The latter of which, in my opinion, is especially tragic.) I hope that, somewhere in the future, drugging toddlers with psychotropic medications (Zito et al., 2000) will be considered at least as barbaric—by the mainstream, that is—as shoving an ice pick through someone's eye socket. It is actually not even working; one need only review the statistics for the incindence of mental illness to quickly see that orthodox psychiatric medicine isn't taking us

anywhere nice (CDC Statistics for Autism; NIMH Statistics for Mental Illness; Statistics for Dementia; Xu et al., 2018).

> I'm not lost for I know where I am. But however, where I am may be lost.
> (Winnie the Pooh)

For many people, myself included, the human being is body, soul and spirit, and the isolation and disconnection of any of these systems from the others may result, depending on our object and purpose, in a crippling lack of information that can render the whole endeavour perfectly useless. I started this Thesis with lofty hopes that it would have some sort of clinical and social repercussion—the initial dream was to improve our diagnostic capabilities for neurodegenerative diseases. However, I fear that if it is a step at all, it is probably in the wrong direction—or at least, in a direction that will not serve people in the way that is most relevant.

All this is not to say, however, that any effort to know more with the resources we have available, even (and especially!) in Neuroscience, is futile. We probably just need a little perspective. If we do keep in mind that all models are wrong (Schiff, 2012, Chapter 8), that we now know that much of what was known before is wrong (and therefore that much of what we know now may also be wrong—why not?), and that anything short of x-raying a whole human being from a superior dimension will be isolating and reducing systems to a potentially disabling degree, we will doubtless be more cautious with what we think we do know, and with what we do about it. We want to know, we need to know, and we need to seek the answers we naturally crave. That is why the poet plucked the flower.

But perhaps, if the poet dwelt a little more on the thought of God, he would more easily come to know what the flower is.

Those who have dissected or inspected many [bodies] have at least learnt to doubt; while others who are ignorant of anatomy and do not take the trouble to attend it are in no doubt at all.

Giovanni Battista Morgagni

2

Physiological basis of brain modelling

Few systems known to man are more complex in their configuration and operation than the human brain. Cerebral dynamics are an incredibly complicated and excellently coordinated dance in which all participants must do just the right thing, in the right place, and at the right time. This section presents an overview of the anatomy and physiology of the brain and the basis of its electrical functioning, along with a description of some conditions that seemingly arise when there is an anomaly.

2.1 Neural signalling

The ground-breaking neuroanatomical work of Santiago Ramón y Cajal brought forth, around the turn of the 20th century, the establishment of the neurone doctrine, basically reducing cerebral activity to being originated in the group of discrete cells that the nervous system is supposed to be and based on the interactions thereof. The discovery of electron microscopy in the 1950s consolidated this belief and to date it remains one of the cornerstones of modern neuroscience (López-Muñoz et al., 2006). However right or wrong this may be, we are in no place to venture a judgement; in this Thesis we conform to this pattern of thought for the remainder of the work.

As often happens with other theories, and following the reflections in chapter 1, we have heard the neurone doctrine being called by a learned scientist in the field "the greatest punishment Neuroscience has ever faced". Again as with other theories, time will tell.

The basic unit of neural processing is thought to be the neuron. Neurones have a soma, or body, which contains the dendritic arbour that receives incoming signals from other cells, and the nucleus. This then travels down the axon, a very variably long projection, that in turn connects to the receptors of other cells, most commonly the dendrites of other neurones, by means of synapses. (There are an estimated three times more glial cells (Purves et al., 2004) with supportive functions that have a great influence on brain activity, to the point of bidirectionally communicating with neurones and acting as a third element in the synapse (Perea and Araque, 2010; Perea et al., 2009). Nevertheless, the models we consider here do not take glia into account.)

The neurone is delimited by the membrane, which is impermeable to water molecules and ions and contains gated pores, the ion channels, whose selective permeability is a fundamental characteristic of the cell's electrical function. These ion channels can be either opened or closed to permit the

passage of certain ions, the most important of which are sodium, potassium, magnesium, calcium, and chloride. The activity of ion channels can depend on several factors, but the passage of ions through them tends to diminish the concentration gradient. However, ion pumps, which are also key constituents of the membrane, forcefully pump certain ions and molecules against the concentration gradient.

The activity of the neuronal membrane and its channels and pumps result in a difference of voltage across the membrane, the membrane potential. Typically, the resting membrane potential is about −65 mV, the intracellular medium being more negative than the outside. Changes in the membrane potential (brought about by the activity of other cells, by the presence of neurotransmitters or by changes in ionic concentrations) may cause the cell to fire an electric action potential, or spike, down its axon, eventually acting on a downstream neurone (or neurones) and possibly causing them to react in turn. Spikes are an all-or-nothing event; the differences in the input intensity will not alter the strength of an action potential, although it might change the rate at which the neurone fires. It is interesting to note that synapses act stochastically and their reliability is highly variable (Branco and Staras, 2009); this is a complicating factor when attempting to model networks of neurones at a single-cell level (see section 3.2).

2.2 Cortical columns

In the very midst of the heated discussion between proponents and detractors of the neurone doctrine, Brodmann already suggested in 1909 that it is cell groupings, not individual cell types, that are responsible for any cortical function (Brodmann and Garey, 2006). Vernon Mountcastle suggested in

1957, after his experiments with the cat's somatic sensory cortex, that "the elementary pattern of organisation in the cerebral cortex is a vertically oriented column or cylinder of cells" (Mountcastle, 1957), a finding that Hubert and Wiesel confirmed with further experiments two decades later (Hubert and Wiesel, 1977).

Since then, the existence of such entities in the cerebral cortex as neuronal clusters grouped in the vertical (or, rather, radial) direction is not questioned. The actual definition of what a cortical column is, and the relationship between structure and function, are nevertheless a matter of debate. Also, to date it is unexplainable why a columnar structure does exist (Goodhill and Carreira-Perpiñán, 2002). Neurones within a cortical column will be intrinsically connected in the vertical dimension and share similar connections to and from remote regions; so much appears to be under consensus (Horton and Adams, 2005).

However, anatomical considerations make classification very difficult; whereas some structures appear to be clearly visible and distinguishable (de Nó, 1949), other cases show fuzzy and overlapping boundaries. Furthermore, the definition of columns at different scales, due in part to the existence of radial cell units observed during cerebral development, has contributed to further confuse the issue, bringing additional concepts like mini– and macrocolumns into play (Buxhoeveden and Casanova, 2002; Horton and Adams, 2005; Rakic, 2008). Finally, some authors, e.g. Szentágothai (1978), have proposed the cortical column as a theoretical concept, albeit based on experiments, considering it a module of a constant diameter of 200–300 μm. Two years later, a highly influential work was published, in a similar line, that suggested that the structure of the neocortex was more uniform than

had been thought previously (Rockel et al., 1980). Although this study was fraught with problems at every level (Rakic, 2008), many liked this idea for its simplicity, since the uniformity of the neocortex across modalities as well as during expansion brings forth other deeper and more philosophical implications that, for some reason, always seem attractive, such as that the differences between human and animal neocortices are merely quantitative, or that the specialisation of cytoarchitectonic areas is just due to input from the periphery (Rakic, 2008).

To this date, cortical columns, as defined under anatomical considerations, have failed to serve as a unifying principle to relate structure to function. However, the idea of groupings of neurones (functional or not) is still a useful concept and is attracting both basic research and applied efforts in innovative directions, e.g. a project that maps all the cortical columns with brain-computer interfaces in view (Goebel, 2016). In this Thesis, we consider a cortical column as described by Mountcastle (1978, 1997), namely, a cluster of neurones with a set of common characteristics that is about 300–600 μm wide in diameter, and which acts as a processing and distributing unit that links a number of inputs to a number of outputs via overlapping internal processing chains (Mountcastle, 1997).

2.3 Measuring brain activity

Electricity is a very important component of cerebral activity, and even though this has been implicitly accepted for several centuries, in medical practices such as the application of electric eels to help with migraine (Koehler and Boes, 2010), it wasn't until the 18th century that the concept of bioelectricity was more explicitly and systematically studied, most famously by Luigi

Galvani with his experiments on neuromuscular stimulation (Malmivuo and Plonsey, 1995). Towards the end of the 19th century, Caton (1875) was the first to record the electric activity of a brain, and his work, if not the discovery of the electroencephalogram itself, is at least its precursor. A few decades later, Berger (1933) recorded alpha waves in the first human electroencephalogram. Other technologies, such as electrocorticography or, less related conceptually, BOLD-fMRI—whose biological basis had also been lain in the 19th century (Mosso, 1880; Roy and Sherrington, 1890)—, made their clinical debut only decades later (Jasper, 1941; Ogawa et al., 1990), thus adding to the wide array of brain imaging techniques available today.

2.3.1 Electroencephalography

The electroencephalogram, or EEG from now on, measures the electric activity that is detectable by electrodes placed on the scalp. Most of the signal is thought to come from the post-synaptic potentials of groups of similarly oriented pyramidal neurones, which induce currents in the extracellular matrix with a potential field strong enough to be measurable (Marcuse et al., 2016; Silva, 2011). EEG detects mostly currents very near the skull, since the sources that are located deeper in the brain are very difficult to detect and discern (Klein and Thorne, 2006).

As more information about glia is uncovered, it is hypothesised that even they too play a role in the signal detected by EEG (Marcuse et al., 2016).

The setup for an EEG recording involves a set of electrodes placed on a subject's scalp, with their number and position usually decided by an international standard (Klem et al., 1999); an amplifying unit to allow to display the signal on a computer screen, since the signal on the scalp is of the order of microvolts; an A/D converter; and a visualising and/or recording device. The electrodes may be placed in one of two montages.

Bipolar recordings link successive electrodes to one another in such a manner that the voltage of one electrode is compared to that of the adjacent electrodes (see figure 2.1); the difference between the potentials measured at the two electrodes forms a channel. In referential recordings, however, the voltage of a scalp electrode is compared to one referential electrode, usually on the ear and sometimes on the vertex (the highest point of the skull); here, the channel is formed by the difference between the electrode under consideration and the reference.

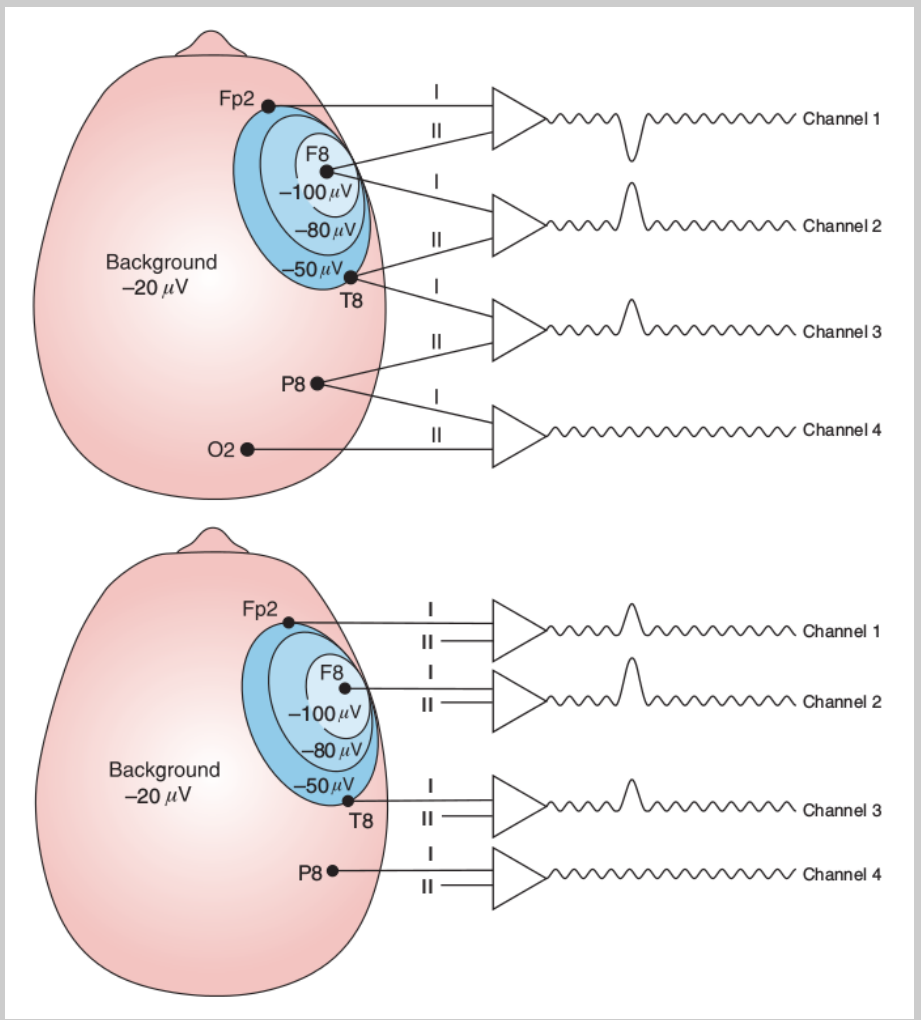

Figure 2.1 Focal activity and its corresponding traces as seen with a bipolar montage (above) and a referential montage (below). Adapted from Marcuse et al. (2016).

In both montages—in actual fact, the two modalities are complementary—an electroencephalogram can show oscillations whose frequency, spatial distribution, shape, and pattern point to different neurological states and conditions. According to their frequency, neural oscillations may be classified into four groups: gamma (38–42 Hz), beta (13–38 Hz), alpha (8–13 Hz), theta (4–8 Hz), and delta (0.5–4 Hz). The alpha frequency is the most studied, and it is associated to a restful, relaxed state; it is visible on an EEG as sinusoidal waves with a typical peak-to-peak amplitude of 50 μV (Teplan, 2002). Beta, theta, gamma and delta waves differ in amplitude and pathophysiological meaning and relevance, and will not be discussed here.

Of interest in an EEG are very sharp waves, or spikes. They arise suddenly from the background, with a duration of 20–70 ms, and their upward slope is typically steeper than the downward slope; they are usually followed by a low-voltage slow potential of about 200 ms, and after that the baseline is re-established. See figure 2.2 for several examples. Spikes are almost always associated to epileptiform discharges, and this and other similar considerations make EEG a very valuable tool in the diagnosis and monitoring of epilepsy (Marcuse et al., 2016).

The second feature of EEG of interest for this Thesis is phase reversal. Phase reversal is very useful in detecting potential fields, and it can be visible using the bipolar montage; see figure 2.1 for a clear visualisation of the concept. Where there is a local activity focus, and considering a three-electrode chain for this example (in upper panel of the the figure, Fp2, F8 and T8), the subtraction of the (more negative) signal from the focus (electrode F8) minus the background signal (electrode Fp2) will result in a downward deflection; however, the following electrode in the chain, T8, will

be at a similar potential to the first electrode, Fp2, and the subtraction will result in an upward deflection, thus placing the focus of activity under the second electrode. With a referential montage, the focus would be localised under the electrode that yields the signal with the most amplitude (lower panel of figure 2.1).

Electroencephalography is used to monitor coma, alertness and brain death; to find damaged areas (for example, following a stroke or trauma); to investigate sleep disorders; to locate and study epileptic foci; to test and monitor drug effects, including anticonvulsants and anaesthesia; and in other medical and research applications (Bickford, 1987). It is extremely non-invasive, relatively inexpensive and especially fast (both in the sense of processing measurements with speed and having very good temporal resolution); its main drawbacks are the lack of spatial resolution (due to volume conduction and to the translation of a three-dimensional structure of activity into a two-dimensional array) and the obscurement of the signal (due to the direction of the electrical field, the physical distance and tissues between electrode and focus of activity, and several artifacts) (Chong et al., 2007).

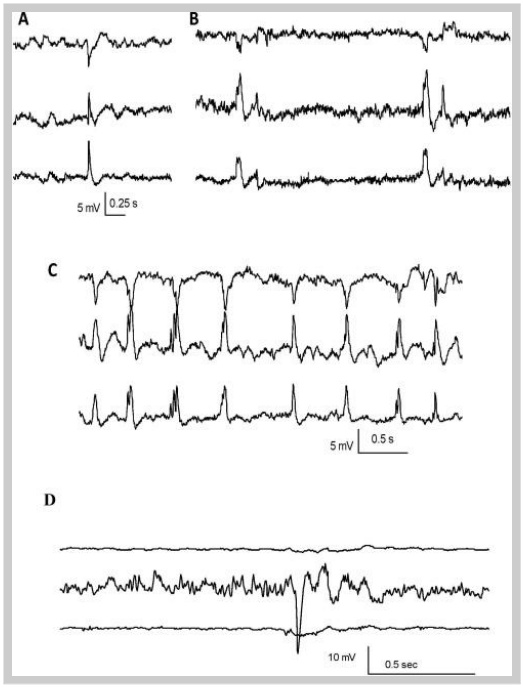

Figure 2.2 Several examples of spike discharges in a rat EEG. Reproduced integrally from White et al. (2010).

The EEG oscillations in many clinical scenarios may be modelled by means of differential equations (Babajani-Feremi and Soltanian-Zadeh, 2010; Hashemi et al., 2014; Kuhlmann et al., 2016; Sotero et al., 2007). Indeed, this is an important aspect in this Thesis, in view of assimilating experimental data into theoretical models (see Mesoscopic models, section 3.2).

2.3.2 Electrocorticography

Electrocorticography (ECoG) is also called intracranial electroencephalography and is in essence very similar to EEG, the main difference being that the electrodes are not placed on the skull, but directly on the exposed surface of the brain. This makes it a highly invasive technique, since it necessarily requires a craniotomy to implant the electrodes. Electrodes may be implanted on or under the dura mater, either mounted on a flexible frame (which allows to use multiple electrodes simultaneously) (Schuh and Drury, 1997) or individually. Of special interest are depth electrodes, which, in adequate conditions, can measure action potentials (Ulbert et al., 2001).

ECoG shares with EEG the nature of the signals they record and their origin. However, where EEG has little spatial resolution due to the attenuation of the bone, ECoG is more advantageous in this sense; this makes it an especially indicated tool for the localisation of both epileptogenic zones and functional areas to avoid during surgery. Indeed, it is for this purpose that its use was pioneered in the 1950s by Jasper and Penfield (1954).

Electrocorticography signals may be simulated by means of mathematical models, in the same manner as EEG. Indeed, this Thesis is heavily inspired on the work of Freestone et al. (2013b), who used ECoG data to estimate the parameters of a neural mass model with the aim of tracking brain states

in a personalised manner. Another exciting perspective is using ECoG as a recording technique for applications in brain-computer interfaces (Shenoy et al., 2008). The next chapter reviews some of the most well-known models used to reproduce physiological measurements, with a special emphasis on EEG and ECoG.

...[the brain] is very big and complicated and made of stuff that dies when you poke it around.

Geoffrey Hinton

3

Modelling cerebral activity

There are many problems in neuroscience that warrant a mathematical approach. Only recently, however, have computational techniques been advanced enough to make whole-brain modelling feasible—to a certain extent.

In 1907, Louis Lapicque studied the excitability of nerves and developed a model that would later serve as the basis for the integrate-and-fire model of neuronal membranes (Brunel and van Rossum, 2007; Lapicque, 1907).

Nevertheless, the fathers of computational neuroscience are considered to be Alan L. Hodgkin and Andew F. Huxley, who won the Nobel prize in 1963 for their description of the action potentials of the giant squid axon in 1952 (Hodgkin and Huxley, 1952).

However, although modelling has a strong component in both of these significant developments, the use of computational methods wasn't promoted until Wilfrid Rall used mathematics to defend how strongly synaptic currents affect the processing of the synaptic input in the soma (Rall, 1959, 1962). The opposition he had to deal with is very interesting to consider, as it highlights two important problems that modern neuroscience has faced since its inception. On the one hand, the experimental techniques available have inevitably shaped our understanding of brain dynamics for many decades (Yuste, 2015). This is problematic, especially because experimental evidence is often rejected if it doesn't conform to orthodox theories. On the other hand, the general scepticism of experimentalists towards the usefulness of computational approaches to neuroscience (and, indeed, to biomedicine in general) opens a wide gap between theory and clinical application that is still to be bridged—to which end this Thesis is but a small effort.

3.1 Microscopic models

Microscopic models reproduce the dynamics of single cells or, even at a greater level of detail, the dynamics of ion channels in their membranes (Hille, 2001) (the latter lie out of the scope of this work). Communication between neurones is based on electrical impulses called action potentials, or spikes. These come into a cell and are then transformed into a sequence of output

spikes. Spikes are all almost indentical to one another and are an all-or-nothing type of response; as a consequence, neuronal computations are based on the inter-spike intervals, rather than on the spikes themselves. The emission of a spike depends not only on the incoming information from other neurones, but also on the membrane potential and by other elements such as heat, stretching, and the presence of ligands, all of which affect the ion channels and their permeability (Purves et al., 2004).

Microscopic models can be highly realistic biologically, but this comes at a considerable computational expense. In efforts to reduce the computational burden while still preserving a reasonable amount of biological plausibility, there are many simplified models that have been in use for decades. The following sections provide an overview to some of the most relevant.

3.1.1 Integrate-and-fire model

As mentioned previously, Louis Lapicque's work in 1907 established a precedent for what would later become the integrate-and-fire model of a neurone. Despite the fact that the model is often attributed to him, in reality the model as we know it was defined in the 60s, and the first papers to mention the name *integrate-and-fire* appeared in the 70s (Brunel and van Rossum, 2007; Knight, 1972a,b), with earlier work done in 1936 (Hill, 1936).

The integrate-and-fire model basically describes a passive patch of membrane as an RC circuit, where an input current eventually causes the membrane potential to reach a specified threshold. This short-circuits the membrane resistance and ellicits a spike followed by a reset and a refractory period, after which the membrane may charge again (Sterratt et al., 2011). Equation 3.1

shows the integrate-and-fire model. This equation comes from solving the differential equation for the membrane potential V:

$$V = E_m + R_m I(1 - e^{-\frac{t}{\tau_m}}) \tag{3.1}$$

In this equation, V is the membrane potential, E_m is the reset potential (to which the membrane is reset after a spike), R_m is the membrane resistance, I is the total current input, and τ_m is the membrane time constant (the product of the membrane resistance R_m and the membrane capacitance).

Hodgkin pioneered the study of bifurcation mechanisms of excitability and identified two groups: class I, where action potentials may be generated on a low frequency depending on the strength of the applied current, and class II, where spikes are generated within a frequency band that is relatively independent of changes in the intensity of the applied current (Izhikevich, 2007).

The integrate-and-fire model falls in class I, according to Hodgkin's classification by neural excitability (Izhikevich, 2007). It has many variants that add realism to its behaviour (Fourcaud-Trocmé et al., 2003; Gerstner and Kistler, 2002; Hansel and Mato, 2000; Koch, 1999; Latham et al., 2000). Overall, it is a relatively simple model and fast to implement, which makes it especially useful for simulating large networks.

3.1.2 Hodgkin-Huxley model

The Hodgkin-Huxley model describes the action potential of a neurone and originated from the authors' careful observations of the giant squid axon (Hodgkin and Huxley, 1952). It merited the Nobel Prize in 1963 and is still to date one of the most important tools in computational neuroscience. In this model, the membrane acts as a capacitance C and voltage-dependent electrical conductances represent voltage-gated ion channels. One formulation (Rabinovich et al., 2006) follows:

$$C\dot{V}(t) = g_L\,[V_L - V(t)] + gN_a m(t)^3 h(t)\,[VN_a - V(t)] + gKn(t)^4(V_K) - v(t) + I \tag{3.2}$$

$$\dot{m}(t) = \frac{m_\infty\,(V(t)) - m(t)}{\tau_m\,(V(t))} \tag{3.3}$$

$$\dot{h}(t) = \frac{h_\infty\,(V(t)) - h(t)}{\tau_h\,(V(t))} \tag{3.4}$$

$$\dot{n}(t) = \frac{n_\infty\,(V(t)) - n(t)}{\tau_n\,(V(t))}, \tag{3.5}$$

where V(t) is the membrane potential; m(t), h(t), and n(t) are empirical variables that describe the activation and inactivation of the ionic conductances; and I is an external current. The steady-state values of m_∞, h_∞, and n_∞, which are the conductance variables, depend on the voltage in a nonlinear fashion.

3.1.3 Morris-Lecar and FitzHugh-Nagumo models

The Morris-Lecar model (Morris and Lecar, 1981) is also a widely used and well-known microscopic model that is derived from experiments on the barnacle giant muscle fiber. Despite the fact that it is only two-dimensional, it is capable of reproducing a wide array of oscillating states and can simulate both class I and class II neurones (see page 22), all of which make it one of the most popular microscopic models available. It is a conductance-based model, comparable to the Hodgkin-Huxley model, except that its dimensionality is lower while still reproducing a similar array of behaviours.

This model reproduces the oscillatory behaviour of the membrane potential of a nerve cell with respect to the activation of the ion channels in the membrane. It reduces the voltage dynamics to being dependent on Ca^{2+}, by means of an instantaneously responding voltage-sensitive conductance, for excitation; and K^+, with a delayed voltage-dependent conductance, for recovery. The initial model accounted for Ca^{2+} ion dynamics; however, a set of safe assumptions were made that allowed to simulate the entire set of two-dimensional oscillation phenomena that had been observed experimentally without this third variable. The final model therefore relies on two variables: the membrane potential, V, and the recovery variable, N—the fraction of open K^+ channels—, as presented in the following equations:

$$C\dot{V}(t) = I - g_L\,(V(t) - V_L) - g_{Ca}M_\infty\,(V(t))\,(V(t) - V_{Ca}) - g_K N\,(V(t) - V_k) \tag{3.6}$$

$$\dot{N}(t) = \lambda_N\,(V(t))\,(N_\infty\,(V(t)) - N(t))\,, \tag{3.7}$$

where

$$M_\infty\,(V(t)) = \frac{1}{2}\left(1 + \tanh\left(\frac{V(t) - V_1}{V_2}\right)\right) \tag{3.8}$$

$$N_\infty\,(V(t)) = \frac{1}{2}\left(1 + \tanh\left(\frac{V(t) - V_3}{V_4}\right)\right) \tag{3.9}$$

$$\lambda_N\,(V(t)) = \overline{\lambda_N}\cosh\left(\frac{V(t) - V_3}{2V_4}\right) \tag{3.10}$$

In these equations, I is the applied current; g_L, g_{Ca} and g_K are leak, Ca^{2+} and K^+ conductances, respectively; $\lambda_N(V)$ and λ_N are the rate constant and maximum rate constant for K^+ channel opening, respectively; $M_\infty(V)$

and $N_\infty(V)$ are the fractions of open Ca^{2+} and K^+ channels at steady state, respectively; V_1 and V_3 are the potentials at which $M_\infty = 0.5$ mV and $N_\infty = 0.5$ mV, respectively; and V_2 and V_4 are reciprocals of slope of voltage dependence of M_∞ and N_∞, respectively.

The Morris-Lecar model allows to reproduce several dynamic behaviours by altering its parameters, thus generating different types of stability. Also, because the parameterisation is relatively simple, one may use the model to build networks of coupled oscillators and describe collective oscillations whose behaviour depends on the coupling.

The FitzHugh-Nagumo model (FitzHugh, 1961; Nagumo et al., 1962) is related to the Morris-Lecar model, in the sense that it is a conductance-based model and a simplification of the Hodgkin-Huxley model to a 2D space:

$$\dot{x} = x - cx^3 - y - I \tag{3.11}$$

$$\dot{y} = x + by - a, \tag{3.12}$$

where x(t) is the membrane potential, y represents fast currents, I is an external current, and a, b, and c are chosen to allow the model to spike (Rabinovich et al., 2006). The FitzHugh-Nagumo model contains the van der Pol oscillator when $a = b = 0$.

3.1.4 Microscopic neural networks

Microscopic neural networks are formed by connecting microscopic models of neurones to one another by transmitting the output signal of one neurone as the input signal to another. Mostly, the signal is the presence or the absence of an action potential (Stepanov, 2011); however, whether it is

the timing of action potentials or the firing rate of neurones which encodes information is still unknown. The presence of connections adds an important element of complexity, as there are many aspects that further complicate finding a good compromise between biological realism and mathematical tractability (Cessac and Viéville, 2008). Indeed, the analysis of a single neurone cannot always be easily extended to a network: whether or not to position neurones in space; the quantity of units and connections, or its scaling; the nature of these connections and their number, as well as their distribution (i.e. resulting in sparse, local or small-world networks); the presence of delays in the communication; and the variability in the properties or characteristics of each unit, these aspects must all be considered in the construction of a neural network. Moreover, in some cases the simplifications in the model may by themselves induce effects not observed in the real system (Cessac and Viéville, 2008), adding to the difficulty.

However big the obstacles, modelling networks of neurones plays a crucial role in understanding the transmission of information and the emergent characteristics of cerebral circuits, especially through their dynamical features (such as the synchronisation between different populations, or the presence and influence of noise). Experimental data reveal how microscopic properties of neural populations shape the processing of information in local networks, and at the same time how the behaviour of networks at a larger scale influences local populations (Guigon et al., 1994; Panzeri et al., 2015; Wright and Liley, 1996). We are especially interested in integrating and relating the knowledge from both scales of operation for a comprehensive global understanding of brain dynamics (see section 3.3).

3.2 Mesoscopic models

Although microscopic networks are currently the most realistic modelling tool we possess, modelling circuits of more than a few dozens of neurones and their interconnections can be computationally expensive to a prohibitive degree. Also, there is much yet to be learnt about the properties of neurones, their placing, and how they interact with each other, not to mention the activity and influence of non-neuronal glia (Araque and Navarrete, 2010; Perea and Araque, 2010; Perea et al., 2009). Additionally, non-deterministic factors affect brain interactions (Branco and Staras, 2009), to the point where any model is inevitably inexact, and often very much so.

Mesoscopic models use concepts from statistical physics to average out large clusters of neurones and model them at a population level, with a single set of parameters describing the dynamics of the neuronal ensemble (Deco et al., 2008). This is especially useful in the context of imaging, where the available technologies—e.g. electroencephalography, magnetoencephalography or functional magnetic resonance imaging—reflect the collective activity of large groups of neurones. Neural mass models, a type of mesoscopic models, do not account for the spatial dimension (see Other approaches, section 3.2.2), but focus on temporal effects. Section 3.3, Bridging the gaps, describes in greater detail the relationship and derivation of mesoscopic formulations from microscopic models.

Although the concept of a neural mass was introduced in the 70s, it was earlier, in the work of Beurle (Beurle, 1956) and then Griffith (Griffith, 1963, 1965) that the first studies involving assemblies of neurones in the mesoscale were conducted. These works did not account for refractoriness

or recovery and neither did they consider any inhibitory components; therefore, they were not very relevant from a physiological point of view (Liley et al., 2012), but they did serve as an important precedent for the more exact models that were to come. Wilson and Cowan proposed what was probably the first neural mass model in 1972 (Wilson and Cowan, 1972), even though they did not use this name themselves. Their model introduced a sigmoidal function to encode the firing rate of the neural mass and defined a series of excitatory and inhibitory interactions between spatially defined populations of neurones, both of which innovations were crucial and have been retained by future models (Liley et al., 2012). Further work by Amari (Amari, 1975, 1977) and Freeman (Freeman, 1975) advanced these efforts with different mathematical approaches.

3.2.1 Jansen-Rit model

Most early models assumed that the effects of synaptic activity are directly felt at the soma (Liley et al., 2012) (except for Freeman (1975)). However, it was found experimentally that the cellular membrane potential peaks and decays in a second-order response to incoming synapses (Kandel et al., 2000), which was later referred to as post-synaptic potential (PSP). Lopes da Silva et al. (1974) and van Rotterdam et al. (1982) were the first to explicitly include PSPs in the formulation of a mean field model. Jansen and Rit extended and systematically investigated the model for its behaviour under parameter changes (Jansen and Rit, 1995; Jansen et al., 1993). It is their studies which present the formulation used in this thesis, and from now on we refer to it as the Jansen-Rit model—the fairness of which is not a subject of debate in these pages.

Jansen and Rit's model simplifies the neuronal diversity of a cortical column in three interacting populations: pyramidal neurones, excitatory interneurones, and inhibitory interneurones. The larger pyramidal population excites both groups of interneurones, which in turn feed back into the pyramidal cells. The pyramidal population is also driven by excitatory noise from distant areas of the brain and by neighbouring columns. (Please see section A.1 on page 113 for the equations of the model and more details.) As with earlier neural mass models, the activity of the cortical column is conducted with two transformations: the first relates the average density of incoming action potentials into an average post-synaptic membrane potential and takes the form of a second-order differential equation; the second converts the net average membrane potential of the population into an average firing rate, and is described by a sigmoid function.

As has been mentioned previously in section 2.3.1, Electroencephalography, electrical activity detected by the electrodes on the scalp in an EEG is thought to be originated by the weighted sum of the averaged membrane potential of the pyramidal cells. In this Thesis, we have chosen the Jansen-Rit model as our tool for reproducing the EEG for its ability to reproduce alpha-like waves and epileptiform spikes.

3.2.2 Other approaches

As has been mentioned in the previous sections, neural mass models are far from being the only modelling tool available in the mesoscopic scale. The first mesoscopic models took the spatial dimension into account (Beurle, 1956; Griffith, 1963, 1965), and therefore fall into the category of neural fields; in fact, neural masses can be regarded as a special case of neural

fields in which conduction times tend to zero (Pinotsis and Friston, 2014). Because of the spatial dimension of neural fields, there are interesting theoretical possibilities of study, perhaps the most notorious of which is pattern formation (Amari, 1975, 1977). Also, the practical applications of neural field models are highlighted in recent and past research on brain imaging (Freestone et al., 2011a; R.G.Abeysuriya and P.A.Robinson, 2016; Wijeakumar et al., 2017), full brain modelling (Spiegler and Jirsa, 2013), neural plasticity (P.K.Fung and Robinson, 2013; P.K.Fung et al., 2013), vision (Adorján et al., 1999; Salmon and Trappenberg, 2008; Wang et al., 2012), pathological states of the brain (Müller et al., 2017), and robotics (Fard et al., 2015; Oubbati et al., 2006).

In the context of data assimilation in brain modelling, and especially inferring connectivity, a notorious tool is dynamic causal modelling (Friston et al., 2003; Stephan et al., 2010). Dynamic causal modelling uses Bayesian model comparison to infer the coupling parameters that characterise the connectivity between different brain regions. These brain regions consist of neural populations that are intrinsically connected and also coupled externally to other regions, and may be described by any model that is biologically plausible and sufficient to describe population phenomenology (Beharelle and Small, 2016). Although it was initially aimed at fMRI BOLD (Havlicek et al., 2015; Stephan and Roebroeck, 2012), later on it was extended to modelling evoked responses with EEG and MEG (David et al., 2005, 2006; Kiebel et al., 2008) using in this case, interestingly, Jansen and Rit's model. Other efforts include the study of seizures (Jedynak et al., 2017; Papadopoulou et al., 2016), using large scale models (Lee et al., 2006), neural fields (Moran et al., 2013; Pinotsis et al., 2012), a scale-bridging model using laminar

recordings (Pinotsis et al., 2017), and combination with cross-spectral density analysis of electrophysiological recordings (Moran et al., 2009).

3.3 Bridging the gaps

Perhaps one of the properties of brain activity that makes it the hardest to decipher is that it operates on different scales: temporally, from the milliseconds a spike takes (Berry et al., 1997) to circadian rhythms and a lifetime of memories (Buhusi and Meck, 2005); and spatially, from the nanometric neurotransmitters to the brainwaves generated by clusters of neurones, to functional areas that encompass several square centimetres (Purves et al., 2004). Relating these scales to each other, or "bridging the gaps", is a basic undertaking when attempting to build a consistent and self-contained picture of brain dynamics. Because the most relevant models for our work fit either in the microscopic or the mesoscopic category, from now on we will refer solely to these two scales and to the relationship between them.

Although it is entirely possible to build a mesoscopic model that is exclusively phenomenological in its inception, i.e. that aims solely to reproduce the dynamics of those time traces obtained by brain imaging, such a model will mostly fail in its interpretation of the underlying physiology of the system that originated these time traces. In our view these models might have great theoretical interest, but probably have no direct or immediate clinical application, whereas most microscopic models are often directly derived from experiments and their parameters respond to concrete biological magnitudes. It is for this reason that we believe that relating these two scales of brain activity is of paramount importance.

Although this holds true for many or most mesoscopic models, Jansen and Rit's model does feature parameters with biological meaning.

The models that have been hitherto discussed all contain, in some measure, more or less implicit information as to where they are situated both in the temporal and spatial scales. Therefore, any effort towards relating two types of models (e.g. mesoscopic to microscopic) will necessarily deal with these two aspects. Essentially, the challenge lays in relating discrete events that take place in milliseconds from cell to cell (neuronal spikes) to continuous waves of activity that may span multiple seconds and are the result of the collective activity of tens of thousands of cells.

In their thorough and exhaustive review, Deco and others (Deco et al., 2008) apply the mean-field approach to describe an ensemble of spiking neurones with the Fokker-Planck equation, which results in the so-called ensemble density models; in the special case where the description of the ensemble density models is summarised with a single number, a neural mass model is obtained. Faugeras and others (Faugeras et al., 2009) derive a mean-field model from an ensemble of spiking neurones (Dayan and Abbott, 2001; Gerstner and Kistler, 2002) by assuming that the mean of the sigmoids of the membrane potentials of each cell in a population is the same as the sigmoid of the mean. This is a very strong assumption but it holds true when the synaptic strength from one population to another remains constant. Another caveat of this derivation is that the microscopic membrane potential and the mesoscopic result of a group of neurones firing together, the synaptic voltage, are essentially considered to be equivalent, which is, at best, a somewhat unjustified assumption.

Conductance-based models of neurones are based on an equivalent electric circuit. The most famous example is Hodgkin and Huxley's model of the giant squid axon (Hodgkin and Huxley, 1952).

Rodrigues et al. (2010) considered two different assumptions when relating a neural mass model and a conductance-based microscopic model. On the one hand, they considered membrane and synaptic temporal scales

as separate, for which two assumptions are needed that are contradicted by experimental evidence: namely, that the synaptic activity varies on a much slower scale than that of the voltage, and that the driving forces are constant for all channels. On the other hand, they considered equal membrane and synaptic temporal scales using Freeman's model (Freeman, 1975), where the precise meaning of the voltage is actually unspecified (which is related to the derivation by Faugeras et al. (2009) already discussed). Additionally, they assumed that intracellular activity is proportional to extracellular activity.

In a more recent work, Zandt et al. (2014) introduce a neural mass model that explicitly includes microscopic dynamics by calculating the population firing rate from the single cell dynamics. This work has the explicit aim of modelling pathophysiology and is therefore brought forth with the intention of corresponding to experimental results. This allows to empirically justify and relax a difficult assumption, namely, that the time scales of fluctuating input currents to a neurone and its instantaneous firing rate are reasonably similar.

It is interesting to note that, as well as the bottom-up approaches hitherto presented—those which derive mesoscopic models of collective behaviour from microscopic descriptions of single cells—, some efforts have been made in the opposite direction, i.e. by attempting to eludidate microscopic characteristics from mesoscopic signals (Hadjipapas et al., 2009). The merit of all these works is undoubtable; however, more experimental work, together with the appropriate theoretical frameworks, are needed to relate scales of brain dynamics and operation on a more solid and undisputable foundation.

3.4 Head model

One of the main contributions of this Thesis is the use of multichannel extracranial data to obtain information about the neuronal populations inside the brain (using data assimilation). To that end, the output of the neural mass models must be transferred outside of the head to resemble EEG signals detected by electrodes on the skull.

This transformation is mediated by a lead field matrix (Mosher et al., 1999), which builds on the basic idea of calculating the electric potential caused by a dipole source (Buzsáki et al., 2012) on a three-layer isotropic hemisphere of radius 1 (Ary et al., 1981; Zhang, 1995) that represents the three main tissues that impact brain activity readings (brain, skull, and scalp). The lead field matrix also contains information about the geometry of the problem (e.g., locations of cortical columns and electrodes) and about the electrophysiology of the head (e.g., conductivities of the different tissues). Please see section A.2 in appendix A for the equations of the head model.

As has already been discussed, the use of dynamical equations to mimic any aspect of brain function is always subject to a compromise between computational feasibility and biological realism. Combining models with experimental data may help in improving the quality and applicability of these efforts. This is made possible by data assimilation, which is discussed in the following chapter.

...since all our measurements and observations are nothing more than approximations to the truth, the same must be true of all calculations resting upon them, and the highest aim of all computations made concerning concrete phenomena must be to approximate, as nearly as practicable, to the truth.

Carl Friederich Gauss

4

Data assimilation and Kalman filtering

Data assimilation is defined as a technique which combines observed data with the output of a theoretical model to produce the best possible estimate of an evolving dynamical system. It has a long and exciting history that started in the field of the geosciences, specifically in meteorology as an aide for numerical weather prediction. In this field, data assimilation is mostly needed to produce the best possible estimate of the system to set the initial conditions for the weather forecasting model. In contrast, in engineering a data assimilation algorithm is most often used for tracking

and estimating the state of the system in real time. This is an important difference that has shaped the evolution of the techniques in the two different fields. Kalman filtering is perhaps the most widely known data assimilation technique, as its applications span fields so diverse as economics, navigation, climate studies, etc.; so much so that it is widely regarded as one of the greatest advances of the 20th century, and certainly the most important contribution to modern systems and control theory.

4.1 Overview of data assimilation methods

Before the advent of data assimilation algorithms, observations were directly inserted into the model of the system, and the experience and intuition of experts was of paramount importance. Panofsky (1949) is credited with the first objective analysis of a weather map for numerical weather prediction. This was followed by the work of Bergthórsson and Döös (1955) and Cressman (1959), who developed the first method in four-dimensional data assimilation. Specifically, they proposed successive corrections to the dynamical model by weighing the observation according to its influence and its distance to the expectation. Nudging methods (Hoke and Anthes, 1976; Kistler, 1974), also referred to as Newtonian relaxation, appeared two decades later. Nudging is reminiscent to the direct insertion of observations used earlier, and is based on adding a term that "nudges" the dynamics of a model towards the observed values by means of tuning parameters. These two approaches, successive corrections methods and nudging, are mainly of historical interest and almost out of use (Kalnay, 2003).

Four-dimensional data assimilation, or 4DDA, takes time into account as the 4th dimension, in contrast to methods in the 3DDA family.

To be fair, however, it is Gauss (1809) who should be credited for the first recorded attempt at assimilating observed measurements into a dynamical

model, while determining the orbit of Ceres. He stated that the best estimate for the values that characterised the motion of the satellite were those most probable, defining them with the following condition: *"...the most probable value of the unknown quantities will be that in which the sum of the squares of the differences between the actually observed and the computed values multiplied by numbers that measure the degree of precision is a minimum"* (Gauss, 1809). Legendre independently arrived to similar results in 1806, and both their names are associated to the development of what later would be known as least squares estimation.

Most data assimilation techniques currently in use aim to minimise a cost function derived from a multivariate Gaussian distribution, such as

$$J(\mathbf{x}_i) = \frac{1}{2}\left(\mathbf{x}_i - \mathbf{x}_i^f\right)^T \mathbf{P}_i^{-1}\left(\mathbf{x}_i - \mathbf{x}_i^f\right) + \frac{1}{2}\left(\mathbf{y}_i - H(\mathbf{x}_i)\right)^T \mathbf{R}_i^{-1}\left(\mathbf{y}_i - H(\mathbf{x}_i)\right), \quad (4.1)$$

where the first term is related to the distance between the model projection $\mathbf{x}_i^f$—the theoretical knowledge of the system—and the estimate $\mathbf{x}_i$ of the state of the system, and the second term measures the distance between the model projection and the observations $\mathbf{y}_i$. The matrices $\mathbf{P}$ and $\mathbf{R}$ are covariance matrices that measure the error of the estimate and that of the measurement, respectively.

This can be done with a large variety of algorithms, depending on the application and the tradition of the field. However, most fall in two categories, sequential and variational (Lorenc, 1986). Sequential algorithms involve direct algebraic solutions of equation 4.1 (see, e.g., Aldrich (1997) or Kalman (1960)); variational algorithms, in contrast, solve it by a numerical minimisation (Sasaki, 1970).

4.1.1 Sequential algorithms

This group contains some of the techniques that are most used in control and signal engineering, namely optimal interpolation and its variants and derivatives. Optimal interpolation is a minimum variance estimator, first introduced and named by Gandin (1965), although the technique goes back to Kolmogorov et al. (1941) and Wiener (1949). The Kalman filter (Kalman, 1960) was developed in the late 50s and the early 60s by Rudolf Emil Kálmán, whose main contribution was the use of the state space approach to correct Wiener's input-output formulation of the statement and solution of the problem (Kalman, 1960). (Because the Kalman filter is the algorithm of choice for data assimilation in this Thesis, it is discussed in more depth in sections 4.2.3 and 4.2.1, as well as in appendix B.) One of the most relevant differences, compared to optimal interpolation, is that optimal interpolation uses a fixed model error covariance estimate, whereas the Kalman filter uses an evolving model error covariance estimate. The Kalman filter is, in its linear form, the best linear unbiased estimate, provided that the model and observation errors are both zero-mean, and it is one of the best known examples of recursive Bayesian estimation.

Although the Kalman filter is optimal for linear problems, there are many applications that warrant a nonlinear approach. Section 4.2.2 reviews those of the most interest for this Thesis. The engineering community has traditionally favoured the use of sequential algorithms, especially that of Kalman filters—and probably because of Kalman filters—, with the exception of the ensemble Kalman filter (Evensen, 1994), which from its inception belongs mostly in the field of the geosciences.

4.1.2 Variational algorithms

Variational algorithms numerically approximate the solution to equation 4.1 by iteration, thus minimising some measure of the distance to the observations in the presence of a dynamical constraint (Lorenc, 1986). 3D-Var, or 3-dimensional variational assimilation, can be proven to be algebraically equivalent to optimal interpolation, provided the cost function is that in equation 4.1 (Kalnay, 2003; Lorenc, 1986); however, because the methods of solution are different, the results are also different, and 3D-Var is the method of choice in many weather prediction centres because of the improved quality of the numerical forecasts. However, it does have some major drawbacks, perhaps the largest of which is the fact that model errors are assumed to be constant over time, thus ignoring the "error of the day"—when day-to-day variability in the forecast error is approximately as large as the average error. Kalman filtering (above) does update the forecast error covariance with each iteration, but its use is not feasible in large systems due to computational constraints. 4-dimensional variational assimilation, or 4D-Var (Courtier and Talagrand, 1987; Talagrand and Courtier, 1987; Thepaut and Courtier, 1991), considers updates in the forecast error, albeit implicitly; the fourth dimension is time, and the observations are assimilated over a time window (Le Dimet and Talagrand, 1986), and not one at each iteration sequentially, as is done with the previously presented methods. This approach has been very successful, but its implications result in computational costs that are unrealistic for most weather forecasting centres in both its two variants: strong constraint (which assumes the model error is zero) and weak constraint (which accounts for model imperfections).

4.1.3 Particle filters

Particle filters use a set of particles (or samples) to represent the probability density function, rather than using a function over state space; therefore, they are suited to estimating the state of nonlinear dynamic systems. Particle filters represent a whole class of algorithms that have sampling and recursive Bayesian estimation in common; however, what is referred to as the particle filter, also called sequential Monte Carlo filter (SMC filter), is an algorithm proposed by Gordon et al. (1993)—who built on the work of Stewart and McCarty (1992)—to effectively bootstrap a set of samples from the actual distribution in order to approximate the probability density function. The SMC filter can be used in highly nonlinear situations and parallelisation is easy. Furthermore, the estimation error converges to zero as the number of particles drawn approaches infinity (Simon, 2006). One of the major drawbacks of the filter, however, is the computational effort involved in using many particles.

The unscented Kalman filter (UKF) and the ensemble Kalman filter both fall in the category of particle filters, if we take the term in the more generalistic sense. However, one of the main strengths of the UKF is that the particles (known as sigma points) are chosen deterministically, and therefore a fixed and smaller number of them are needed, which lightens the computational load (see section 4.2.2 and Simon (2006)). In the ensemble Kalman filter, the ensembles are the "particles" that condense the statistical information of the state without the need to store first- and second-order moments in what would be unfeasibly large matrices (Fearnhead and Künsch, 2018)

4.1.4 Final remarks

The list of available data assimilation algorithms is very long and includes several variants of the Kalman filter, as well as other approaches, such as H_∞ filters (Khargonekar and Nagpal, 1989). A complete and exhaustive review of these methods is out of the scope of this work. Much research is currently being directed towards developing hybrid methods of the ensemble Kalman filter and the variational methods, to bring together the strengths of both (Lorenc, 2003; Penny, 2017).

Even though these hybrid methods are being developed, they are still used mainly by the climate science community. In the previous paragraphs we have hinted at the wide gulf there exists between the signal processing and control engineering community and the geosciences (Roth et al., 2015), and this is indeed highlighted by the fact, for example, that Kálmán's seminal paper from 1960 isn't even cited in Evensen's first development of the ensemble Kalman filter (Evensen, 1994). Also, the nomenclature in the different fields is different (see table 4.1). However, a better communication between the two disciplines would result in a more fruitful and efficient outcome while choosing between available techniques for a given situation. Especially, we believe that large scale problems in neuroscience would surely benefit from the consideration of variational and ensemble approaches.

As has been mentioned already, the unscented Kalman filter is the algorithm that has been employed for the data assimilation problems in this Thesis. Our choice is defended not only by technical considerations on the superiority of the technique (see section 4.2.2), but also because much of the existent research on which the present work is inspired (Freestone et al., 2011b;

Table 4.1 Concepts in data assimilation and their nomenclature in different fields of application.

Engineering	Geosciences	Definition
A priori estimation	Forecast	Projection through the model of the state at the previous time step
A posteriori estimation	Analysis	Corrected estimate after considering observation
Model	Background	Knowledge of the system independent of observations

Kuhlmann et al., 2016) uses the UKF. This is not to mention that filtering is so far the method of choice for data assimilation in neuroscience (Freestone et al., 2014a; Hamilton et al., 2013, 2014; Li et al., 2016; López-Cuevas et al., 2015; Shan et al., 2015), variational methods having been used very sparsely (Moye and Diekman, 2018).

4.2 The Kalman filter

4.2.1 Description and equations of the Kalman filter

The Kalman filter is essentially an efficient computational solution of the recursive least-squares method—it aims to minimise the mean square error of the estimated values. It considers two basic elements, the state of the system and the measurement thereof, due to the state space formulation of the problem:

$$\mathbf{x_k} = \mathbf{\Phi x_{k-1}} + \mathbf{w_{k-1}} \tag{4.2}$$

$$\mathbf{z_k} = \mathbf{H x_k} + \mathbf{v_k} \tag{4.3}$$

Equation 4.2 describes the state of the system, and equation 4.3 relates the measurement to the state. The state transition $\mathbf{\Phi}$ and the observation $\mathbf{H}$ matrices are assumed to be constant in time. $\mathbf{w}$ and $\mathbf{v}$ are white noise sequences, independent of each other, and assumed to be Gaussian with known covariance.

Note that the Kalman filter does not assume these processes to be Gaussian, but rather, the filter is optimal if they are.

Derivation

The following is one of many derivations of the filter (Sorenson, 1970). It has been chosen for its succintness and proximity to Kalman's conceptualisation of the algorithm. It presents the problem in the state-space approach, and uses the least-squares approach to minimise the error in the estimate.

At any time instant k, the estimate of the signal

$$\mathbf{s_k} = \mathbf{H_k x_k}, \tag{4.4}$$

given the estimated state $\mathbf{\hat{x}_{k|k}}$ (which reads "the state estimate given the state at time k), is expressed as

$$\mathbf{\hat{s}_{k|k}} = \mathbf{H_k \hat{x}_{k|k}}. \tag{4.5}$$

To minimise the mean-square error, the orthogonality principle known as the Wiener-Hopf equation must be satisfied; this states that the error in the estimate must be orthogonal to the measurement data (Sorenson, 1970). Therefore, we write $\mathbf{\hat{x}_{k|k}}$—that is, the estimate of the state $\mathbf{x}$ at the time instant k given the state at the time k—as the linear combination of the predicted estimate and the residual. Then the mean-square estimate is

The Kalman filter is a recursive extension of the Wiener filter to non-stationary stochastic problems.

$$\hat{\mathbf{x}}_{\mathbf{k}|\mathbf{k}} = \mathbf{\Phi}\hat{\mathbf{x}}_{\mathbf{k-1}|\mathbf{k-1}} + \mathbf{K}_{\mathbf{k}}\left[\mathbf{z}_{\mathbf{k}} - \mathbf{H}\mathbf{\Phi}\hat{\mathbf{x}}_{\mathbf{k-1}|\mathbf{k-1}}\right], \tag{4.6}$$

where the second term is the residual.

The matrix $\mathbf{K}$, which is the gain matrix (also known as the Kalman factor), is chosen, to minimise the mean-square error, $\mathrm{E}\left[(\hat{\mathbf{x}}_{\mathbf{k}} - \hat{\mathbf{x}}_{\mathbf{k}|\mathbf{k}})^{\mathrm{T}}(\mathbf{x}_{\mathbf{k}} - \mathbf{x}_{\mathbf{k}|\mathbf{k}})\right]$:

$$\mathbf{K}_{\mathbf{k}} = \mathbf{P}_{\mathbf{k}|\mathbf{k-1}}\mathbf{H}^{\mathbf{T}}\left(\mathbf{H}\mathbf{P}_{\mathbf{k}|\mathbf{k-1}}\mathbf{H}^{\mathbf{T}} + \mathbf{R}\right), \tag{4.7}$$

where $\mathbf{R}$ reflects the measurement error. $\mathbf{P}_{\mathbf{k}|\mathbf{k-1}}$ is the predicted estimate error covariance:

$$\mathbf{P}_{\mathbf{k}|\mathbf{k-1}} = \mathrm{E}\left[\left(\mathbf{x}_{\mathbf{k}} - \hat{\mathbf{x}}_{\mathbf{k}|\mathbf{k-1}}\right)\left(\mathbf{x}_{\mathbf{k}} - \hat{\mathbf{x}}_{\mathbf{k}|\mathbf{k-1}}\right)^{\mathrm{T}}\right] = \mathbf{\Phi}\mathbf{P}_{\mathbf{k-1}|\mathbf{k-1}}\mathbf{\Phi}^{\mathbf{T}} + \mathbf{Q}, \tag{4.8}$$

where $\mathbf{Q}$ is a measure of the model error. Finally, $\mathbf{P}_{\mathbf{k}|\mathbf{k}}$ is the estimate error covariance:

$$\mathbf{P}_{\mathbf{k}|\mathbf{k}} = \mathrm{E}\left[\left(\mathbf{x}_{\mathbf{k}} - \hat{\mathbf{x}}_{\mathbf{k}|\mathbf{k}}\right)\left(\mathbf{x}_{\mathbf{k}} - \hat{\mathbf{x}}_{\mathbf{k}|\mathbf{k}}\right)^{\mathrm{T}}\right] = \mathbf{P}_{\mathbf{k}|\mathbf{k-1}} - \mathbf{K}_{\mathbf{k}}\mathbf{H}\mathbf{P}_{\mathbf{k}|\mathbf{k-1}}. \tag{4.9}$$

The covariance $\mathbf{P}$ satisfies the Riccati equation, which has important implications as to the observability and controllability of the system.

Equations 4.6 to 4.9 are essentially the Kalman filter. There are several other ways of obtaining the Kalman filter equations. Another very common derivation uses Bayesian statistics, in which posterior probability is used to determine the most likely cause for a flawed measurement (Barker et al., 1995; Brown and Hwang, 2012); yet another very intuitive approach combines the Gaussian distributions of model output and measurement to reach a better estimate (Faragher, 2012; Maybeck, 1979).

The linear Kalman filter

The following equations 4.10 to 4.14 contain a more usual and practical form of the Kalman filter, commonly used to implement the algorithm. The linear Kalman filter is the base for the other more complex versions, which still share its chief characteristics.

$$\hat{\mathbf{x}}_{\mathbf{k}}^{-} = \mathbf{\Phi}\hat{\mathbf{x}}_{\mathbf{k-1}} \tag{4.10}$$

$$\mathbf{P}_{\mathbf{k}}^{-} = \mathbf{\Phi}\mathbf{P}_{\mathbf{k-1}}\mathbf{\Phi}^{\mathbf{T}} + \mathbf{Q} \tag{4.11}$$

$$\mathbf{K}_{\mathbf{k}} = \mathbf{P}_{\mathbf{k}}^{-}\mathbf{H}^{\mathbf{T}}\left(\mathbf{H}\mathbf{P}_{\mathbf{k}}^{-}\mathbf{H}^{\mathbf{T}} + \mathbf{R}\right)^{-1} \tag{4.12}$$

$$\hat{\mathbf{x}}_{\mathbf{k}} = \hat{\mathbf{x}}_{\mathbf{k}}^{-} + \mathbf{K}_{\mathbf{k}}\left(\mathbf{z}_{\mathbf{k}} - \mathbf{H}\hat{\mathbf{x}}_{\mathbf{k}}^{-}\right) \tag{4.13}$$

$$\mathbf{P}_{\mathbf{k}} = \left(\mathbf{I} - \mathbf{K}_{\mathbf{k}}\mathbf{H}\right)\mathbf{P}_{\mathbf{k}}^{-} \tag{4.14}$$

There are two steps to every iteration (or every time instant k) of the Kalman filter: the *a priori* step, before incorporating the measurement (marked with the superindex $^{-}$), and the *a posteriori* step, which adds the information of the observation. The *a priori* estimate $\hat{\mathbf{x}}_{\mathbf{k}}^{-}$ is calculated by projecting the state at the previous iteration $\hat{\mathbf{x}}_{\mathbf{k-1}}$ through the state transition function $\mathbf{\Phi}$, and therefore merely takes into account the theoretical knowledge of the system (i.e. the model). The *a posteriori* estimate, however, incorporates the measurement $\mathbf{z}_{\mathbf{k}}$ to obtain a corrected final estimate $\hat{\mathbf{x}}_{\mathbf{k}}$ for the current time iteration, by comparing with the estimation of the state projected onto the measurement space, $\mathbf{H}\hat{\mathbf{x}}_{\mathbf{k}}^{-}$. $\mathbf{P}_{\mathbf{k}}$, $\mathbf{Q}$ and $\mathbf{R}$ are estimate, model and measurement covariance error matrices, respectively. The Kalman gain

$\mathbf{K}$, which is key to the performance of the filter, integrates the knowledge about the precision of both model and sensors to weigh the residual $\left(\mathbf{z_k} - \mathbf{H}\hat{\mathbf{x}}_\mathbf{k}^-\right)$.

4.2.2 Nonlinear versions and the unscented Kalman filter

In the very same paper where Kalman presented his filter he recognised the better adequacy of nonlinear filters to certain tasks, but he stated, textually, "*At present, however, little or nothing is known about how to obtain (both theoretically and practically) these nonlinear filters*" (Kalman, 1960). Nevertheless, he probably missed the important work of Stratonovich, who by that time had developed a nonlinear filter deriving partial differential equations for the *a posteriori* probability density function, based on his theory of conditional Markov processes (Stepanov, 2011; Stratonovich, 1959).

When the filter was being used for the first time, it was quickly seen that most of its applications would feature some kind of nonlinearity. The most popular nonlinear version of the Kalman filter is the extended Kalman filter, which was developed at NASA at the centre in which Kalman himself had worked (Smith et al., 1962). The extended Kalman filter linearises about the mean at each time step with a local Taylor expansion, and therefore uses the Jacobian matrix much as one would use the matrix of a linear transfer function. This is the most well known, well researched and widely used nonlinear filter (Julier and Uhlmann, 2004), but it has two important drawbacks: first, the Jacobian matrix must be calculated (if it exists) and hard-coded into the algorithm; second, the first-order approximation at every time step of the nonlinear function often causes the filter to diverge in very little time, as this assumption does not hold well in the presence of severe nonlinearities.

The next most popular nonlinear Kalman filter is probably the unscented Kalman filter (UKF) (Julier and Uhlmann, 2004; van der Merwe and Wan, 2000). This is the filter that has been used in this thesis. The UKF deals with the nonlinearity using the unscented transform (UT), which was invented by Jeffrey Uhlmann, and which is based on the idea that *it is easier to approximate a probability distribution than it is to approximate an arbitrary nonlinear function or transformation* (Uhlmann, 1994). At each time step, therefore, the UKF propagates a set of deterministically chosen points through the nonlinear transformation and recovers the statistical information of the distribution from these (instead of attempting to propagate the statistical information of the distribution directly). Figure 4.1 illustrates the idea behind the propagation of the state through a nonlinearity from different approaches. In the first column, multiple samples are drawn from the distribution to approximate its statistical information. This is the approach used in particle filters (see section 4.1.3). The second column illustrates how, in the extended Kalman filter, the linearisation approach is often insufficient to handle the transmission of information through a nonlinearity. Finally, the third column shows how projecting a set of points through the nonlinearity allows to recover the information with fewer points than particle filters (hence, less computational effort) and more faithfully than the EKF.

The somewhat esoteric term *unscented* has, in reality, a very simple explanation: late one evening, while alone in his lab, Jeffrey Uhlmann saw a men's deodorant on someone's desk and thought it was the perfect absurd, abstract and distant name for his new development (Jeffrey Uhlmann, 2016).

The UKF has been shown to be superior to the extended Kalman filter in several ways. It is more precise, as it captures up to the second-order moment of the state distribution; more stable, as the UT can handle higher nonlinearities; and still computationally efficient, at a computational complexity of $O(L^3)$ (where L is the dimension of the state) (Julier and Uhlmann, 2004;

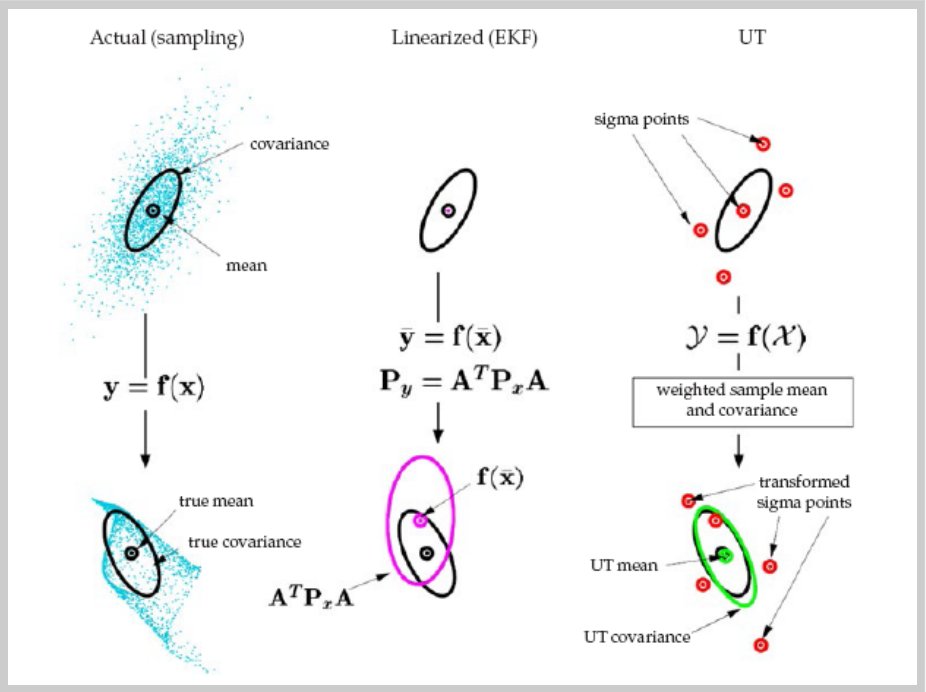

Figure 4.1 The unscented transform and how it compares to the approach of the extended Kalman filter. Reproduced integrally from van der Merwe and Wan (2001).

van der Merwe and Wan, 2000). For a detailed formulation of the UKF, see section B.1 in appendix B.

There are several other nonlinear versions of the Kalman filter that will not be discussed here. For reference, the reader is invited to see van der Merwe and Wan (2001) for the square-root unscented Kalman filter; Arasaratnam and Haykin (2009) for the cubature Kalman filter; and Evensen (1994) and Gillijns et al. (2006) for the ensemble Kalman filter.

4.2.3 Kalman filtering in neuroscience

The application of Kalman filtering to problems in neuroscience is relatively new; it is only recently that efforts have been made to bridge the gap that has traditionally existed between experimental measurements of brain states and characteristics, and theoretical models of the system (Hamilton

et al., 2013, 2014, 2016). However, data assimilation algorithms and their application to neuroscience have met with fair success. The Kalman filter has been used on microscopic problems to estimate neurone membrane dynamics (Moye and Diekman, 2018), with corresponding mathematical contributions to the filtering technique (Lankarany et al., 2014; Rigatos, 2014). At the mesoscopic level, much work has been done integrating experimental recordings into neural mass models (Aram et al., 2015; Freestone et al., 2011a, 2013a,b); this has many clinical applications, such as tracking of brain states in anaesthetised individuals (Bojak and Liley, 2005; Kuhlmann et al., 2016), monitoring (Nguyen et al., 2017) and control (Cao et al., 2015) of epileptic seizures, and estimation of effective brain connectivity during seizures (Freestone et al., 2014b).

Nevertheless, the approach used in these works has one major drawback, and that is the use of highly invasive intracortical data. The problem of inferring brain states from extracranial data, or the inverse problem, goes back long in time and has been researched extensively (Brookes et al., 2008, 2009; Caune et al., 2014; Gotman, 2003; Haufe et al., 2011; Lamus et al., 2012; Lehnertz et al., 2001; Verhellen and Boon, 2007; Whittingstall et al., 2003). The solutions that have been found are greatly useful for adding valuable information and constraints to data assimilation approaches that seek to estimate brain states from exclusively extracranial information. Also, there are theoretical models that translate intracranial signals onto extracranial recordings (this is known as the forward problem) (Mosher et al., 1999; Zhang, 1995), which is fundamental when comparing extracranial and intracranial information.

This work aims to relate extracranial measurements to states and characteristics of the brain, which are obviously intracranial. The possibilities of this approach seem, at present, endless and of enormous importance: among others, developing stimulation devices (Blankertz et al., 2011; Chi and Snyder, 2012; Helbling et al., 2015; Kringelbach et al., 2007; Perlmutter and Mink, 2006; Sadaghiani et al., 2010; Turi et al., 2012; Wagner et al., 2007), contributing to automatic biometric-based user recognition systems (Campisi and Rocca, 2014; Hema et al., 2008), tracking changes in brain dynamics due to aging (Anokhin et al., 1996; Nelson et al., 2010; Yang et al., 2017), monitoring the evolution of disease (Soekadar et al., 2015; Yoo, 2017), tracking the evolution of brain states during motor imagery-control (Zich et al., 2015), task-switching control (Phillips et al., 2014), efficient control of epilepsy (Shan et al., 2016), improving performance in brain-machine interface tasks (Del R. Millán et al., 2008; Kao et al., 2015; Sussillo et al., 2016), detecting and controlling transcranial brain stimulation (Krause et al., 2013), and rehabilitation tasks (Aram et al., 2015; Stephan et al., 2015). These, to name but a few, are all important fields that will be greatly advanced with a successful algorithm that infers brain dynamics from non-invasive recordings.

The introduction to this Thesis has aimed to describe some basic concepts related to brain function, the efforts that have been made to describe it with mathematical models, and how experimental data may be used in conjunction with these to increase our knowledge and to develop novel and important applications. The following part shows some results we have obtained in this direction.

Part II

Results

The brain highlights what it imagines
as patterns; it disregards contradictory
information. Human nature yearns to
see order and hierarchy in the world.
It will invent it where it cannot find it.

Benoît Mandelbrot

5

Matching mesoscopic and microscopic neural dynamics with Kalman filtering

In chapter 3 we have introduced two scales of operation in the brain, microscopic and mesoscopic, and have briefly reviewed the efforts made to relate them to one another (section 3.3). Indeed, the brain operates at multiple temporal and spatial scales, and current experimental techniques show different aspects of cerebral activity in different scales in both the temporal and spatial dimensions. Multi-neurone recordings offer information about both

the temporal and the spatial dimensions, which allows to infer a neurone circuit and the functional connections between its elements (Berényi et al., 2014), with the caveat that recordings at a neuronal scale, which have been studied extensively, do not take higher structures into consideration. Imaging techniques, such as two-photon imaging and functional magnetic resonance imaging, have good spatial resolution (the former at a neuronal level and the latter with brain regions), but have poor temporal precision. This limits their ability to describe the dynamical changes produced at their measuring scale in detail. Finally, measures of neural mass activity, such as EEG or magnetoencephalography, have a high temporal resolution while capturing the averaged activity of large groups of neurones, but lack spatial precision and cannot discern the location of individual neurones and their spike timing (Panzeri et al., 2015). These all allow to discern healthy brain activity from pathological presentations and have been extensively studied and used in both research and clinical settings.

The wide array of available dynamic models of brain activity necessarily reflects the experimental stage (Yuste, 2015). Microscopic models can be very detailed, some to the point of describing compartments in neuronal dentrites (Ermentrout and Terman, 2010), and all focusing on the neurone as the basic computation unit of the brain. However, the diversity of neuronal types and the rich complexity of their connectivity patterns greatly difficult the task of modelling the whole brain at this level, not to mention that it is still not clear how information is encoded within the neurone's action potentials (Dayan and Abbott, 2001; Middleton et al., 2003; Shimokawa et al., 1999; Vargas-Irwin et al., 2010). Several dynamic features such as noise (Mainen and Sejnowski, 1995), excitation and inhibition coupling, and transmission delays have played an essential role in explaining the

variability of synchronisation responses and the stability of different dynamical states in large networks (Hansel and Mato, 2001; Hansel et al., 1995; Roxin et al., 2005). While these features add realism to the dynamics of models, they also pose an additional complicating factor, as they must be properly tuned to reflect the experimentally observed behaviours.

Moreover, attempts at modelling full brain dynamics with networks of individual networks have shown emergent properties that arise from the interactions among anatomical and dynamic processes, such as the sensitivity to changes in individual neurones, the emergence of activity waves, and the functional connectivity on different scales (Izhikevich and Edelman, 2008). This suggests that, in order to model full brain dynamics with neuronal networks, it is necessary to understand how the brain operates at the mesoscopic scale also (Panzeri et al., 2015), and some efforts have been directed this way, by Hagen et al. (2016), for instance.

As well as a better understanding of brain dynamics in the mesoscale, it would also be helpful to improve our understanding of the relationship between the microscopic scale and the mesoscopic. In section 3.3 we have given an overview on the different approaches that have been taken to derive mesoscopic models from microscopic networks, and the simplifications and assumptions that must be made. In this chapter we propose the use of Kalman filtering as a way to bypass these approximations and we study simple situations, in which the standard assumptions are valid, and more complex situations in which they are not.

To this end, we have generated data with a series of microscopic neural networks, first in a trivial situation in which the neurones are uncoupled, and next in more complicated situations where normal derivation of mesoscopic

models fails. We have used the uncoupled configuration to fit the sigmoidal function that relates the average firing rate and the average input synaptic current for each population (see section 5.3). Finally, we have fitted the mesoscopic model to the data generated with the microscopic networks in a variety of interesting situations, and studied the relationship between the output of the two scales.

5.1 Synaptic current

Neurones in the network are coupled with synapses. Even though their dynamical evolution can be very complex, here we work with simplified current-base synapses (Graham et al., 2011):

$$I^{(e,i)}(t) = \sum_{t_s^{(e,i)}} \hat{I}^{(e,i)} \exp\left(-\frac{t - t_s^{(e,i)}}{\tau_{syn}}\right), \tag{5.1}$$

where the action potentials, or spikes, arrive a times $t_s^{(e,i)}$ either from a Poissonianly distributed spike train (Burkitt, 2006) or from the presynaptic neurones coupled to the cell under consideration. The current may be excitatory, $I^e(t)$, or inhibitory, $I^i(t)$. Upon the arrival of a spike, the excitatory current $I^e(t)$ increases by a factor of $\hat{I}^e$, and after that time instant, t_s^e, this contribution to the total current decreases exponentially with a time constant τ_{syn}. This behaviour is analogous in the inhibitory case, except that the current is negative and not positive.

5.2 Mesoscopic model

To model the dynamics of the neurones at a mesoscopic scale, we consider again an excitatory population and an inhibitory population coupled as described in equation 5.1 and following, for the derivation, Faugeras et al. (2009). Taking into account the previous considerations regarding the average firing rate, we arrive to the following equations for the average synaptic input current for the excitatory population I_e and the average synaptic input current for the inhibitory population I_i:

$$\frac{dI_e}{dt} = \frac{-I_e}{\tau_{syn}} + J_{ee}S(I_e) - J_{ei}S(I_i) + J_{e,ext}\lambda_e \tag{5.2}$$

$$\frac{dI_i}{dt} = \frac{-I_i}{\tau_{syn}} + J_{ie}S(I_e) - J_{ii}S(I_i) + J_{i,ext}\lambda_i, \tag{5.3}$$

where the subscripts e and i refer to the excitatory and the inhibitory populations, respectively. The J_{ab} terms are the synaptic weights and λ_x are the external Poissonian firing rates injected to the populations. We consider the shape of the post-synaptic potentials to be identical for both populations (equation 5.1) and described by the time constant τ_{syn}. This set of equations, with the appropriate choice of the coupling constants J_{ab}, may produce oscillatory dynamics. However, the local interaction field may cause the system to become non-Markovian and, to be rigourous, the evolution in time of the microscopic models should be integrated over its complete history. However, the above equations disregard this memory term. We propose that the use of Kalman filtering may account for this loss of information.

5.3 Fitting the sigmoid function

At the microscopic scale, the response of the neurones in the network to the incoming spikes determines the post-synaptic potential (PSP) of the neurones. The resulting input drives the dynamics of the neurone: when the current is large enough, spikes are ellicited whose rate depend on the magnitude of the input current. For instance, the firing rate of an integrate-and-fire neurone is given by

$$f(I) = \frac{1}{\tau_r - \tau_m \ln(1 - \frac{\theta_{IF}}{R_m I})}. \tag{5.4}$$

Zandt et al. (2014) have shown that for a network of active/inactive cells that receive the same input, and whose voltage thresholds follow a Gaussian distribution, the average firing rate of the network can be approximated as a sigmoidal function:

$$S(V) = \frac{f_{max}}{1 + e^{r(V_0 - V)}}. \tag{5.5}$$

As a matter of fact, this behaviour has been often assumed in neural mass models (see, for example, Jansen and Rit's model of a neural mass, page 113). However, the characterisation of the conditions in which the network behaves this way has been addressed in several studies, which put limits to the validity of the approximation (Amit and Tsodyks, 1991; Kilian and Siegelmann, 1996; Roxin et al., 2011).

Indeed, it is not possible to obtain a sigmoidal curve for the average firing rate if the individual f-I curves of each neurone (which show the average

firing rate versus the input current) are anything more complicated than a step function. As this is the case with the integrate-and-fire model, using a sigmoid to approximate the average firing rate is not rigorously correct (Kuhn et al., 2002). However, it is the approach that is commonly used, and in our work, the Kalman filter allows us to overcome this simplification by correcting this wrong information with the rest of the state measured at the mesoscopic scale (that is, the average synaptic current). Figure 5.1, which shows the reasoning made by Zandt et al. (2014), justifies their approximation by fitting a sigmoid curve to a distribution of 5000 Heaviside functions centred around $V_0 = 10$ and with a standard deviation $\sigma = 2$.

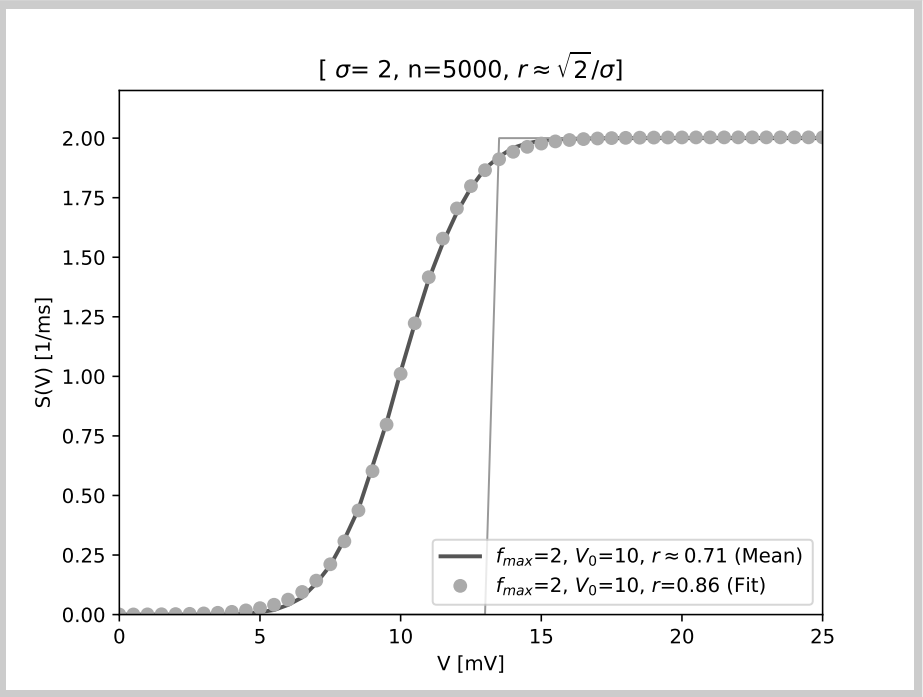

Figure 5.1 Approximation of the sigmoid function made in Zandt et al. (2014). This curve is the result of 5000 step functions of height FR and centred in V_0 with a Gaussian standard deviation σ. The average of these 5000 curves (solid line) is fitted to a sigmoid fuction (grey dots). The approximation of a sigmoid to average the firing rates of the cells in a network is valid only if the firing response of the cells is a step function; however, this is the standard approach in most cases and we aim to address its shortcomings in this work with the UKF.

For our first case, the uncoupled network in a stationary situation, we have fitted a sigmoid with 10 realisations of the network for each value of the average firing rate λ (here, $\lambda_e = \lambda_i = \lambda$). We show the result in figure 5.2.

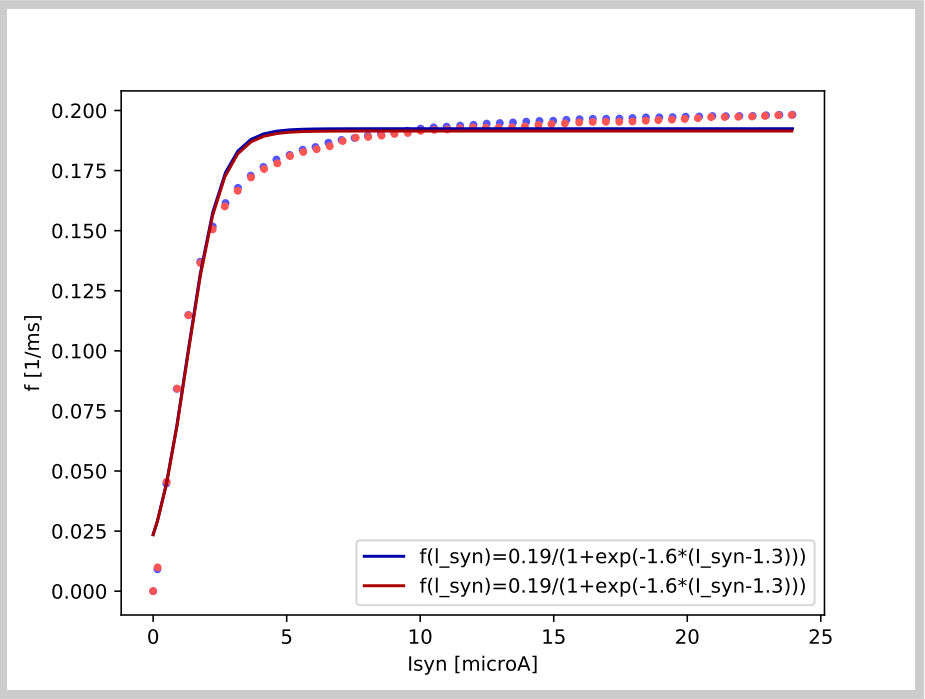

Figure 5.2 Estimated sigmoid function for the uncoupled network.

5.4 Uncoupled network of integrate-and-fire neurones

The first situation considers a simple network of non-interactive neurones, the so-called Freeman's KO sets. This network consists of an excitatory and an inhibitory population. The input to the neurones comes from spikes that follow a Poisson distribution and which cause the synaptic current to increase, followed by an exponential fall. Given the stochasticity of the incoming signal, the current of each neurone is different and somewhat erratic, as seen in figures 5.3 and 5.4. As can be seen in the plots, once the system has reached a stationary state, at around t = 100 ms, we decrease the value of λ_x, upon which change the system evolves towards a new stationary state. The parameters that configure the network are subject

to variability to mimic real-life behaviours more faithfully; their nominal values are shown in table 5.1.

Parameter	Description	Value
τ_m	Membrane time constant	5 ms
R_m	Membrane resistance	25 kΩ
θ_{IF}	Threshold potential	20 mV
E_m	Membrane reset potential	−10 mV
τ_r	Refractory period	5 ms
$\hat{I}^e$	Maximum excitatory current	1 μA
$\hat{I}^i$	Maximum inhibitory current	1 μA
τ_{syn}	Synaptic time scale	5 ms

Table 5.1 Parameters of the uncoupled microscopic neural network. In order to attain the desired variability, the nominal values shown here are multiplied by a factor of (1 + X), where X is a random number that introduces some variability (in percentage). These parameters are used in our simulations unless otherwise specified.

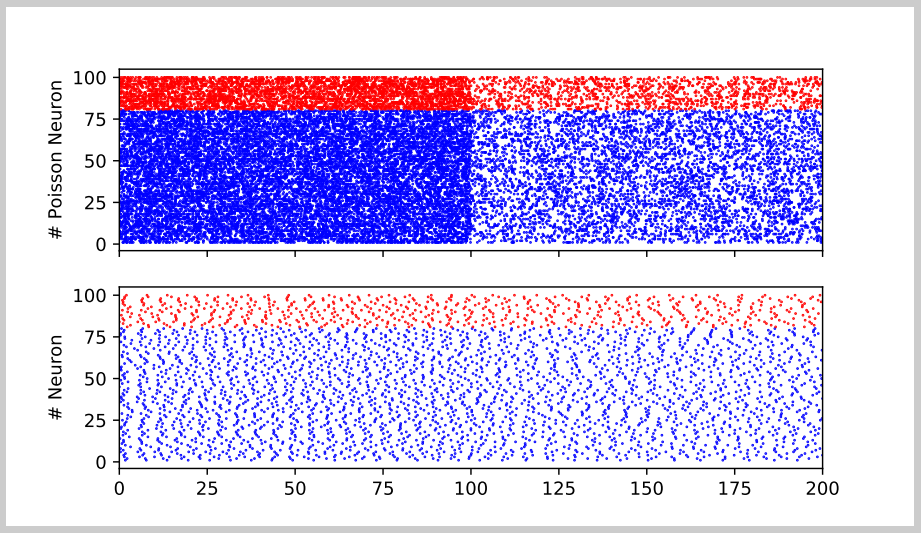

Figure 5.3 Raster plots for the uncoupled network. The above plot shows the Poissonian inputs to the network and below is the firing of the uncoupled network. Here, and hereafter, blue is for the excitatory population and red is for the inhibitory.

In such an uncoupled network, the synaptic responses of the neurones are trivial and are determined exclusively by $J_{x,ext}\lambda_x\tau_{syn}$, the Poissonian external input, and the dynamics of the synapses described in equation 5.1. There is a non-obvious relationship between $J_{x,ext}$ and $\hat{I}^x$ (equation 5.1), mediated by the value of λ_x. There is no presence in the mesoscopic equation

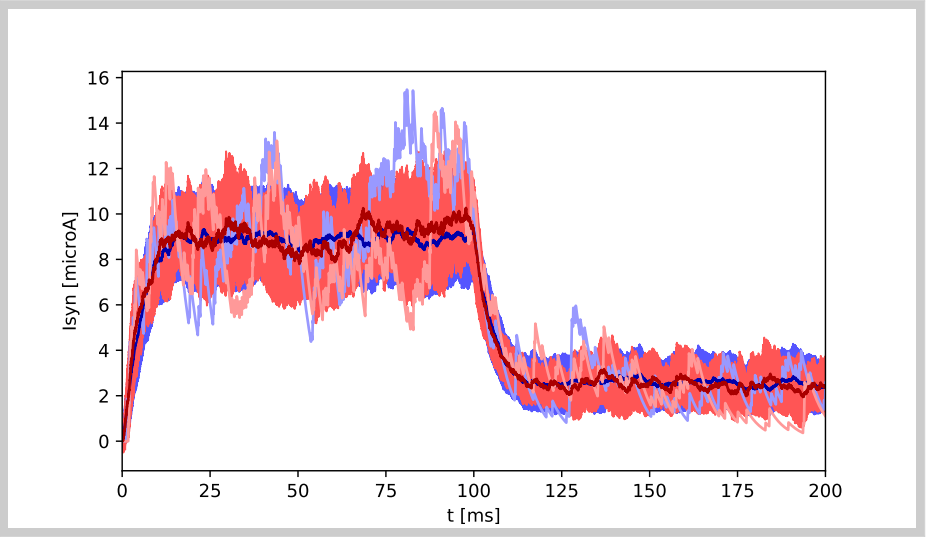

Figure 5.4 Temporal evolution of the synaptic current of the excitatory and inhibitory neurones in the uncoupled network for one realisation in which the excitatory and inhibitory Poissonian firing rates are $\lambda_x = 2\ ms^{-1}$ during the first 100 ms. At $t = 100ms$, they are reduced to $2/3\ ms^{-1}$. The dark solid blue (red) line shows the average synaptic current for all the excitatory (inhibitory) neurones. The shaded blue (red) area shows the standard deviation of the synaptic currents of all the excitatory (inhibitory) neurones in the network. The synaptic current of only one excitatory (inhibitory) neurone is shown in light blue (red) as an example.

of the sigmoidal terms (see equations 5.2 and 5.3); therefore, for any microscopic model that has the same synaptic response to the Poissonian input we will obtain the same dynamics—an uncoupled network will allow us to infer only its synaptic response. However, for each value of the synaptic current we may obtain an average response firing rate (see figure 5.3, below plot). This enables us to characterise the response of the network (i.e. to define its characteristic sigmoid function) by means of the relationship between the values of I_{syn} and the external input to the network, and those of λ_x.

We define $X_x = J_{x,ext}\lambda_x$ (see 5.2 and 5.3). We performed a preliminary fitting with the unscented Kalman filter (UKF) in this uncoupled situation to show how we may obtain information from the network through the mesoscopic model. Firstly, we estimated the terms X_e and X_i of the mesoscopic model by the average synaptic currents shown in figure 5.4. We then used the Rauch-Tung-Striebel smoother on the estimates, wherewith we obtained a smoother version of X_x versus time. With this, we solved equations 5.2

and 5.3 without the sigmoid terms, with which we obtained $I_X(t)$, shown in the following figures 5.5 and 5.6:

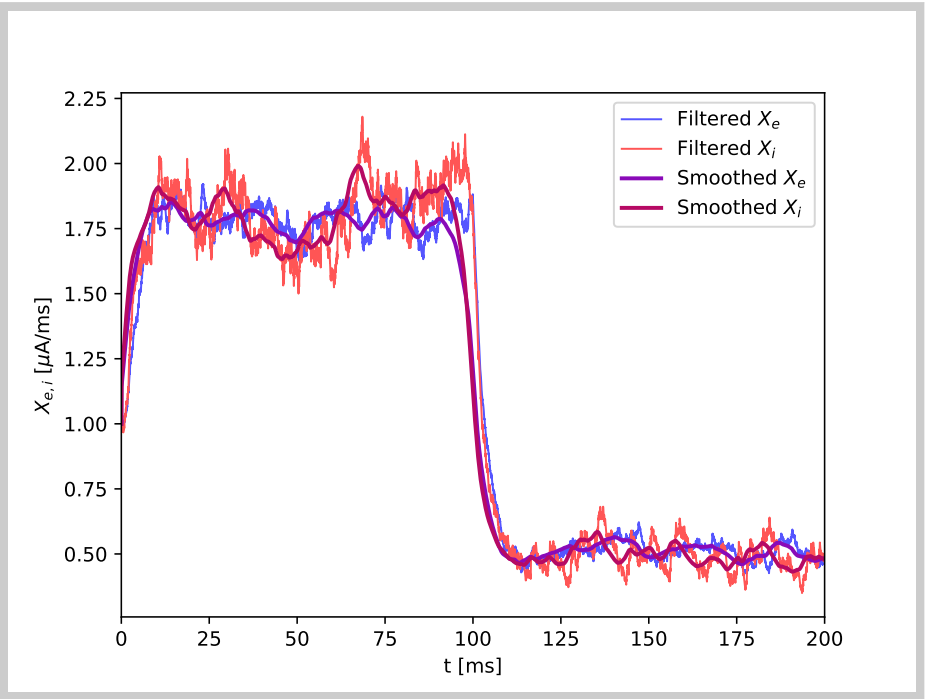

Figure 5.5 Estimated X_X before smoothing (light coloured lines) and after smoothing (dark coloured lines). This is the input to the mesoscopic model.

The pink and purple lines in figure 5.6 are the result of solving equations 5.2 and 5.3 without the sigmoid term and with the values for X_X found with the UKF. The good correspondence between these two magnitudes, which should be the same for a correct mesoscopic model, show the validity of the algorithm in a simple case, which serves as the basis for the more complicated problems that follow.

5.5 Coupled networks

As mentioned previously, the validity of the sigmoidal approximation to the average firing rate of a network has been contended. In the following

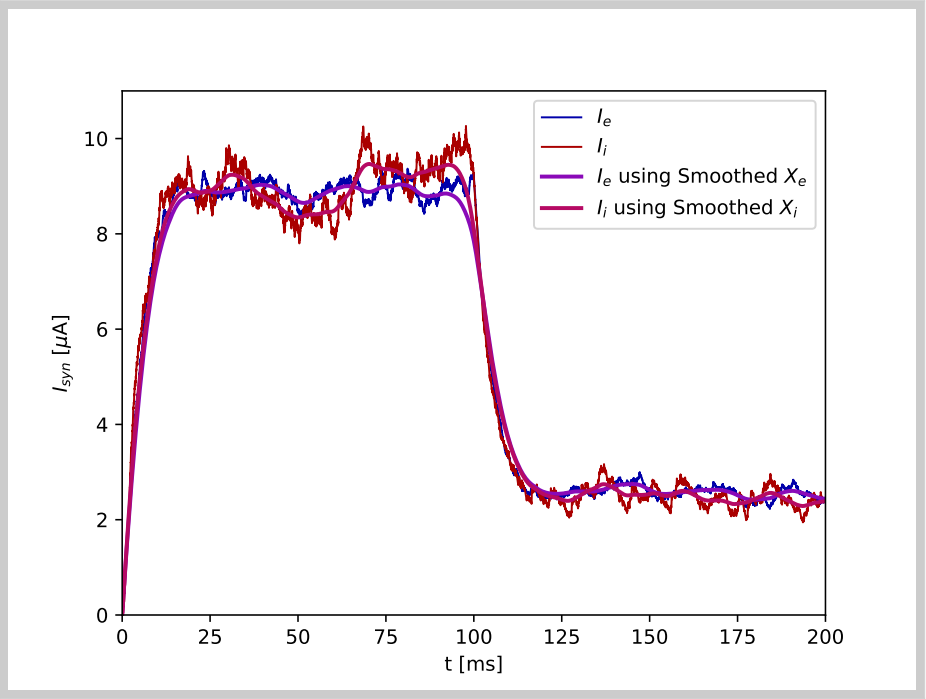

Figure 5.6 Original average synaptic currents of the network (blue and red) and the solution of the mesoscopic model (equations 5.2 and 5.3) for the input, X_x, represented by the dark coloured lines shown in figure 5.5. The good correspondence between the curves show the validity of this process.

sections we address this question using Kalman filtering in more complicated, non-stationary conditions.

5.5.1 Randomly coupled network

In this section we repeat the process we outlined in section 5.4 with a coupled network. In this case, the excitatory population is coupled to the inhibitory in a way that there is a 20% probability that an excitatory neurone will be connected to an inhibitory neurone. The input to the network is a Poissonian spike train with firing rates $\lambda_e = 2/3$ ms^{-1} and $\lambda_i = 2$ ms^{-1}.

For this network, as for the previous one, we fitted the mesoscopic model (equations 5.2 and 5.3) to the output of the network using the UKF. This resulted in a set of estimated parameters for the mesoscopic network. Then,

we used these parameters to simulate the system with the mesoscopic equations and compared the output with the microscopic data.

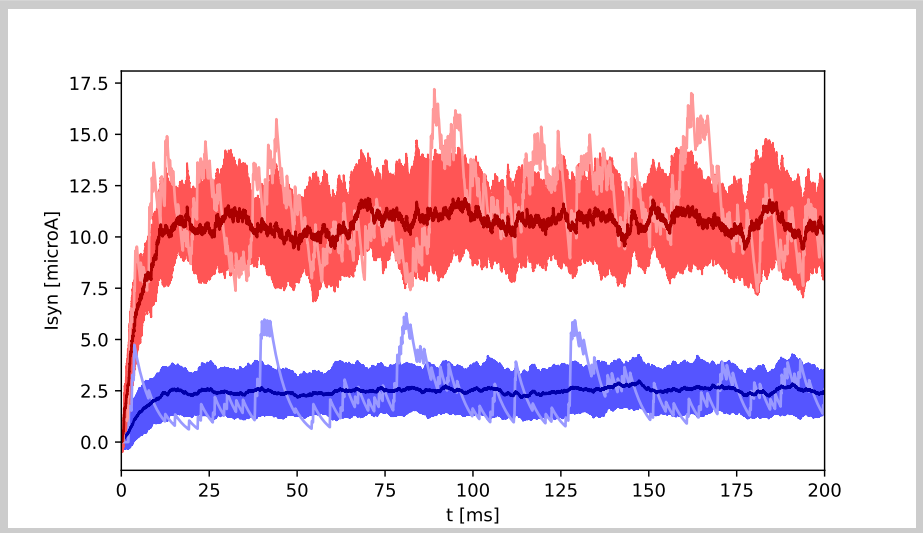

Figure 5.7 Synaptic current of the neurones in the randomly coupled network. The dark solid blue (red) line shows the average synaptic current for all the excitatory (inhibitory) neurones. The shaded blue (red) area shows the standard deviation of the synaptic currents of all the excitatory (inhibitory) neurones in the network. The synaptic current of only one excitatory (inhibitory) neurone is shown in light blue (red) as an example.

Figure 5.7 shows the synaptic currents in the randomly coupled network and the estimated values after filtering. The estimation proves to be accurate even though this network is coupled.

Figure 5.8 shows the estimated X_x terms X_{ei}, which we define as $X_{ei} = J_{ei} f_{max}$ (see equation 5.5). Finally, in figure 5.9 we can see the good correspondence between the output of the microscopic network and the simulation with the mesoscopic equations with the estimated parameters.

The results we have obtained in this section are similar to those in the previous section, in that we have been able to find, with the UKF, a set of parameters for the mesoscopic model that adequately characterise the activity of the microscopic network. However, in this particular case, the relevance of the result is higher. In a coupled network, the presence of local interactions makes the system non-Markovian, which is not taken

Figure 5.8 Estimated X_x and X_{ei} for the randomly coupled network.

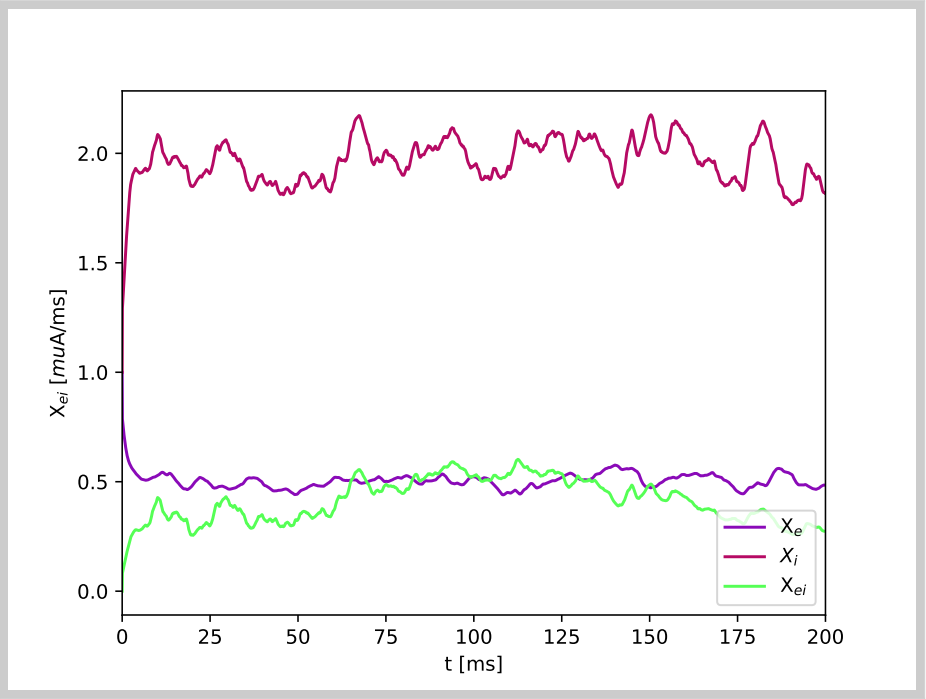

Figure 5.9 Original average synaptic currents of the coupled network (dark blue and red) and the solution of the mesoscopic model represented (light blue and red).

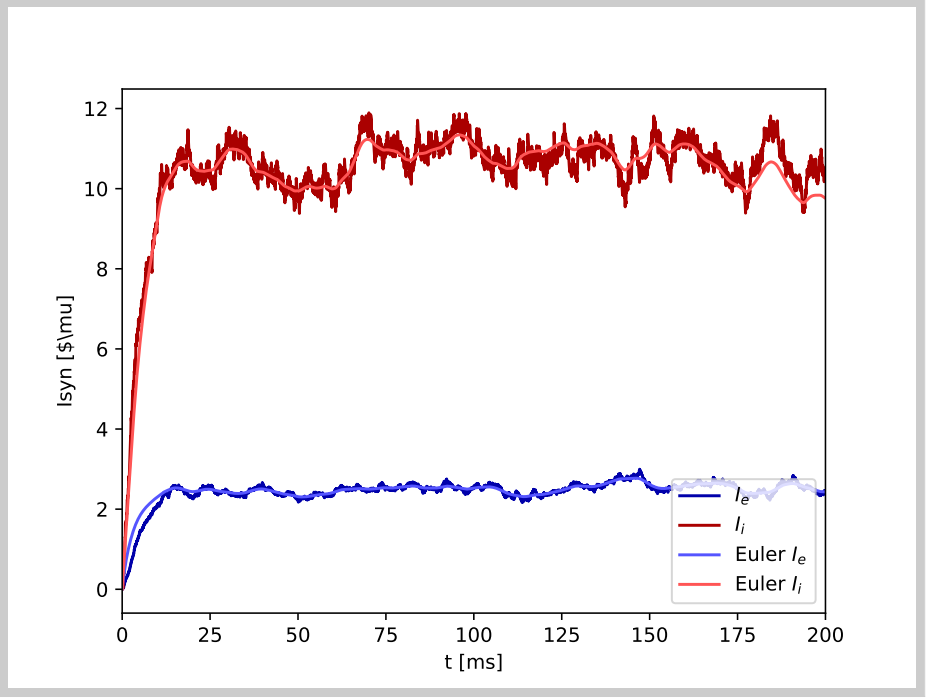

into account in the derivation of the mesoscopic equations. Yet, as we hypothesised in section 5.2, the UKF makes up for this loss of information. Seeing that the resulting set of parameters is able to characterise the model in a way that follows the network so closely, we can see that they encode this additional complexity implicitly.

5.5.2 Coupled network with Lorenzian input

In this new scenario we maintain the same coupling parameters as in the previous network. However, the external input to the network are time traces for the normalised x and y variables of the Lorenz model, shown in figure 5.10. This input has been normalised to fit within a range for which the behaviour of the network is most stochastic.

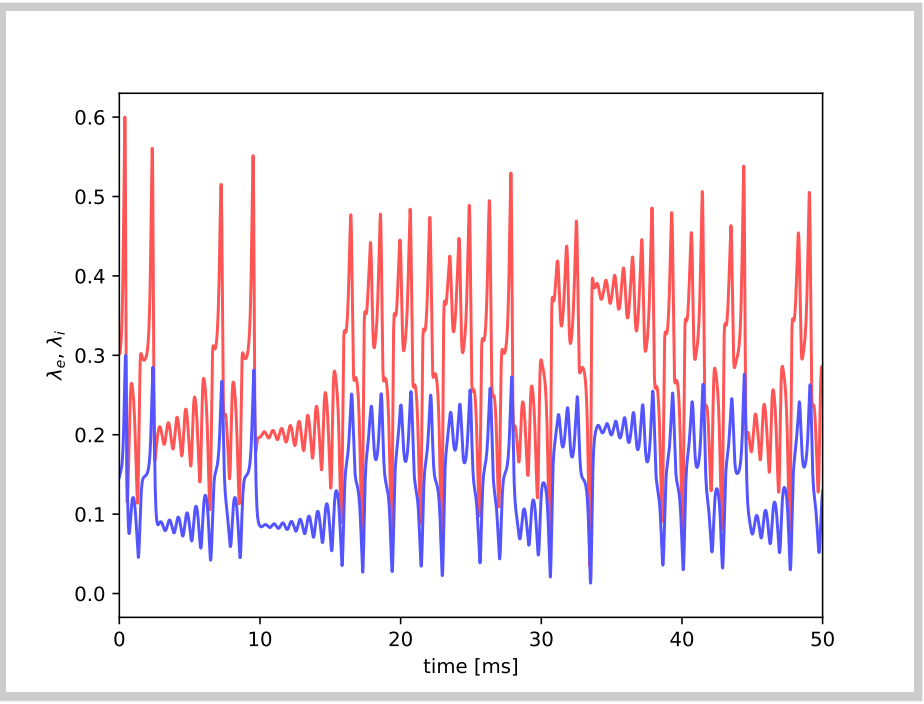

Figure 5.10 Variables of the Lorenz model (x and y) that feed the network. In here they have been scaled to force the network to the maximum possible stochasticity.

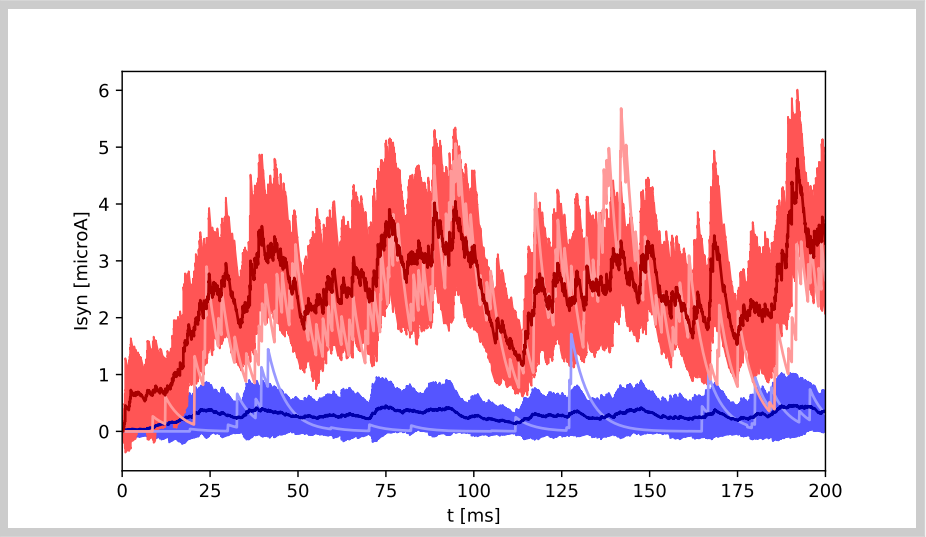

Figure 5.11 Synaptic current of the neurones in the coupled network with Lorenzian input. The dark solid blue (red) line shows the average synaptic current for all the excitatory (inhibitory) neurones. The shaded blue (red) area shows the standard deviation of the synaptic currents of all the excitatory (inhibitory) neurones in the network. The synaptic current of only one excitatory (inhibitory) neurone is shown in light blue (red) as an example.

As in the previous section, figure 5.11 shows the synaptic currents of the network: their variability, their average value, and the current associated to one neurone as an example. The stochasticity in the external input is translated in the form of a highly noisy behaviour of the cells.

Figures 5.12 and 5.13 show the estimates obtained with the UKF. Figure 5.12 shows the X parameters we estimate from the microscopic network—which, as a reminder, are the products of the firing rate and the coupling parameter in each given case. These parameters are then used to forward simulate the mesoscopic system, with the results observed in figure 5.13.

Given the great stochasticity of the system, and bearing in mind the limitations of the analytical derivations of mesoscopic models we have already discussed, it is remarkable that the mesoscopic model is able to reproduce the activity of the network so accurately. Indeed, it is hardly possible that any analytical development be capable of translating the evolution of a network that is excited by chaos modulating a stochastic probability distribution, into a set

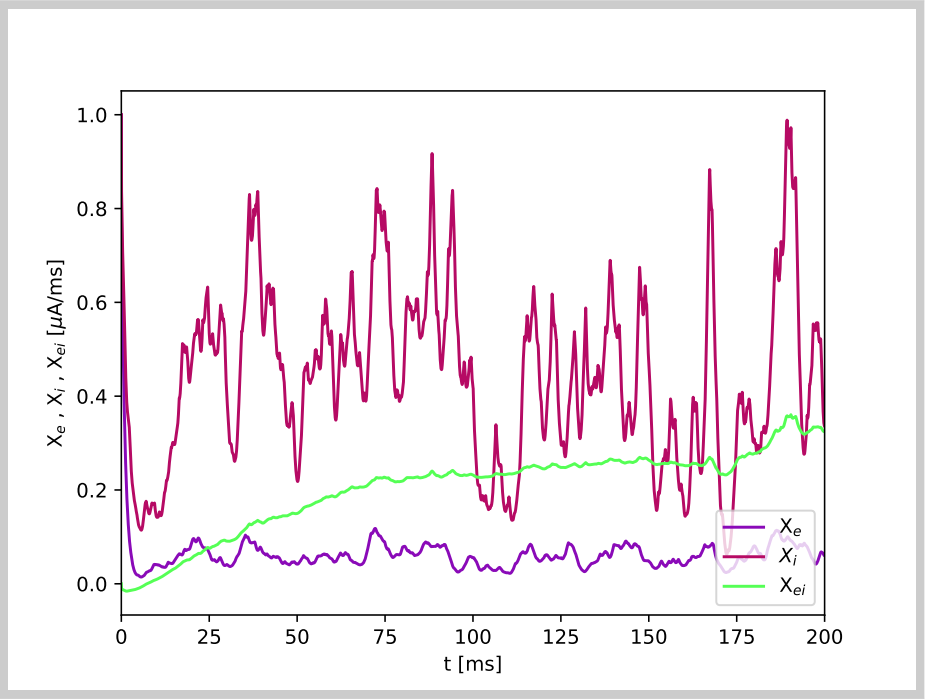

Figure 5.12 Estimated X_x and X_{ei} for the coupled network with Lorenzian input.

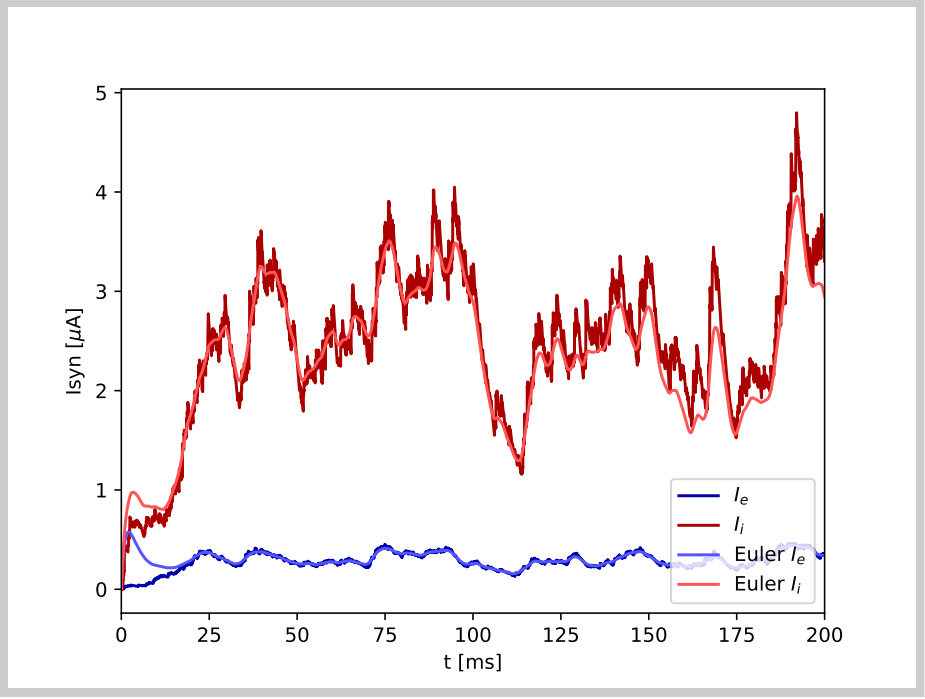

Figure 5.13 Original average synaptic currents of the coupled network with Lorenzian input (dark blue and red) and the solution of the mesoscopic model (light blue and red).

of two simple mesoscopic equations. However, using the UKF we have been able to find a set of parameters that faithfully captures these dynamics to the point of closely reproducing them.

5.5.3 Scale-free network

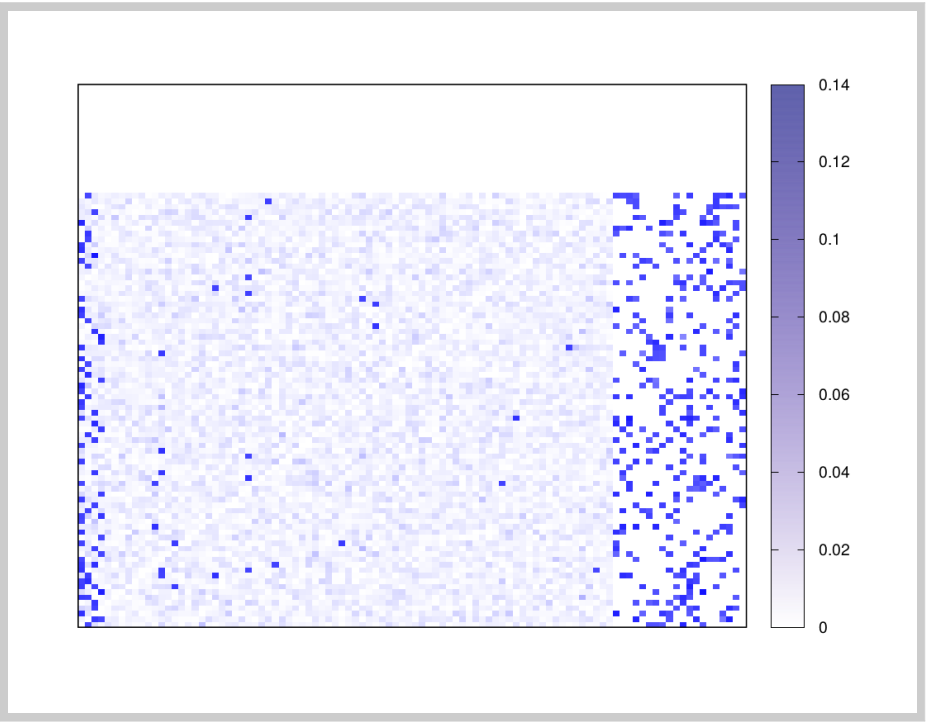

Figure 5.14 Coupling matrix for the scale-free network. The fist 80 cells both to the right and to the top represent the excitatory neurones, which are followed by the 20 cells that represent the inhibitory neurones.

The final situation we consider in this chapter is a scale-free network with a Poissonian input of a spike train with firing rates $\lambda_e = 2/3\ \text{ms}^{-1}$ and $\lambda_i = 2\ \text{ms}^{-1}$. The assumption made by Zandt et al. (2014), that the average firing rate of the network becomes a sigmoidal function for a network of active/inactive cells that receive the same input and whose voltage thresholds follow a Gaussian distribution (see section 5.3), is often used in practice. However, this is providing the coupling of the network follows a uniform and predictable pattern. In this last section we test our algorithm to

see if the results are valid even in this case of hierarchical coupling (whose matrix is shown in figure 5.14).

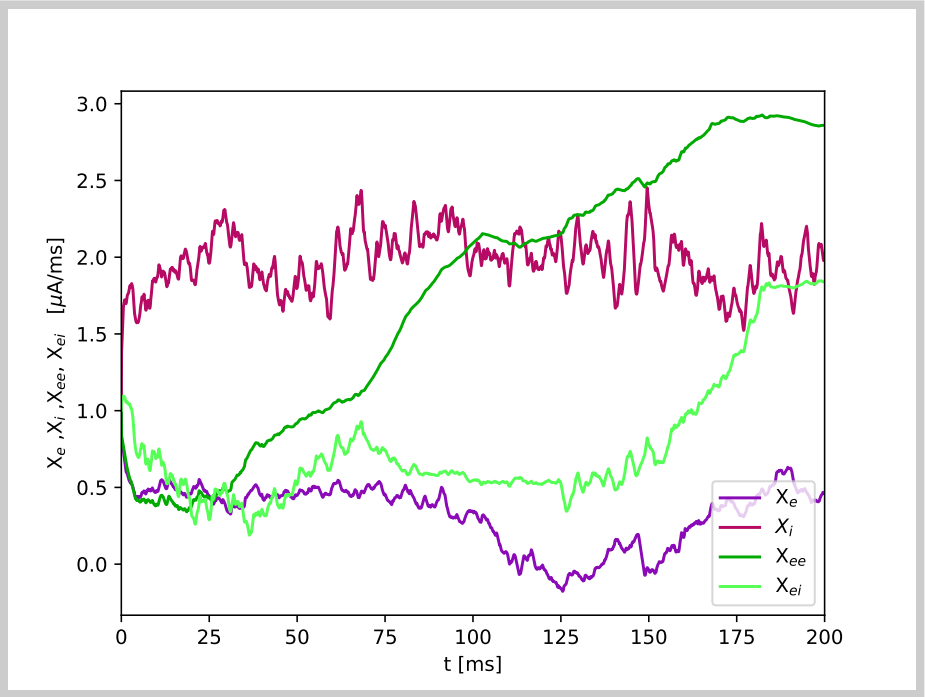

Figure 5.15 Estimated X_x, X_{ee}, and X_{ei} for the scale-free network.

The synaptic currents of the network are not shown here as they are similar to those in the first coupled network (see figure 5.7). However, figures 5.15 and 5.16 are of great interest. Again, these figures show the parameters that have been estimated with the unscented Kalman filter for the mesoscopic equations with data from the microscopic network (figure 5.15), and the forward simulation of the mesoscopic model using these parameters, and how it conforms to the microscopic data (figure 5.15).

These results show that, even in the absence of the conditions in which analytical derivations of mesoscopic models may hold in practice, a set of parameters may be found that allow mesoscopic equations to describe the behaviour of a neural network.

5.6 Conclusions

Taken as a whole, this chapter describes how we have used Kalman filtering to overcome the analytical limitations even in very stochastic dynamics and with non-uniform coupling patterns. Thus we have filled in the inevitable loss of information that is always present in mathematical simplifications when trying to represent the activity of tens (or thousands) of neurones in a single dynamic equation. While we have met with considerable success in this theoretical study, on the other hand it could be thought it is hardly surprising, since the very mesoscopic model we use to fit the data from the network is itself derived from the microscopic network model. Indeed, fitting a mesoscopic model to the activity of a group of real neurones, for instance, is far from being trivial. The following two chapters describe our efforts in this direction.

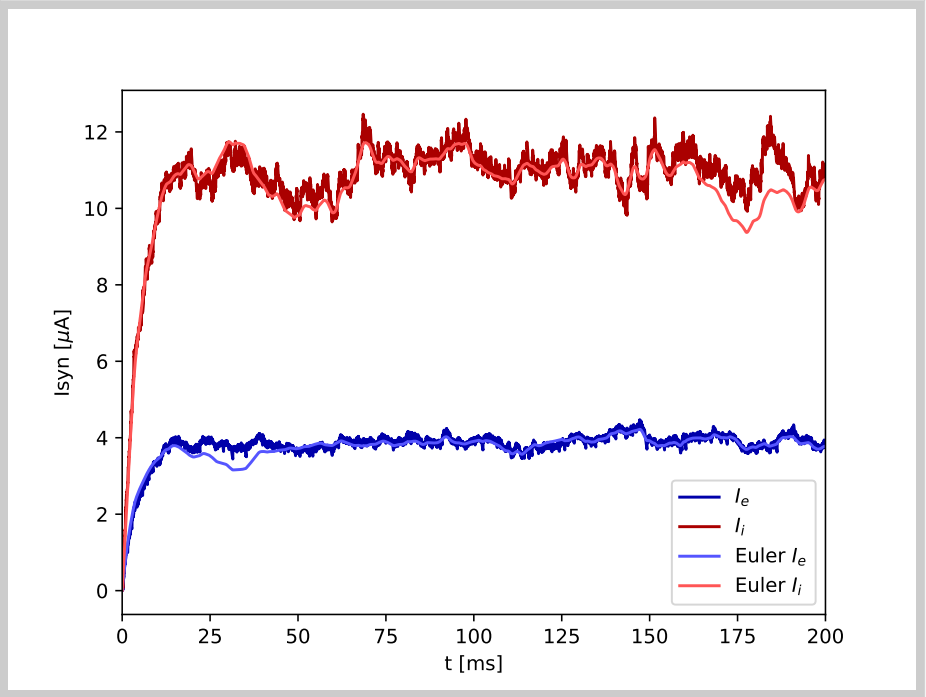

Figure 5.16 Original average synaptic currents of the scale-free network (dark blue and red) and the solution of the mesoscopic model (light blue and red).

There is always much to be said for not attempting more than you can do and for making a certainty of what you try. But this principle, like others in life and war, has its exceptions.

Sir Winston Churchill

6

Extracranial estimation of neural mass model parameters *in silico*

Fitting data with Kalman filtering to neural mass models shows promise in several contexts and applications (Freestone et al., 2011b; Kuhlmann et al., 2016); however, the most important limitation of this approach as of now is that the appropriate experimental recordings are usually intracranial. This chapter describes an attempt at extending

the current methodologies with a head model, thus allowing to compare between the output of neural masses and simulated EEG signals (see figure 6.1).

Even though the quality of the experimental measurements at the scalp might be, in general, worse than the intracranial recordings, an EEG can always be measured from several positions. This allows to obtain measurements for patients without intracranial implants and also to compensate the potentially low quality of the data by having many recordings at the same time. Besides, the spatial distribution of the electrodes on the scalp allows the information arriving from the whole cortex to be available during the assimilation process. In order to address these strengths and weaknesses of the scalp recordings with respect to intracranial measurements, we have analysed situations where assimilation with only intracortical recordings may be wanting. This is the case, for instance, when diverse dynamical regimes coexist due to large differences in control parameters in the cortical columns, or when fine changes of the parameters make the discrimination dificult. While the final goal is to use real experimental data, here we have explored the limitations and advantages of our approach using *in silico* data in very well controlled conditions.

To this end, we have generated three sets of simulated EEG data to explore the capabilities of the unscented Kalman filter with our extended model. While the number of neural masses ant their location are the same in all three analysed situations, the datasets differ in the coupling between them (see figure 6.2 for the different coupling motifs) and the parameters that govern their activity. We use three sources, which provides a considerable spatial and temporal richness in the resulting signals, while keeping the system reasonably simple and still biologically plausible (Cantero et al.,

2009; Richards, 2004). For details on the generation of the data, including the locations of the dipoles and the standard parameters of the model, see appendix A.

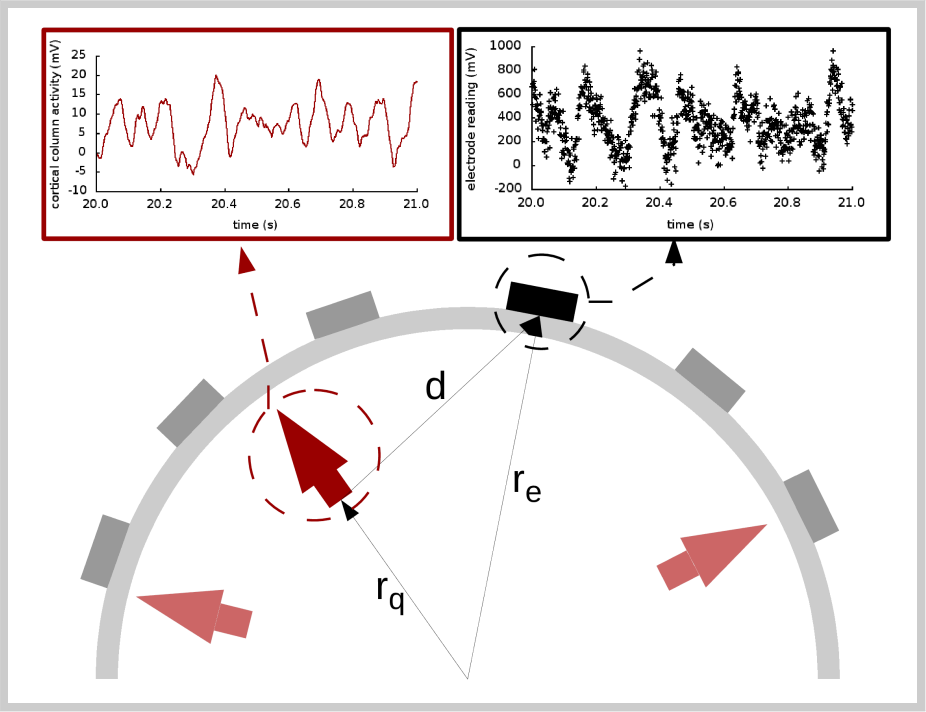

Figure 6.1 Extracranial data generation and illustration of Ary's model of the head. The upper left plot shows the simulated time trace of a cortical column, while the upper right plot shows the *in silico* measurements that would thereby be obtained.

Figure 6.1 provides an illustration of the problem under consideration. The cortical columns (light and dark red arrows) are all driven by a noisy input coming from the rest of the brain and sensory stimuli. The signal from the cortical columns (top left panel) is then transferred to the skull by means of the lead field matrix, after which it is corrupted with Gaussian noise to simulate electrode readings from EEG (top right panel; the electrodes are shown as grey and black rectangles). These are then used to estimate the amplitude of the excitatory post-synaptic potentials—the parameter A in equations A.4 to A.6 (appendix A).

In this drawing, $\mathbf{r_q}$ is the distance from the origin to the cortical column under consideration; $\mathbf{r_e}$ is the distance from the origin to the electrode; and $\mathbf{d}$ is the distance from the cortical column to the electrode (see section A.2 in appendix A). The placement of the arrows here is for illustration purposes only; in our study, the cortical columns are placed on the surface of the brain, close to the skull.

6.1 Three unidirectionally coupled cortical columns

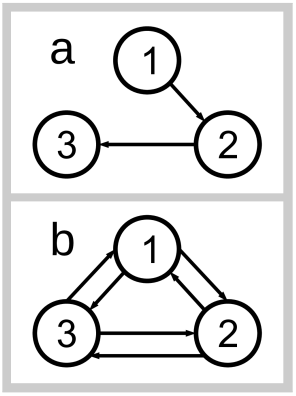

Figure 6.2 The two cortical column motifs used in this chapter. Unidirectionally coupled cortical columns have no backflow, and bidirectionally coupled columns are coupled all-to-all.

For the first study, the cortical columns were coupled unidirectionally (panel (a) of figure 6.2), as described in Liu and Gao (2013). The parameters were set to standard values (Jansen and Rit, 1995) for the three cortical columns, except for the first column, in which A_1 was set to 3.58 mV to bring it into a hyperexcitable regime, in which spikes are driven by the noise present in the system. This first hyperexcitable column causes a spiking cascade in the other two columns. With this study, we aimed to compare how extra- and intracranial electrodes perform in the case of a behaviour being induced by an input from another column, and not by the column's own set of parameters.

The upper panels of figure 6.3 show the intracortical and extracranial estimations of A for the three cortical columns. The solid lines show the averages of the 50 realisations of the estimation, and the shadowed areas indicate the standard deviation. The estimation for A_1 of the first column converges to its correct value, with both the intra- and extracortical approaches.

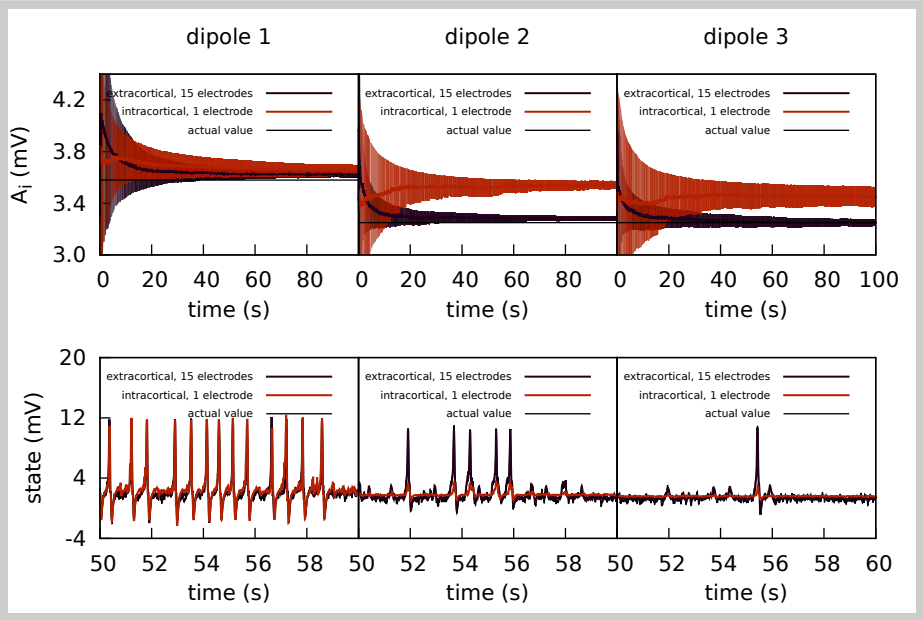

Figure 6.3 Intracranial and extracranial fittings with propagated excitation along unidirectionally coupled cortical columns (panel (a) of figure 6.2).

This was to be expected, since the first cortical column receives no inputs from other elements of the system: information flows unidirectionally because of the way the cortical columns are coupled (Liu and Gao, 2013). In contrast, the intracortical estimations for cortical columns 2 and 3 converge to values significantly higher than their actual value of 3.25 mV. We conjecture that this is caused by the spiking of these two cortical columns, which as mentioned above is due to the influence of cortical column 1. Multi-channel extracranial information, however, allows to see the complete picture of the coupled cortical columns and treat them as a single composed system, contrary to the partial picture obtained from the information provided by the single intracranial recordings.

The lower panels of figure 6.3 show the estimation of the state. The first cortical column has a random spiking activity, due to the increased value of A and the presence of noise (Grimbert and Faugeras, 2006). Because of

the architecture of the coupling, cortical column 1 causes cortical columns 2 and 3 to spike also, when otherwise they would have simply fluctuated around their resting level. With the exception of cortical column 1 (because it has no input from other cortical columns), the filter shows great efficacy when the estimation is extracranial, but performs poorly in the case of intracortical estimation.

6.2 Three bidirectionally coupled cortical columns: coarse parameter estimation

In this second dataset, the three cortical columns are located as in the previous section (Richards, 2004), but coupled bidirectionally (panel (b) of figure 6.2). However, for this study the maximum amplitudes of the excitatory PSPs were set to $A_1 = 4.25$ mV, $A_2 = 10.00$ mV, and $A_3 = 3.25$ mV (the other values being set to standard values). These values were chosen to cause the three cortical columns to be in very different dynamical regimes: cortical column 1 operates in a spiking regime; cortical column 2 oscillates with alpha frequency but with an amplitude similar to that of the spikes; and cortical column 3 oscillates in a more standard regime, as described in Jansen and Rit (1995). Our aim here was to study how the filter performs in an extreme situation, in which the dynamics of the columns are widely different from one another. We intended to explore the outcome of estimating with single extracranial electrodes as well as the complete set, and to compare with intracranial single-channel estimation. To this end, we will add two different noise levels to the data generated by the model.

6.2.1 Moderate intracortical measurement noise

The extracranial data for this study were corrupted with a measurement Gaussian noise of zero mean and standard deviation 100 mV; the intracortical data were corrupted with a measurement noise of standard deviation 5 mV in order to maintain similar levels of signal-to-noise ratio.

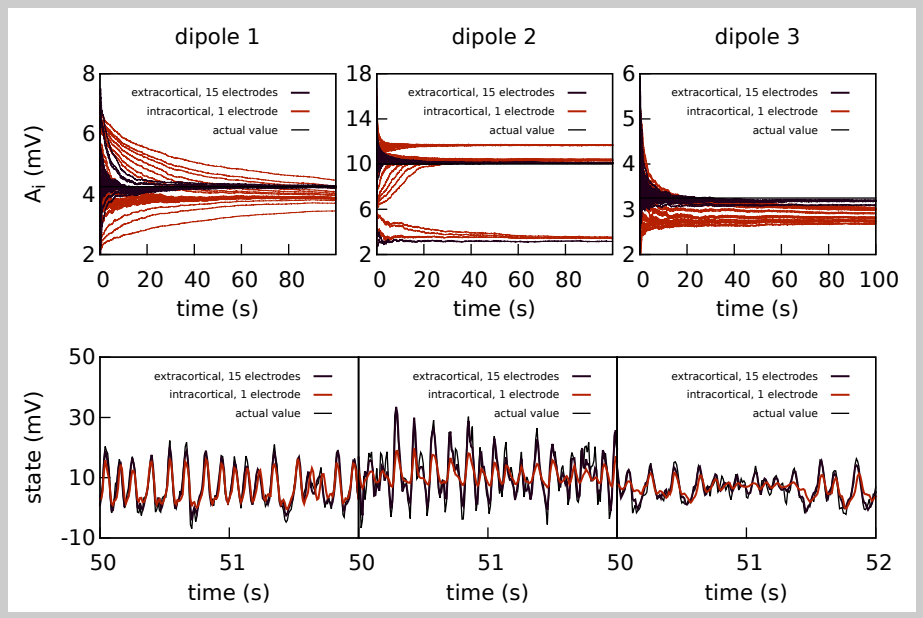

Figure 6.4 Intracranial and extracranial fittings for coarse parameter estimation in the case of bidirectional coupling (panel (b) of figure 6.2).

Figures 6.4 and 6.5 show the performance obtained using the simulated data from a set of extracranial electrodes compared to using individual intracortical electrodes for each cortical column. In this case we show the 50 realisations of each filtering, without showing the average. The upper panels show the estimation of A for each cortical column and the lower panels show the estimations of the observed states. The intracortical parameter estimations do not approximate the target value very well. In particular, the estimations of A for cortical column 2 converge to three different values depending on the initial conditions. The state estimation

follows the actual state of the system closely only for cortical column 1. The situation is very different with extracranial electrodes, where all 50 realisations of the estimations converge with much more precision and speed to the correct values for both state and parameters (with the exception of A_2, which still tends to lower values in a very small quantity of the realisations). Again, extracranial performance is better, in general, than in the intracortical case.

6.2.2 High intracortical measurement noise

Here the amount of noise in the intracortical data was set to the same value as the noise in the extracranial data: the intracortical measurements were corrupted with Gaussian noise of mean 0 and standard deviation 100 mV—about an order of magnitude higher than the noise in the previous study—, while the noise in the extracranial measurements has standard deviation 100 mV.

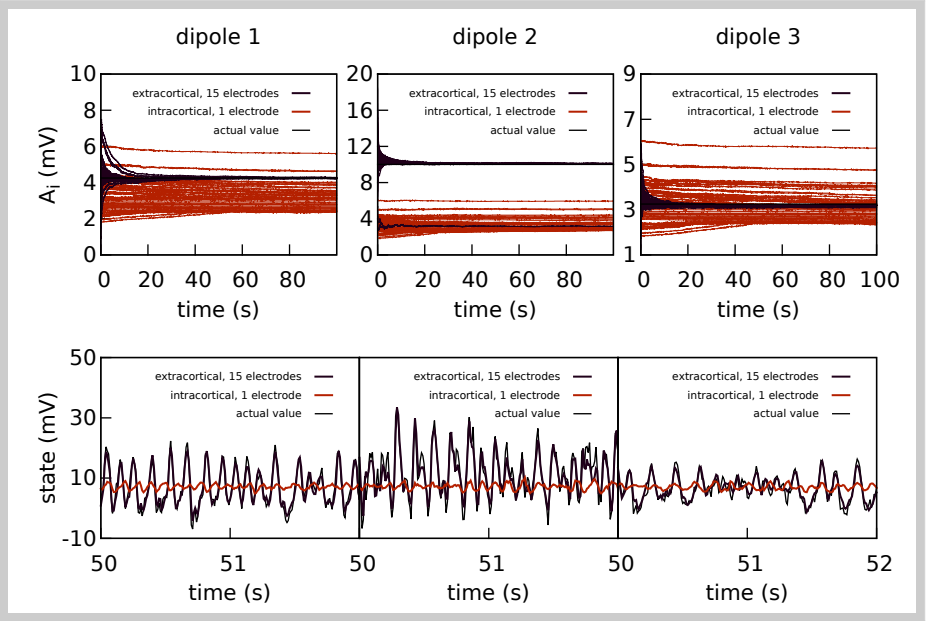

Figure 6.5 Intracranial and extracranial fittings for coarse parameter estimation, with a higher amount of intracortical measurement noise.

The upper panels of figure 6.5 show the estimation of the excitatory post-synaptic potentials for each cortical column and the lower panels show the estimations of the observed states. Extracranial estimations of the parameters are also faster and more accurate than intracortical estimations, more markedly so in this case. As to the state, in this more extreme case, the intracortical estimation does not mimic the evolution of the system in any way even though the value of **R** (the measurement error covariance matrix) was tuned to reflect the increase in measurement noise.

6.2.3 Using one single extracranial electrode

With the same dataset we aimed to investigate the outcome of analysing each extracranial electrode individually (Freestone et al., 2014a), as opposed to using the complete subset as until now. Therefore we studied each electrode separately to estimate the state and parameters of the complete system, with 50 realisations of the estimation for each electrode. By doing so, we show that the quality of the estimations is strongly dependent on the relative positions of sources and electrodes.

In Figs. 6.6 to 6.8 we present the results for the estimation of parameter A of each of the three cortical columns separately. The histograms show the distribution of the 50 estimations of A using each electrode, placed in the respective position of the electrode in question. Vertical coloured lines in the histograms mark the value of the three A parameters being estimated (one in each figure). The histograms show a strong dependence on space of the quality of the estimations. As a general trait, the estimations are better when the electrodes are near the cortical column whose value of A is being

estimated, whereas the more distant electrodes show a wider distribution of final values for the parameter.

In figure 6.6 the distribution of the estimations of A_1 are shown. The distributions tend to be narrowest in the vicinities of the cortical column whose A value is being estimated. However, it is noteworthy that the histograms obtained from the observations in distant electrodes tend to group not around the actual value of $A_1 = 4.25$ mV (red vertical line), but of $A_3 = 3.25$ mV (blue vertical line). This result suggests that the algorithm is unable to distinguish the origin of the EEG activity when sources and electrodes are distant from each other.

Figure 6.7 shows the results of the estimation of $A_2 = 10.00$ mV (actual value shown by vertical green lines), revealing wider distributions in general, which indicates a stronger dependence on initial conditions. Although it is true that the electrodes near cortical column 2 (solid green circle) perform better in estimating A for that column, the difference with more distant electrodes is not as large as for the estimates of A for cortical column 1 and cortical column 3.

Finally, figure 6.8 shows the performance of each electrode when $A_3 = 3.25$ mV is being estimated (actual value shown by vertical blue lines in the figure). Interestingly, even the electrodes located at the far left of the figure lead to a good estimate of A with narrow distributions in the histogram, comparable to that coming from the electrodes in the far right, which are closer to column 3 and could therefore be expected to provide a much more accurate estimation.

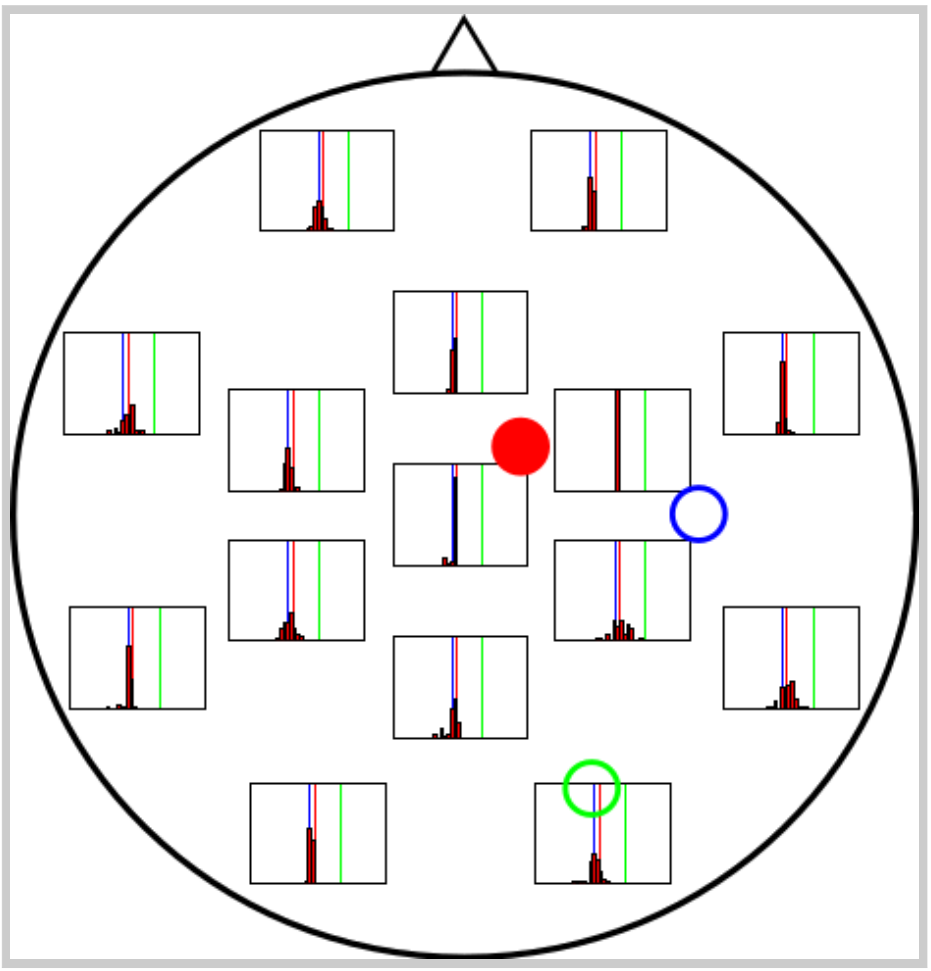

Figure 6.6 Distribution of 50 realisations of A estimations for cortical column 1 (solid red circle) from a single electrode (red bars). The red, green and blue lines correspond to the actual values of A_1, A_2 and A_3, respectively.

While the estimations arising from single electrodes are reasonably accurate in some cases, using the complete set of 15 electrodes invariably yields better results. This is because, in Kalman filtering, combining many sources of information always improves the final estimation, even if some of the sources are inaccurate or incomplete (Schiff, 2012).

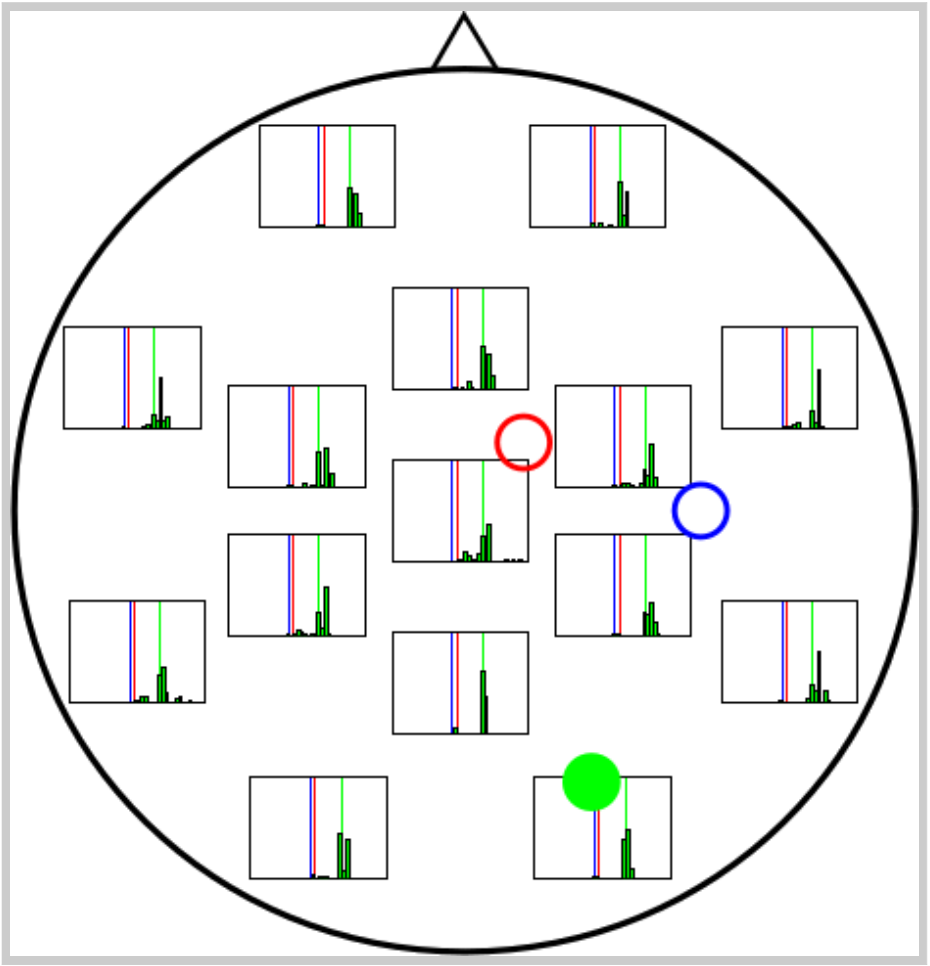

Figure 6.7 Distribution of 50 realisations of A estimations for cortical column 2 (solid green circle) from a single electrode. The red, green and blue lines correspond to the actual values of A_1, A_2 and A_3, respectively.

6.3 Three bidirectionally coupled cortical columns: fine parameter estimation

In the previous section, the value of A of one of the cortical columns was much larger than the other two, as the aim was to generate widely different dynamics in each column. We now consider the same coupling motif, but with values of the A parameter that are much closer together in value: A_1 = 3.58 mV, A_2 = 3.25 mV, and A_3 = 3.10 mV. (The rest of the parameters

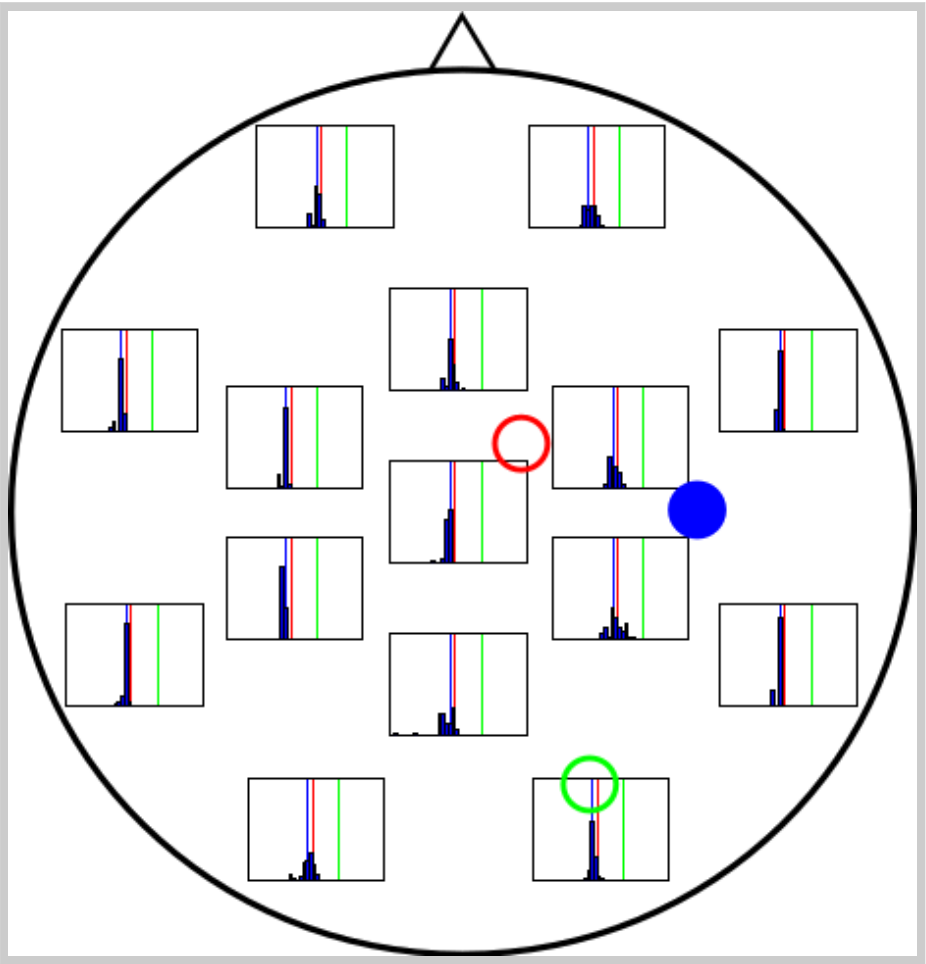

Figure 6.8 Distribution of 50 realisations of A estimations for cortical column 3 (solid blue circle) from a single electrode. The red, green and blue lines correspond to the actual values of A_1, A_2 and A_3, respectively.

were set to standard values (table A.1).) The purpose of this test was to ascertain whether the filter could differentiate between parameters with smaller differences in value—this ability is very important if we expect to use the technique in clinical applications.

As seen in figure 6.9, the estimations of the amplitude of the excitatory post-synaptic potentials of the three cortical columns are shown after averaging over 50 realisations (solid lines); the shadowed areas indicate

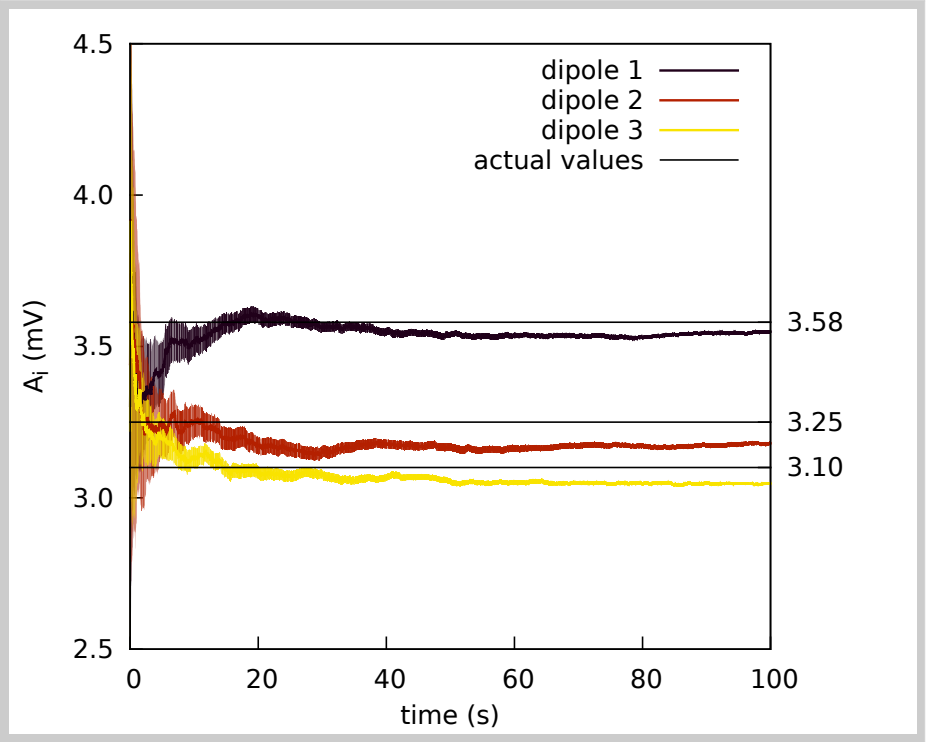

Figure 6.9 Extracranial fit with parameters close together in value.

the standard deviation. The estimation of the parameters is fairly accurate, which gives hope towards employing the technique in clinical scenarios.

6.4 Conclusions

In order to compare the performance of the extra- and intracranial approaches to Kalman filtering, we have analysed three different cortical column configurations, each using one of the two motifs shown in figure 6.2. Where relevant, two different types of estimations have been used: intracranial and extracranial. Intracranial estimation uses simulated data that would have hypothetically been obtained from electrocorticography, that is, using a single intracortical electrode, and is estimated with the data provided by a single location—in other words, the direct output of Jansen and Rit's model. Extracranial

estimation, on the other hand, employs simulated data originated from *in silico* EEG recordings, using several electrodes placed on the skull, and is implemented here with the projection on the head of the model output.

The first study considered here involves three columns that are coupled unidirectionally with no backflow. The first cortical column is made hyperexcitable by increasing the excitatory post-synaptic potential to $A_1 = 3.58$ mV; this cortical column causes the second cortical column and, indirectly, the third, to modify their behaviour by inducing spiking. For the intracranial estimations, single intracortical electrodes measured the evolution of the three cortical columns independently; for the extracranial estimations, 15 extracranial electrodes were used simultaneously. Applying the Kalman filter to the extracranial data provided a good estimation of the A parameters and of the dynamical state of the model; the intracortical measurements, however, yielded mixed results. The estimation for cortical column 1 was accurate, whereas for cortical columns 2 and 3 the estimation of A was above the target value and very close to the estimation for cortical column 1 (see orange dashed lines in figure6.3). The estimation of the dynamical state of cortical columns 2 and 3 was also worse than the estimation for cortical column 1. We attribute this to the fact that columns 2 and 3 are excited by column 1, which spikes due to a higher value of A. As a consequence, when independently evaluated using the intracranial information, the estimation is higher than the actual value. Therefore we suggest that one intracranial electrode provides only a partial view of the system, and thus cannot capture the behaviours of all three cortical columns and the interactions between them; the use of many electrodes provides a more complete view of the system.

Next we considered a situation in which the dipoles were coupled bidirectionally in an all-to-all configuration. The A parameters were chosen such as to cause different dynamic behaviours in the cortical columns. Three types of fitting via Kalman filtering were performed, using (i) independent intracortical recordings of single cortical columns, (ii) the complete subset of 15 extracranial electrodes, and (iii) single extracranial electrodes. The intracortical data were corrupted with two different levels (medium and high) of measurement noise. For both cases, the multi-electrode extracranial estimation surpasses the intracortical results in both speed of convergence and quality. The difference, however, is more marked in the presence of higher measurement noise in the intracortical recordings.

In all these cases, the representation of the dynamical state of the three cortical columns using the complete set of 15 extracranial electrodes nicely matched the actual dynamical state, contrary to the limited match obtained using single intracranial or extracranial recordings. The results for the single electrodes show a significant influence of space on the quality of the estimations, in the sense that estimations of electrodes close to the source are relatively accurate, and electrodes further away from the source might not allow to discriminate the source of the information correctly, or might completely fail to represent the system.

Finally, we considered the situation of an identical cortical column configuration —in terms of situation and coupling—to the previous one, except for the values of the excitatory post-synaptic potentials of the cortical columns. This dataset was filtered only extracranially, with the purpose of evaluating the filter's ability to discriminate parameter values within narrower ranges. The results in this case were also reasonably good, even though the real

values of the parameter were much closer to one another, which makes data assimilation more challenging.

Even though the results shown here are better when considering extracranial electrodes, the method has, of course, limitations. For instance, the head model introduces new parameters which should be realistic. The use of Jansen's model, while being a very standard choice in the field, is not mandatory and could be substituted by others. There several alternatives to Ary's head model too. The succesful application of the method with different combinations of these models will, for sure, guide researchers to choose which models are more suitable for the theoretical description of the mesoscale in the brain. Even though the exploration of the dynamics for the different neural mass models or of the different head models might be worth exploring in future works, it lays outside of the scope of this work.

Taken as a whole, our results show that, independently of the need to explore more realistic situations, extracranial EEG recordings constitute a good candidate to be used together with neural mass models and Kalman filters, provided the method is extended with a head model. With its management of the noise in the system and the necessary and of the inherent simplifications in neurological models, the Kalman filter is an appropriate tool for tackling the challenges of brain data processing. Applications of the method presented here will certainly appear in the field of brain-machine interface, long-term tracking for early diagnosis of degenerative diseases, or short-term tracking during rehabilitation of traumas and strokes. Using non-invasive techniques in these processes widens the applications of Kalman-based data assimilation methods in neuroscience. However, the succesful application of the method

in each of these fields will require further research. In the next chapter we describe our preliminary efforts to apply this method to real EEG measurements.

The strongest arguments prove nothing so long as the conclusions are not verified by experience. Experimental science is the queen of sciences and the goal of all speculation.

Roger Bacon

7

Data assimilation of extracranial EEG observations into neural mass models

In the previous chapter we have combined *in silico* data with neural mass models under very well controlled conditions. This was done in order to study the performance of the unscented Kalman filter (UKF) with this type of data and its applicability and potential. However, the ultimate goal in mind is to use the algorithm in real life situations with data from electrophysiological signals. In the following pages we take the results from

chapter 6 a step further to assimilate real EEG data into Jansen and Rit's neural mass model.

7.1 Description of the dataset

We used a publicly available dataset that was collected by a team of investigators from the Children's Hospital Boston and the Massachussetts Institute of Technology (Goldberger et al., 2000; Shoeb, 2009). The dataset consists of EEG recordings from 22 paediatric subjects with intractable seizures; these were obtained after their medication was withdrawn to characterise their seizures and assess their elligibility for surgery. We chose dataset `chb01_03` for our study because it features a seizure towards the end of the segment, after two apparently different dynamic regimes. This dataset contains 23 signals, one for each of the channels in the International 10-20 System (Malmivuo and Plonsey, 1995) (see figure A.1 on page 120). Figure 7.1 shows the time trace belonging to the first channel, FP1-F7 (chosen arbitrarily), as an illustration of the evolution of the time traces. The signal shows a change in regime from t = 1800 s onwards, followed by a seizure, which occurs between t = 2996 s and t = 3036 s.

7.2 EEG data filtering

For this dataset, a larger number of cortical columns was warranted, given the significant difference in predictibility of experimental data. Therefore, we considered 21 dipole sources in place of the 3 cortical columns described in chapter 6, and located them under the electrodes. The parameter we chose to study was the amplitude of the excitatory post-synaptic potential,

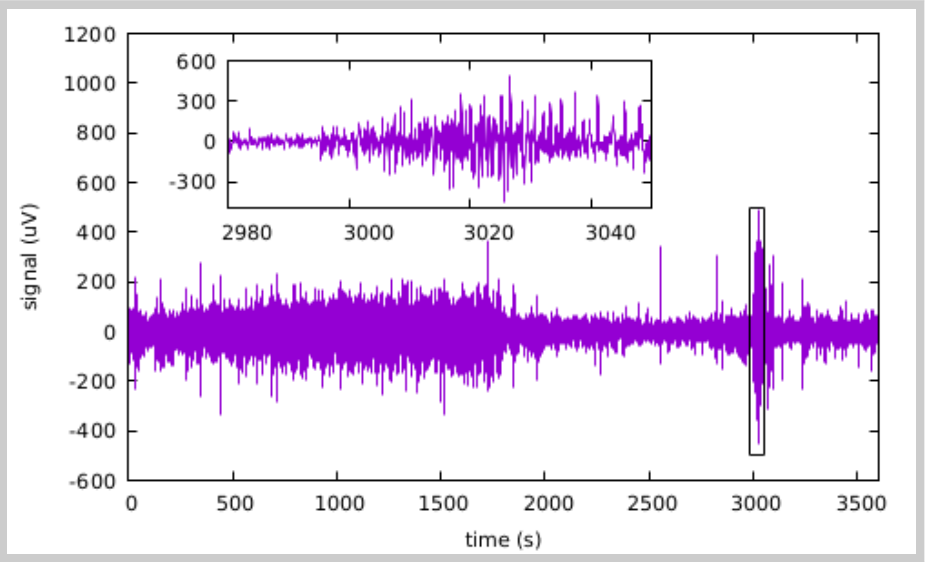

Figure 7.1 Signal from channel FP1-F7. A change in regime can be seen at around t = 1800 s precluding a seizure, which takes place between t = 2996 s and t = 3036 s.

or A (see table A.1 on page 116), following the work presented in the previous chapter. The data were run through the UKF as described in section B.2.2 of appendix B, yielding the estimation presented in figure 7.2.

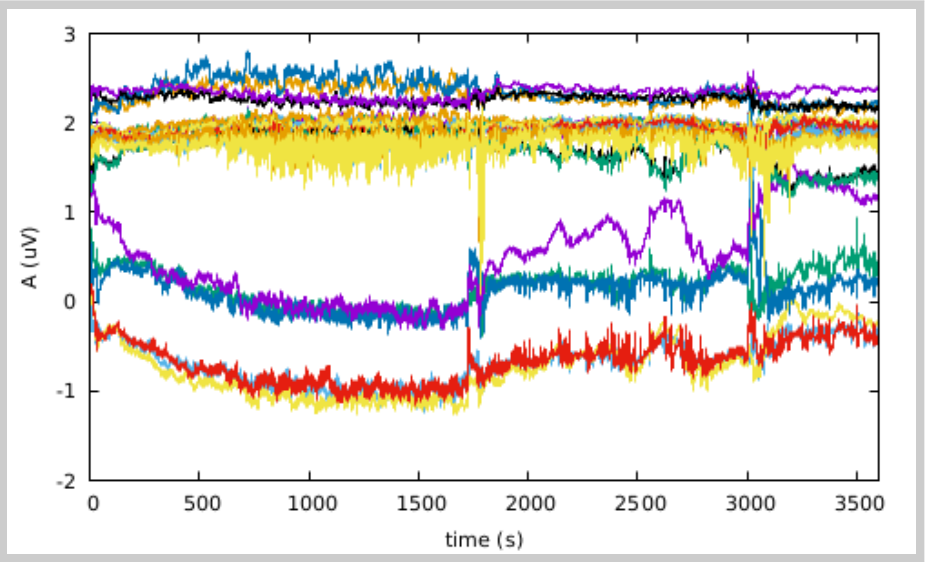

Figure 7.2 Estimations of A, the excitatory post-synaptic potential, for all 21 cortical columns.

The fact that the estimations of the parameters stabilise to a given value after some time, and that they are sensitive to changes in dynamical regimes,

may be considered a success of the UKF at fitting the EEG to Jansen and Rit's model. This is reinforced by the fact that the state estimations are fairly accurate. Figure 7.3 shows the state estimations calculated with the filter and projected onto measurement space, which allows to compare with the data; this good correspondence shows that the estimation is satisfactory.

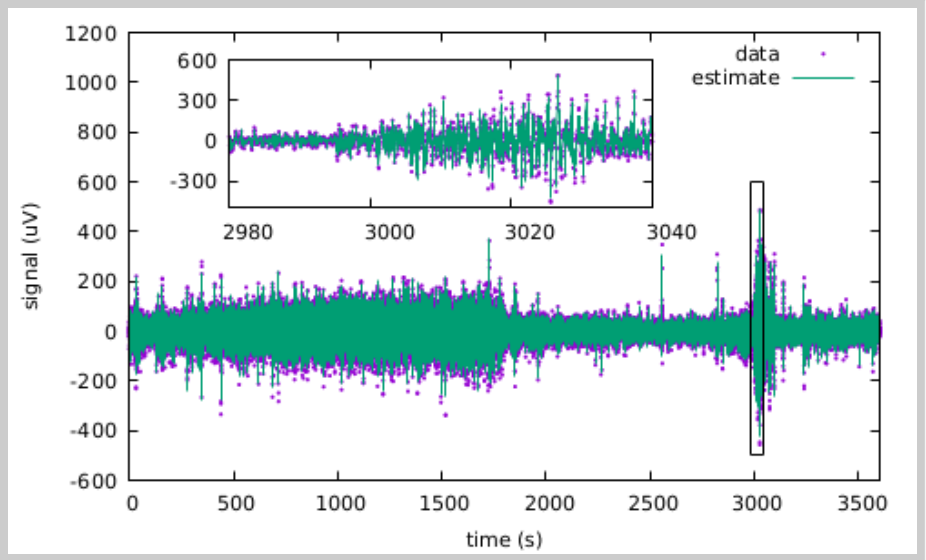

Figure 7.3 Comparison of the projected state estimate and the experimental data. The close correspondence is an indicator of good filter performance.

A striking feature can be observed in figure 7.2, and that is that several of the parameter estimations group together and stabilise to similar values. Figure 7.4 shows the locations of the cortical columns that are responsible for this behaviour. The most distinct groups are colour-coded, and the cortical columns whose parameters fall in a certain group have been coloured accordingly. We use an image of the electrode layout because for this study we placed a cortical column under each of the electrodes for the forward modelling in the filter (see section B.2.2).

The figure shows a surprising symmetry in the positions of the cortical columns whose parameters stabilise at similar values. This may be due

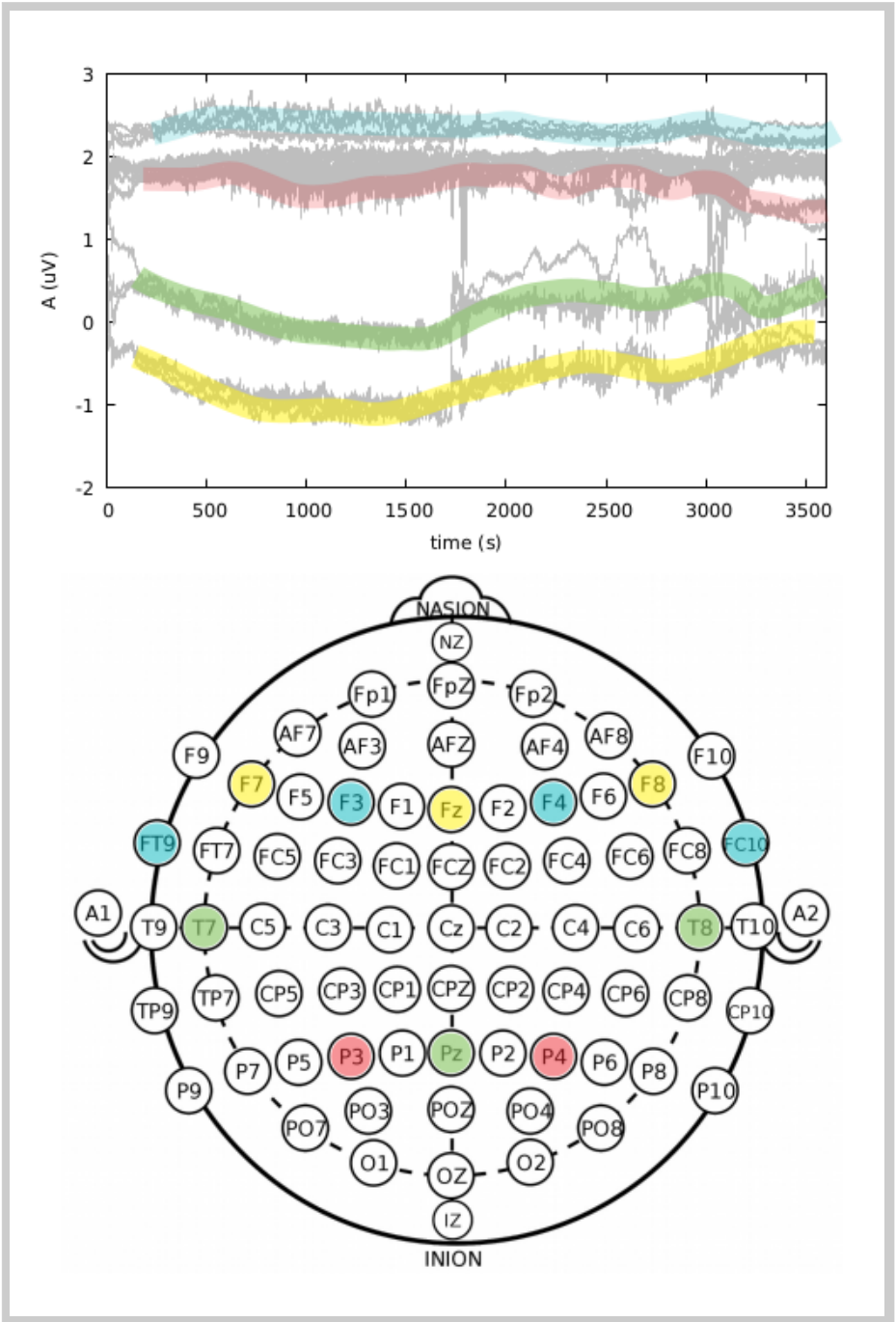

Figure 7.4 Locations of the cortical columns whose parameter A falls into the most distinct groups, colour-coded according to the group to which the parameter belongs. A striking symmetry is observed.

in part to the symmetric disposition of the cortical columns. Surprisingly, however, the fact that cortical columns are in the same scalp region doesn't result in parameters with similar estimated values, but quite the opposite (see, for instance, the blue and yellow groups). There is also the possibility of this being an artifact.

Unoubtedly, much remains to be done in this direction, as these are only very preliminary results. However, the possibility of using real EEG data in combination with neural mass models opens the door to multiple applications —mostly in medical technology—and exciting new lines of research.

Part III

Conclusions

"The time has come," the Walrus said,
"To talk of many things:
Of shoes—and ships—and sealing-wax—
Of cabbages—and kings—
And why the sea is boiling hot—
And whether pigs have wings."

Lewis Carroll

8

Discussion

The human brain is a wondrously complex structure that is responsible for enabling us to operate at many levels. Mathematical modelling has a long and rich trajectory as an aid to understanding brain structure and its related function, and undoubtedly this history is thickly dotted with successes; however, it is also faced with the intrinsical challenges involved in attempting to describe any aspect of reality with mathematical equations, and especially one so fraught with unknowns as the brain.

Indeed, the brain has hitherto resisted absolute reduction and quantification at all scales. Precise knowledge of the function and components of nervous cells has yielded single neurone models such as the integrate-and-fire model, or the Hodgkin-Huxley model, which have been central to Neuroscience to understand many principles of neural communication. However, the brain is a superior structure that is probably best understood as a network, and we are far from being able to detail the characteristics of all the neural and the so-called auxiliary species (which might be more central than we currently imagine), not to mention their relationships to one another and the emergent behaviours their couplings may bring forth. Indeed, at the present moment the very mechanisms of neural communication haven't been completely elucidated.

However, modern imaging techniques allow us to detect signals in the mesoscopic scale that average over large groupings of neurones, resulting in a mass signal that disregards or lumps together much of the microscopic uncertainty. These mesoscopic signals may also be modelled by means of mathematical equations, where the greatest challenge is the characterisation of the parameters that govern their behaviour. Observations of the brain inevitably lie in the realm of phenomenological measures whose underlying mechanisms may not always be well known.

In this work we have used data assimilation in an attempt to bypass these limitations and, at the same time, bring together the best of two worlds. By fusing mathematical descriptions of brain function with experimental recordings we hope to overcome the limitations of both purely theoretical speculation, on the one hand, and of real-world data in which it may be hard to find a pattern or generalisation, on the other hand.

We have done this by means of two distinct studies: in the first (chapter 5), we have aimed to overcome the existing limitations in bridging two scales of operation in the brain: microscopic (single-cell level) and mesoscopic (cortical columns that are used to describe electrophysiological data). In the second study we have seeked to improve existing neural mass models by assimilating both *in silico* (chapter 6) and *in vivo* (chapter 7) electroencephalography (EEG) observations into them. In both cases we have used the unscented Kalman filter (UKF), a tool that is particularly suited to nonlinear dynamics in complex systems. The following sections discuss the results obtained in the three relevant chapters.

8.1 Matching mesoscopic and microscopic neural dynamics using Kalman filtering

In this first study we aimed to use the UKF to lay bridges between microscopic scales of brain description and mesoscopic equations that describe the averaged behaviour of the whole network. To attain this, we first described the dynamics of an uncoupled microscopic network. These depend solely on the dynamics of the synapses, characterised by exponential functions, and on the external Poissonian spike trains input to the network. Then we used the UKF to feed microscopic data into a mesoscopic model and estimate parameters that govern its activity. We judged the capabilities of the filter to capture information by how well the behaviour of the microscopic neural network was reproduced by the mesoscopic model (using the estimated parameters mentioned).

Secondly, we studied three different situations in which the network is coupled. The first was randomly coupled; it was the simplest case of all three, and the UKF provided a set of parameters that described the system well. The second and third scenarios pushed the algorithm to situations where the common assumptions for the derivation of mesoscopic equations do not hold: feeding the network with very stochastic input from the Lorenz model, and a scale-free coupling that removes all possible uniformity. Even in these situations there is good correspondence between the output of the mesoscopic model and that of the microscopic network.

This shows that the filter is capable of surmounting the obstacles in dynamical situations in which the analytical descriptions proposed so far cannot be considered. However, it must be considered that these results are purely theoretical, and that real-life data complicate matters to an extent not so easily surmountable, even by the Kalman filter.

8.2 Extracranial estimation of neural mass model parameters *in silico*

This goal of this study was to test the possibilities of the filter and the complete algorithm under well controlled conditions. To this end, we generated three sets of data of different dynamical properties and explored how well the filter performed at estimating the state and a targeted parameter.

The first test was for a set of three cortical columns coupled unilaterally, with no backflow. The parameter configuration of the first column only was chosen to display hyperexcitability; the rest were set to the standard configuration. The influence of the first column caused the second and

third columns to spike when they wouldn't have otherwise. The filter was then run on each column individually, mimicking electrocorticography (ECoG), and then on the complete set of columns from the scalp, imitating EEG signals. In the first case, single estimation of the first column yielded good results, but the second and third did not. We hypothesise that the filter performed well for the first column because it received no influence from the rest of the system. Similarly, the poor results for the second and third columns may have been caused by the fact that their behaviour was influenced not by their own parameters, but by other elements in the network not accounted for by the filter. In the second case, the estimation with simulated EEG data gave good results for state and parameter of all the cortical columns. From the previous paragraph it follows that this is probably due to simultaneously taking into account the complete system as a whole, which provides a complete picture of the behaviour of all the elements and the interactions between them.

The second study used three bidirectionally coupled dipoles with different parameter configurations that resulted in very different dynamical behaviours. We used simulated intracortical data for each of the cortical columns (with two different levels of measurement noise), extracranial data with the complete set of electrodes, and then we studied the performance of each electrode independently. As before, extracranial estimation with the complete set of electrodes greatly improves the results of intracranial estimation, especially in the presence of high measurement noise; additionally, the results obtained from using each of the electrodes on its own show a marked influence of space and location on the quality of estimations, in the sense that electrodes close to the source of activity provide a good estimation of

the parameters, whereas those far from the source fail to discriminate the origin of the observed activity, or fail to represent the system altogether.

Lastly, we considered a third situation in which the cortical column configuration was identical to the previous one, except that values of the estimated parameters were within a much narrower range. The filter, however, provided a reasonably good estimation even though the parameters were closer together in value, which makes data assimilation more challenging. This gives hope to the applicability of this algorithm to clinical scenarios, in which it may be useful to discriminate between more similar numerical values.

8.3 Data assimilation of extracranial EEG observations into neural mass models

After testing the performance of the unscented Kalman filter with *in silico* data, the natural continuation was to apply the same algorithm to experimental data. The data we chose feature diverse dynamic regimes, the most notable of which are episodes of epileptic convulsions. The goal here was to obtain a reasonable estimation of the state and of one chosen parameter.

We were able to tune the filter in a way in which we obtained a good fit of the estimation to the data. The parameter estimate stabilises to a given value but is sensitive to changes in regime, varying to correctly adjust. Although these are very preliminary results and warrant further efforts, they are highly promising and their potential applicability spans a wide range of medical and research developments.

Taken as a whole, our work shows that the unscented Kalman filter is of extraordinary value in current open problems in the study of brain dynamics. We have used it with success to bridge gaps and join information from different sources (microscopic/mesoscopic and experimental/theoretical). On the one hand, we have been able to characterise the relationship between neural structures at the microscopic and the mesoscopic scales. Our filtering approaches allow us to bypass common analytical limitations, overcoming the obstacles posed by the loss of information in current derivations of mesoscopic models. On the other hand, we have studied the possibilities of applying the UKFto EEG data and shown that we may also assimilate experimental EEG data to existing mathematical models of the brain. This may enable us to determine the underlying dynamics of observed physiological signals, and at the same time to improve our models with real, patient-specific information. The potential of these enhanced algorithms spans a wide range of brain-related applications, from brain-computer interfaces and other related research to all manner of uses in personalised medicine, including early diagnosing of neurodegenerative diseases, seizure prediction, and monitoring of rehabilitation from trauma and strokes, to name but a few.

One never goes further than when they
do not know where they are going.

Johann Wolfgang von Goethe

9

Perspectives

This Thesis has built upon the foundations laid down in previous efforts involving data assimilation and models of the brain. As the first main contribution, it introduces the use of the unscented Kalman filter to study the interaction between the microscopic and the mesoscopic scales of brain modelling, and to bypass some shortcomings in the analytical derivation of mesoscopic model equations from microscopic neural network models. The other most significant outcome is the assimilation of extracranial, non-invasive experimental data from electroencephalography into neural

mass models that imitate the dynamics of cortical columns. Both efforts aimed to bridge existing gaps between different approaches to the study of the brain and its function. However, they are far from being complete and have opened several interesting possibilities that we would like to explore in the future.

Firstly, we plan to submit the results outlined in chapters 5 for publication. Secondly, another open question that deserves our immediate attention is the preliminary work that has been described in chapter 7. We hope to further explore the database and estimate other meaningful parameters, such as B, the inhibitory post-synaptic potential amplitude, and p, the external input.

The *in silico* study of the capabilities of the UKF would be greatly improved with a makeover of the algorithm. Ary's model of the head, while enabling us to compare the output of Jansen and Rit's model with actual experimental data, is obviously a gross simplification of the physiology and shape of the skull and other tissues. Also, although our choice of Jansen and Rit's model has been justified in the corresponding sections, it is far from being the only suitable model. Subsequent work on the filter will doubtlessly consist of investigating other possibilities for our neural mass model and our model of the head. Also, we hope to improve the speed with which the filter perfoms its calculations; to this end, we will study other alternatives to the UKF and make our code more efficient.

Moreover, we also plan to improve the neural mass model so that it is capable of forward-simulating events observed in clinical EEG, such as phase opposition, for instance. This would make our algorithm more valuable in medical applications. An immediate consequence of the results drawn

from chapter 7 would be to attempt early seizure prediction. Although this has received considerable attention from the machine-learning community, we propose that a model-based algorithm would have its own value and would therefore be worth developing.

Finally, another exciting possibility of estimating parameters from EEG data is source localisation, or the resolution of the inverse problem. This is an ill-posed problem that has attracted much attention for its clinical relevance, and we feel our approach might be a valuable complement to the techniques that already exist. For this application, as for the previous one, collaboration with neurologists and imaging specialists will be essential; we plan to seek such collaborations in the near future as a key step in the further development of our research.

Appendices

A

In silico data generation

A.1 Jansen and Rit's model of a neural mass

The dynamics of each neural mass rely on two different transformations. The first converts the average density of incoming action potentials into an average post-synaptic membrane potential (excitatory or inhibitory). It takes the form of a second-order differential equation for excitatory inputs,

$$\ddot{x}_e(t) + 2a\dot{x}_e(t) + a^2 x_e(t) = Aa\, u_e(t), \tag{A.1}$$

and for inhibitory inputs,

$$\ddot{x}_i(t) + 2b\dot{x}_i(t) + b^2 x_i(t) = Bb\, u_i(t), \tag{A.2}$$

where $u_{e,i}(t)$ and $x_{e,i}(t)$ are the input and output of the transformations, respectively, A and B are the amplitudes of the excitatory and inhibitory post-synaptic potentials, and a and b are the lumped representations of the sums of the reciprocal of the time constant of the passive membrane, and all other spatially distributed delays in the dendritic network.

The second transformation converts the net average membrane potential of the population, v, into an average firing rate, and is described by the following sigmoid function:

$$\mathrm{Sigm}(v) = \frac{2e_0}{1 + e^{r(v_0 - v)}} \tag{A.3}$$

where e_0 is the maximum firing rate of the population, r controls the slope of the sigmoid, and v_0 is the post-synaptic potential for which a 50% firing rate is obtained.

The following equations define Jansen and Rit's model for each cortical column i:

$$\ddot{x}_0^i(t) + 2a\dot{x}_0^i(t) + a^2 x_0^i(t) = Aa\, \mathrm{Sigm}[x_1^i(t) - x_2^i(t)], \tag{A.4}$$

$$\ddot{x}_1^i(t) + 2a\dot{x}_1^i(t) + a^2 x_1^i(t) = Aa \left(p(t) + k \sum_{j=1}^{N_d} K^{ij}\, \mathrm{Sigm}(x_1^j(t - \tau^{ij}) - x_2^j(t - \tau^{ij})) + C_2\, \mathrm{Sigm}[C_1 x_0^i(t)] \right), \tag{A.5}$$

$$\ddot{x}_2^i(t) + 2b\dot{x}_2^i(t) + b^2 x_2^i(t) = Bb\left(C_4\ \mathrm{Sigm}[C_3 x_0^i(t)]\right), \tag{A.6}$$

where C_1 to C_4 are connectivity constants that govern the interactions between populations, p(t) is a noisy external input, and the summation term includes the delayed input from other coupled cortical columns. The connectivity constant k modulates the strength of the coupling, K is the adjacency matrix, and τ^{ij} is the delay with which column i receives the signal of column j. Table A.1 provides the descriptions and values of these parameters.

The presence of additional dipoles in the brain, and its influence on the sources of study, is accounted for in the stochastic external input to the sources (p(t), see equation A.5):

$$p(t) = p_0 + \xi(t), \tag{A.7}$$

where $p_0 = 200\ s^{-1}$ and $\xi(t)$ is Gaussian white noise (Gardiner, 2004) of zero mean and correlation $\langle \xi(t)\xi(t') \rangle = 2\epsilon\delta(t - t')$ (Garcia-Ojalvo and Sancho, 1999). At the extracranial level, the other sources also affect the final EEG signal, as well as the different tissues (brain, skull, scalp, and even hair). This is modelled by adding Gaussian noise with zero mean and standard deviation 100 mV (unless otherwise stated) to the simulated EEG.

Table A.1 Description and default values of the parameters for the system of neural masses. Here, PC refers to pyramidal cells, EI to excitatory interneurones, II to inhibitory interneurones, EPSP to excitatory post-synaptic potential, and IPSP to inhibitory post-synaptic potential.

Par.	Description	Value
A	EPSP amplitude	3.25 mV
B	IPSP amplitude	22.00 mV
a	Rate constant for the excitatory population*	$100\ s^{-1}$
b	Rate constant for the inhibitory population*	$50\ s^{-1}$
C_1	Strength of synaptic connections from PC to EI	135
C_2	Strength of synaptic connections from II to PC	108
C_3	Strength of synaptic connections from PC to II	33.75
C_4	Strength of synaptic connections from EI to PP	33.75
e_0	Maximum firing rate of the population	$2.5\ s^{-1}$
v_0	Mean threshold of the population	6 mV
r	Steepness of the sigmoidal transformation	$0.56\ mV^{-1}$
k	Coupling constant	10
K	Adjacency matrix	$K_{ij} = 1, i \neq j$; $K_{i,j} = 0, i = j$
τ	Delay	Varies with distance (Pons et al., 2010)
p	External input	$200\ s^{-1}$

*Lumped representation of the sum of the reciprocal of the time constant of passive membrane and all other spatially distributed delays.

A.2 Ary's model of the head. Equations

Ary's model of the head reproduces the behaviour of a spherical head comprised by three layers, which correspond to three different tissues (brain, skull, and scalp). The following equations show the potential $V^{e,i}$ on an electrode e, located at $\mathbf{r}_\mathbf{e}^e$ (Jurcak et al., 2007), caused by the dipole $\mathbf{q}^i(t) = x^i(t)\hat{\mathbf{q}}^i$ generated by the cortical column i, located at $\mathbf{r}_\mathbf{q}^i$ and oriented as $\hat{\mathbf{q}}^i$ (where $x^i(t)$ is the output $x_1^i - x_2^i$ of Jansen and Rit's model). In these

equations, $e = 1, \ldots, N_e$, where N_e is the total number of electrodes, and $i = 1, \ldots, N_d$, where N_d is the total number of dipoles.

$$V^{e,i}(\mathbf{r}_\mathbf{e}^e; \mathbf{r}_\mathbf{q}^i, \mathbf{q}^i) \approxeq v^1(\mathbf{r}_\mathbf{e}^e; \mu_1 \mathbf{r}_\mathbf{q}^i, \rho_1 \mathbf{q}^i) + v^2(\mathbf{r}_\mathbf{e}^e; \mu_2 \mathbf{r}_\mathbf{q}^i, \rho_2 \mathbf{q}^i) + v^3(\mathbf{r}_\mathbf{e}^e; \mu_3 \mathbf{r}_\mathbf{q}^i, \rho_3 \mathbf{q}^i), \tag{A.8}$$

$$v^1(\mathbf{r}_\mathbf{e}^e; \mathbf{r}_\mathbf{q}^i, \mathbf{q}^i) = \left((c_1^{e,i,1} - c_2^{e,i,1}(\mathbf{r}_\mathbf{e}^e \cdot \mathbf{r}_\mathbf{q}^i)) \mathbf{r}_\mathbf{q}^i + c_2^{e,i,1} (r_q^i)^2 \mathbf{r}_\mathbf{e}^e \right) \cdot \mathbf{q}^i, \tag{A.9}$$

$$v^2(\mathbf{r}_\mathbf{e}^e; \mathbf{r}_\mathbf{q}^i, \mathbf{q}^i) = \left((c_1^{e,i,2} - c_2^{e,i,2}(\mathbf{r}_\mathbf{e}^e \cdot \mathbf{r}_\mathbf{q}^i)) \mathbf{r}_\mathbf{q}^i + c_2^{e,i,2} (r_q^i)^2 \mathbf{r}_\mathbf{e}^e \right) \cdot \mathbf{q}^i, \tag{A.10}$$

$$v^3(\mathbf{r}_\mathbf{e}^e; \mathbf{r}_\mathbf{q}^i, \mathbf{q}^i) = \left((c_1^{e,i,3} - c_2^{e,i,3}(\mathbf{r}_\mathbf{e}^e \cdot \mathbf{r}_\mathbf{q}^i)) \mathbf{r}_\mathbf{q}^i + c_2^{e,i,3} (r_q^i)^2 \mathbf{r}_\mathbf{e}^e \right) \cdot \mathbf{q}^i. \tag{A.11}$$

In these expressions,

$$\begin{aligned} c_1^{e,i,s} &= \frac{1}{4\pi\sigma^s (r_q^i)^2} \left(2 \frac{\mathbf{d}^{e,i} \cdot \mathbf{r}_\mathbf{q}^i}{(d^{e,i})^3} + \frac{1}{d^{e,i}} - \frac{1}{r_e^e} \right), \\ c_2^{e,i,s} &= \frac{1}{4\pi\sigma^s (r_q^i)^2} \left(\frac{2}{(d^{e,i})^3} + \frac{d^{e,i} + r_e^e}{r_e \Gamma(\mathbf{r}_\mathbf{e}^e, \mathbf{r}_\mathbf{q}^i)} \right), \\ \Gamma(\mathbf{r}_\mathbf{e}^e, \mathbf{r}_\mathbf{q}^i) &= d^{e,i} \left(r_e^e d^{e,i} + (r_e^e)^2 - (\mathbf{r}_\mathbf{q}^i \cdot \mathbf{r}_\mathbf{e}^e) \right). \end{aligned} \tag{A.12}$$

Parameter	Layer 1	Layer 2	Layer 3
Tangential conductivity σ^s	1.0	0.0125	1.0
Berg parameter ρ_s	0.9901	0.7687	0.4421
Berg parameter μ_s	0.0659	0.2389	0.3561

Table A.2 Values of the Berg parameters for the three layers (Ary et al., 1981; Berg and Scherg, 1994).

The tangential conductivity of each layer is represented by σ^s (Ary et al., 1981) and ρ_s and μ_s are the Berg parameters relative to it (Berg and Scherg, 1994) (see table A.2). The parameter $\mathbf{d}^{e,i} = \mathbf{r}_\mathbf{e}^e - \mathbf{r}_\mathbf{q}^i$ is the relative position

of the electrode e under consideration with respect to the position of the dipole i.

A.3 Numerical solver: Heun algorithm

The numerical solver used to generate the *in silico* time series was the Heun algorithm (Toral and Colet, 2014) with a time step of $\Delta t = 1$ ms. The length of the data is 100 s in all cases. Using the Heun algorithm together with Eqs. A.4 to A.6 to update the state variables and the lead field matrix (in order to get the potential in the electrodes of the scalp in Eqs. A.8 to A.12), we generate the required map to apply Kalman filtering in Eqs. 4.2 and 4.3. The following equations implement the stochastic Heun algorithm used to update $\mathbf{x}_k$:

$$\mathbf{x}_{k+1} = \mathbf{x}_k + \frac{1}{2}\left(\mathbf{F}\left(\mathbf{x}_k\right) + \mathbf{F}\left(\tilde{\mathbf{x}}_k\right)\right)\Delta t + \frac{1}{2}\sum\left(g\left(\mathbf{x}_k\right) + g\left(\tilde{\mathbf{x}}_k\right)\right)X_k, \tag{A.13}$$

$$\tilde{\mathbf{x}}_k = \mathbf{x}_k + \mathbf{F}\left(\mathbf{x}_k\right)\Delta t + g\left(\mathbf{x}_k\right)X_k. \tag{A.14}$$

Where g(...), together with equation A.7, introduces the noise term in equation A.5 and is zero for Eqs. A.4 and A.6. In $X_k = \sqrt{2\epsilon\Delta t}\gamma$, γ are gaussianly distributed random numbers with zero mean and unit variance. At different instants of time, these random numbers are independent from one another.

A.4 Data generation and design of the experiments in chapter 6

Here we describe the generation of the data for chapter 6 and the design of the study. Three different *in silico* datasets were generated, using Jansen and Rit's neural mass model (section A.1). We simulated both electrocorticography

(, intracortical) and electroencephalography (EEG, extracranial) readings, using Ary's model (section A.2) additionally in the latter case. The series were generated numerically using Heun's algorithm (section A.3).

All datasets used the same locations for the cortical columns (Richards, 2004), as seen in table A.3. The electrodes were placed using a subset of the equidistant layout, a standard layout for EEG (Easycap, 2018) illustrated in figure A.1. The strength of the coupling was set at a medium value so that the cortical columns have a visible effect on one another without fully synchronising behaviours and locking their dynamics (between $k = 5$ and $k = 10$), and the configurations of the couplings are as shown in figure 6.2. Table A.1 shows representative values for the parameters used in all analyses unless otherwise specified. We focus on estimating the amplitudes A of the EPSPs of the different cortical columns, and therefore we choose values for these amplitudes that produce signals that reflect various dynamic regimes that we wish to explore. (The rest of the parameters were fixed to their standard values (Jansen and Rit, 1995; Jansen et al., 1993), as described in table A.1.)

	x	y	z
dipole 1	0.1688	0.2242	0.2597
dipole 2	0.3766	-0.8520	0.2597
dipole 3	0.6622	-0.2242	-0.1948

Table A.3 Cartesian coordinates of the dipoles used throughout the study. The origin of coordinates is the centre of the perimeter of the head.

A.4.1 Three unidirectionally coupled cortical columns

For the first study, the cortical columns were coupled unidirectionally (panel (a) of figure 6.2), as described in Liu and Gao (2013). The parameters were set to standard values Jansen and Rit (1995) for the three cortical

columns, $A_2 = A_3 = 3.25$ mV, except for the first column, in which A_1 was set to 3.58 mV to make it hyperexcitable. Additionally, the three cortical colums had $p_0 = 90\ s^{-1}$ and $\epsilon = 2\ s^{-1}$. The coupling constant was set to the value of $k = 10$.

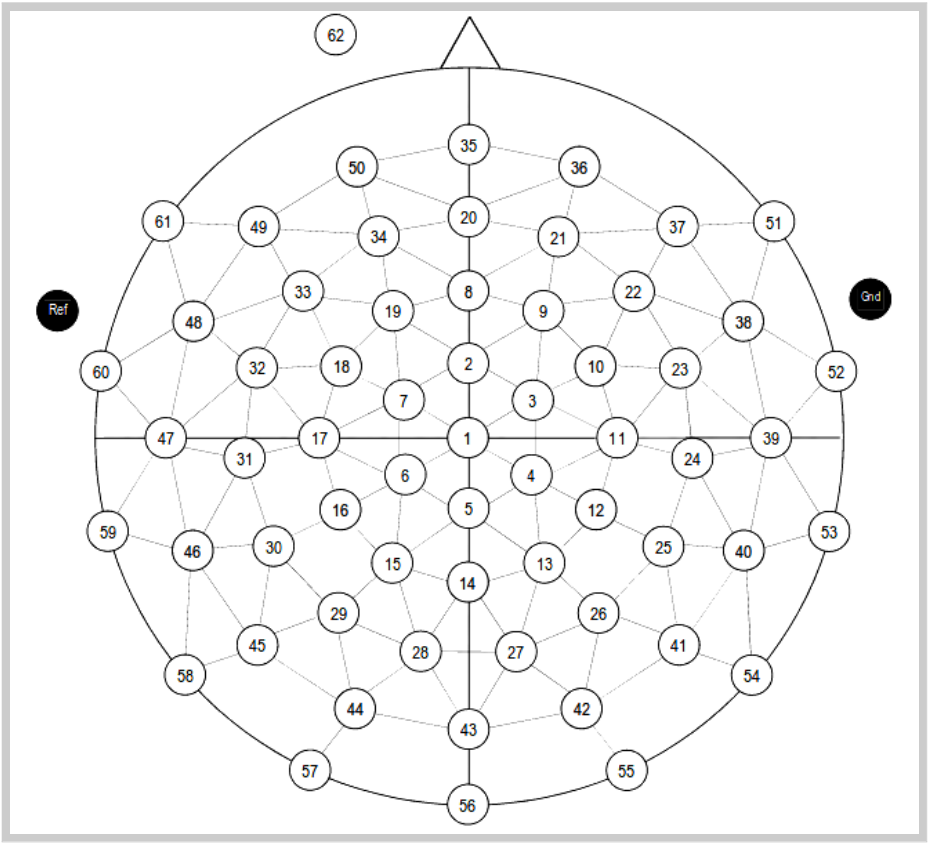

Figure A.1 61-channel equidistant layout. Adapted from Easycap (2018).

The measurements were corrupted with Gaussian noise of mean 0 and standard deviation 5 mV for intracortical measurements and standard deviation 100 mV for extracranial measurements.

A.4.2 Three bidirectionally coupled cortical columns: coarse parameter estimation

The three cortical columns are located as in the previous section, but coupled bidirectionally (panel (b) of figure 6.2). Additionally, the maximum amplitudes of the excitatory PSPs were set to $A_1 = 4.25$ mV, $A_2 = 10.00$ mV, and $A_3 = 3.25$ mV. The external input p(t) for each of the three cortical columns was set using $p_0 = 200\ s^{-1}$ and $\epsilon = 100\ s^{-1}$. The coupling constant was set to $k = 5$.

Moderate intracortical measurement noise

The intracortical measurements were corrupted with Gaussian noise of mean 0 and standard deviation 5 mV, while the noise in the extracranial measurements has standard deviation 100 mV.

High intracortical measurement noise

The intracortical measurements were corrupted with Gaussian noise of mean 0 and standard deviation 100 mV—about an order of magnitude higher than the noise in the previous study—, while the noise in the extracranial measurements has standard deviation 100 mV.

A.4.3 Three bidirectionally coupled cortical columns: fine parameter estimation

The three cortical columns are coupled bidirectionally (panel (b) of figure 6.2). The maximum amplitudes of the excitatory PSPs were set to $A_1 = 3.58$ mV, $A_2 = 3.25$ mV, and $A_3 = 3.10$ mV. The coupling constant was set to $k = 5$. The values for p(t) remain $p_0 = 200\ s^{-1}$ and $\epsilon = 100\ s^{-1}$.

B

Filtering

B.1 The unscented Kalman filter. Equations

The unscented Kalman filter (UKF) is a predictor-corrector algorithm that estimates the state and parameters at a given time step k in two phases. The first one predicts the state based solely on the dynamical information of the system, i.e., the model. The second incorporates a measurement with which to correct the first estimation. Table B.1 presents the symbols used in this Thesis for the variables of the Kalman filter.

Table B.1 Variables of the unscented Kalman filter.

Par.	Description
$\hat{\mathbf{x}}$	state estimate
$\hat{\mathbf{x}}^-$	*a priori* state estimate
$\boldsymbol{\Sigma}$	sigma points
$\mathbf{X}^*$	transformed sigma points
$\mathbf{X}$	redrawn sigma points (van der Merwe and Wan, 2001)
$\boldsymbol{\Upsilon}$	sigma points projected to measurement space
$\mathbf{y}^-$	estimated measurement
$\mathbf{z}$	measurement
f	model of the system
$\mathbf{H}$	observation model
n	state size
λ	scaling parameter
α	primary scaling factor
β	secondary scaling factor
κ	tertiary scaling factor
W^{m}	weight vector for the mean
$\mathrm{W}^{\mathrm{cov}}$	weight vector for the covariance
$\mathbf{P}$	state covariance estimate
$\mathbf{P}^-$	*a priori* state covariance estimate
$\mathbf{P_{yy}}$	predicted measurement covariance
$\mathbf{P_{xy}}$	state-measurement cross-covariance
$\mathbf{Q}$	state error covariance*
$\mathbf{R}$	measurement error covariance*
$\mathbf{K}$	Kalman gain

*To set the matrices $\mathbf{Q}$ and $\mathbf{R}$—which reflect the quality of measurement and model, and which crucially affect the output of the filter—, we used our knowledge of the characteristics of the data to fix an initial guess (Liu and Gao, 2013), then adjusted it to meet performance criteria.

The first step of the algorithm involves computing the expectation of the state and of the state covariance at time instant k + 1, known as the *a priori*

estimation. For this we use a numerical implementation (using Heun's solver) of our dynamical equations, e.g. Jansen and Rit's model of a cortical column (Jansen and Rit, 1995; Jansen et al., 1993).

The nature of the nonlinearities of this model prevents us from using a simple linearisation approach to propagating the statistics of the state variables across the transformation. Therefore, we incorporate the unscented transform (UT) in our formulation of the Kalman filter, which, instead of attempting to propagate a distribution through the nonlinearity, first propagates a series of deterministically chosen points through the nonlinearity and then recovers the statistical information of the distribution from these.

The *a priori* estimation of the state, $\hat{\mathbf{x}}_{\mathbf{k}}^{-}$, is obtained as follows, beginning with the calculation and projection of the 2n + 1 (where n is the state size) sigma points,

$$\begin{aligned}
\boldsymbol{\Sigma}_{\mathbf{k-1,0}} &= \hat{\mathbf{x}}_{\mathbf{k-1}} \\
\boldsymbol{\Sigma}_{\mathbf{k-1,i}} &= \hat{\mathbf{x}}_{\mathbf{k-1}} + \left(\sqrt{(n+\lambda)\mathbf{P}_{\mathbf{k-1}}}\right)_{i}, \quad i = 1,\ldots,n \\
\boldsymbol{\Sigma}_{\mathbf{k-1,i}} &= \hat{\mathbf{x}}_{\mathbf{k-1}} - \left(\sqrt{(n+\lambda)\mathbf{P}_{\mathbf{k-1}}}\right)_{i-n}, \quad i = n+1,\ldots,2n
\end{aligned} \tag{B.1}$$

where $\mathbf{P}_{\mathbf{k-1}}$ is the estimated state covariance matrix for the previous time step. The square root of this matrix is well-defined, and can be calculated efficiently via a Cholesky decomposition (van der Merwe and Wan, 2001).

This continues with the condensation of the projected sigma points into the *a priori* state estimate:

$$\mathbf{X^*_{k|k-1}} = f(\mathbf{\Sigma_{k-1}}) \tag{B.2}$$

$$\hat{\mathbf{x}}^-_{\mathbf{k}} = \sum_{i=0}^{2L} W_i^m \, \mathbf{X^*_{i,k|k-1}} \tag{B.3}$$

$$\mathbf{P}^-_{\mathbf{k}} = \sum_{i=0}^{2L} W_i^{cov} [\mathbf{X^*_{i,k|k-1}} - \hat{\mathbf{x}}^-_{\mathbf{k}}][\mathbf{X^*_{i,k|k-1}} - \hat{\mathbf{x}}^-_{\mathbf{k}}]^T + \mathbf{Q} \tag{B.4}$$

where $\mathbf{Q}$ is the state error covariance and $\mathbf{W^m}$ and $\mathbf{W^{cov}}$ are the weight vectors, defined as

$$\begin{aligned} W_0^m &= \frac{\lambda}{n + \lambda} \\ W_0^{cov} &= \frac{\lambda}{n + \lambda} + 1 - \alpha^2 + \beta \\ W_i^m = W_i^{cov} &= \frac{1}{2(n + \lambda)}, i = 1,...,2n \end{aligned} \tag{B.5}$$

In equations B.1 and B.5, α, β and κ are scaling factors, and λ, which is crucial to guarantee a positive semi-definite covariance matrix $\mathbf{P}$, is calculated as $\lambda = \alpha^2(n + \kappa) - n$. The primary scaling factor α determines the spread of the sigma points around the mean and is set at 0.001, it being usually set between 0.001 and 1 (van der Merwe and Wan, 2000) and chosen according to the quality of the resulting estimation. The secondary scaling factor β contains prior information about the distribution of $\mathbf{x}$; for Gaussian distributions, its optimal value is 2. Finally, κ, the tertiary scaling parameter, is set to 0, as is a usual practice (van der Merwe and Wan, 2000).

We now use a measurement to correct the state estimation, which implies the mapping of the *a priori* estimate onto the measurement space for comparison. In our case, this transformation is a linear matrix $\mathbf{H}$ that relates the state of the cortical columns to an EEG reading (see section A.2 in appendix A for details). The sigma points $\Sigma_{k|k-1}$ are projected into the measurement space (van der Merwe and Wan, 2001)

$$\boldsymbol{\Upsilon}_{\mathbf{k|k-1}} = \mathbf{H}[\boldsymbol{\Sigma}_{\mathbf{k|k-1}}], \tag{B.6}$$

from which the estimation of the measurement, $\hat{\mathbf{y}}_{\mathbf{k}}^{-}$, is calculated:

$$\hat{\mathbf{y}}_{\mathbf{k}}^{-} = \sum_{i=0}^{2L} W_i^m \, \boldsymbol{\Upsilon}_{\mathbf{i,k|k-1}} \tag{B.7}$$

The second step of the algorithm corrects the *a priori* estimation of state and covariance by using the information available from the most recent measurement. The impact of the measurement is determined by the Kalman gain $\mathbf{K}_{\mathbf{k}}$, which essentially expresses the level of confidence on the accuracy of the model and the level of noise in the data.

$$\mathbf{P}_{\mathbf{y}_k\mathbf{y}_k} = \sum_{i=0}^{2L} W_i^{cov} \, [\boldsymbol{\Upsilon}_{\mathbf{i,k|k-1}} - \hat{\mathbf{y}}_{\mathbf{k}}^{-}][\boldsymbol{\Upsilon}_{\mathbf{i,k|k-1}} - \hat{\mathbf{y}}_{\mathbf{k}}^{-}]^T + \mathbf{R} \tag{B.8}$$

$$\mathbf{P}_{\mathbf{x}_k\mathbf{y}_k} = \sum_{i=0}^{2L} W_i^{cov} \, [\mathbf{X}_{\mathbf{i,k|k-1}} - \hat{\mathbf{x}}_{\mathbf{k}}^{-}][\boldsymbol{\Upsilon}_{\mathbf{i,k|k-1}} - \hat{\mathbf{y}}_{\mathbf{k}}^{-}]^T \tag{B.9}$$

$$\mathbf{K}_{\mathbf{k}} = \mathbf{P}_{\mathbf{x}_k\mathbf{y}_k} \, \mathbf{P}_{\mathbf{y}_k\mathbf{y}_k}^{-1} \tag{B.10}$$

$$\hat{\mathbf{x}}_{\mathbf{k}} = \hat{\mathbf{x}}_{\mathbf{k}}^{-} + \mathbf{K}_{\mathbf{k}}(\mathbf{z}_{\mathbf{k}} - \hat{\mathbf{y}}_{\mathbf{k}}^{-}) \tag{B.11}$$

$$\mathbf{P}_{\mathbf{k}} = \mathbf{P}_{\mathbf{k}}^{-} - \mathbf{K}_{\mathbf{k}} \, \mathbf{P}_{\mathbf{y}_k\mathbf{y}_k} \, \mathbf{K}_{\mathbf{k}}^T \tag{B.12}$$

where $\mathbf{P_{y_k y_k}}$ is the predicted measurement covariance, $\mathbf{P_{x_k y_k}}$ is the state-measurement cross-covariance, $\mathbf{R}$ is the measurement error covariance, and $\mathbf{z_k}$ is the measurement for the current time step.

B.2 Application of the filter

B.2.1 *In silico* EEG data

For each of the experiments in chapter 6 we conducted 50 realisations of each estimation for the complete state vector, with different initial conditions; all the figures show averages of the 50 estimations, unless otherwise specified. The initial conditions for state and parameter estimations were randomly generated with a normal distribution of zero mean and unit variance; the parameters, however, were constrained to deviate no more than 90% of their actual value as an initial assumption.

The noise covariances Q and R were chosen according to the best knowledge of the system and of the noise corrupting the data. Therefore, Q was set to contemplate the incoming noise to each dipole, i.e. it was set to a null matrix except for the term corresponding to the equation that contains the input p(t) (see equation A.5 on page 114 and Garcia-Ojalvo and Sancho (1999)). The matrix R was set to $1000\mathbf{I}$ mV^2. (In practice, in most applications of the Kalman filter, the matrix R is fairly easy to set with the knowledge of the measurement precision as a starting point. However, in real life applications Q is often set by trial and error.)

B.2.2 Real EEG data

After filtering *in silico* EEG data, real data were used in chapter 7. Instead of the three dipoles used in chapter 6, here we place one cortical column under each of the 21 electrodes that are used for data collection (Goldberger et al., 2000; Shoeb, 2009) and we position them according to the theoretical coordinates of the electrodes in the International 10-20 System (see figure B.1). In this case, only one realisation of each set of initial conditions was conducted due to the size of the problem. The initial conditions for the state are random numbers between -0.5 and 0.5, while the initial conditions for the parameters were set to their nominal value in Jansen and Rit's model unless otherwise specified.

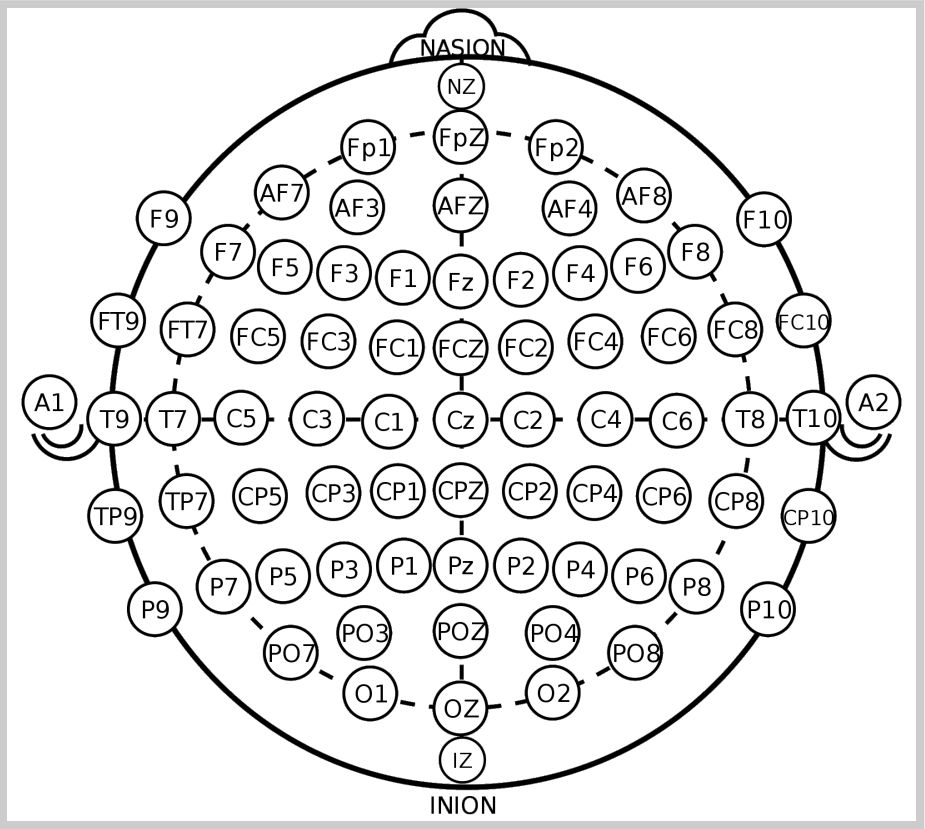

Figure B.1 The International 10-20 system of electrode layout on the scalp (Klem et al., 1999).

The noise covariances Q and R were set heuristically with the output of the filter as the indicator for good performance. Our targets were, on the one hand, smooth and stable estimates of the parameters and, on the other hand, a good correspondence between the measurements and the projected state estimates.

The process noise covariance Q was given values similar to those described in the previous section; additionally, because we are dealing here with real data, we added diagonal terms of value 10^{-6} for the rest of the equations for the state, and of 10^{-9} for the terms in the diagonal corresponding to the parameters. This was done to give more freedom for the filter to adjust to experimental data while constraining it to find parameters with as stable a value as possible. The measurement noise covariance matrix was set to $R = 10^{-2}\mathbf{I}\ \mu V^2$.

Research activities

Publications

Lara Escuain-Poole, Jordi Garcia-Ojalvo, Antonio J. Pons. Extracranial Estimation of Neural Mass Model Parameters Using the Unscented Kalman Filter. *Frontiers in Applied Mathematics and Statistics*, 4, 2018. doi: 10.3389/fams.2018.00046

Conference attendance and presentations

Barcelona Computational and Systems Neuroscience. Barcelona (Spain), 16th and 17th of June 2014.

III Jornada complexitat.cat. Barcelona (Spain), 19th of June 2014. Poster: *EEG correlates of cortical column synchronisation in mesoscopic brain dynamics*

IV Jornada complexitat.cat. Tarragona (Spain), 25th of May 2015.

Barcelona Computational and Systems Neuroscience 2015. Barcelona (Spain), 18th of June 2015. Talk: *Parameter estimation in neural mass models*

International Conference on System Level Approaches to Neural Engineering. Barcelona (Spain), from the 21st to the 23rd of September 2015.

International Conference on Artificial Neural Networks 2016. Barcelona (Spain), 7th of September 2016. Talk: *Data assimilation of EEG observations by neural mass models*

International Conference on Artificial Neural Networks 2017. L'Alguer (Italy), 14th of September 2017. Poster: *Matching mesoscopic neural models to microscopic neural networks in stationary and non-stationary regimes*

Organisation of scientific events

Local Organising Committee of the International Conference on Artificial Neural Networks 2016, held at the Polytechnic University of Catalonia, Barcelona, Spain, from the 6th to the 9th of September 2016.

Co-direction of undergraduate theses

Study of mesoscopic descriptions of neural networks, Alberto Hernández Alcaina. Spring semester 2015–2016.

Nanos gigantum humeris insidentes.

Bernard of Chartres

References

Péter Adorján, György Barna, Péter Érdi, and Klaus Obermayer. A statistical neural field approach to orientation selectivity. *Neurocomputing*, 26–27:313–318, 1999. Page 30

B. Albrecht, P.K. Staiger, K. Hall, P. Miller, D. Best, and D.I. Lubman. Benzodiazepine use and aggressive behaviour: a systematic review. *Australian and New Zealand Journal of Psychiatry*, 48(12):1096–1114, 2014. Page 5

John Aldrich. R. A. Fisher and the Making of Maximum Likelihood 1912 – 1922. *Statistical Science*, 12(3):162–176, 1997. Page 37

Shun-Ichi Amari. Homogeneous nets of neuron-like elements. *Biological Cybernetics*, 17(4): 211–220, 1975. Page 28, Page 30

Shun-Ichi Amari. Dynamics of pattern formation in lateral-inhibition type neural fields. *Biological Cybernetics*, 27(2):77–87, 1977. Page 28, Page 30

Daniel J Amit and M V Tsodyks. Quantitative study of attractor neural network retrieving at low spike rates: I. substrate—spikes, rates and neuronal gain. *Network: Computation in Neural Systems*, 2(3):259–273, 1991. Page 58

Andrey P. Anokhin, Niels Birbaumer, Werner Lutzenberger, Andrey Nikolaev, and Friedrich Vogel. Age increases brain complexity. *Electroencephalography and Clinical Neurophysiology*, 99(1):63–68, 1996. ISSN 00134694. doi: 10.1016/0921-884X(96)95573-3. Page 50

P. Aram, D.R. Freestone, M.J. Cook, V. Kadirkamanathan, and D.B. Grayden. Model-based estimation of intra-cortical connectivity using electrophysiological data. *NeuroImage*, 118:

563 – 575, 2015. ISSN 1053-8119. doi: http://dx.doi.org/10.1016/j.neuroimage.2015.06.048. Page 49, Page 50

Alfonso Araque and Marta Navarrete. Glial cells in neuronal network function. *Philosophical Transactions of the Royal Society*, 365:2375–2381, 2010. Page 27

Ienkaran Arasaratnam and Simon Haykin. Cubature Kalman Filters. *IEEE Transactions on Automatic Control*, 54(6):1254–1269, 2009. Page 48

James P. Ary, Stanley A. Klein, and Derek H. Fender. Location of Sources of Evoked Scalp Potentials: Corrections for Skull and Scalp Thicknesses. *IEEE Transactions on Biomedical Engineering*, BME-28(6):447–452, 1981. Page 34, Page 117

Abbas Babajani-Feremi and Hamid Soltanian-Zadeh. Multi-area neural mass modeling of eeg and meg signals. *NeuroImage*, 52:793–811, 2010. Page 16

Audrey S. Bahrick. Persistence of Sexual Dysfunction Side Effects after Discontinuation of Antidepressant Medications: Emerging Evidence. *The Open Psychology Journal*, 1:42–50, 2008. Page 5

A. L. Barker, D. E. Brown, and W. N. Martin. Bayesian Estimation and the Kalman Filter. *Computers Math. Applic.*, 30(10):55–77, 1995. Page 44

Anjali Raja Beharelle and Steven L. Small. Imaging brain networks for language: Methodology and examples from the neurobiology of reading. In Gregory Hickok and Steven L. Small, editors, *Neurobiology of Language*. Academic Press, 2016. Page 30

P. Berg and M. Scherg. A fast method for forward computation of multiple-shell spherical head models. *Electroencephalography and Clinical Neurophysiology*, 90:58–64, 1994. Page 117

Hans Berger. Über das Elektrenkephalogramm des Menschen. *Archiv für Psychiatrie und Nervenkrankheiten*, 99(1):555–574, 1933. Page 12

Páll Bergthórsson and Bo R. Döös. Numerical Weather Map Analysis. *Tellus*, 7(3):329–340, 1955. Page 36

MJ Berry, DK Warland, and M Meister. The structure and precision of retinal spike trains. *Proceedings of the National Academy of Sciences*, 94:5411–5416, 1997. Page 31

Antal Berényi, Zoltán Somogyvári, Anett J. Nagy, Lisa Roux, John D. Long, Shigeyoshi Fujisawa, Eran Stark, Anthony Leonardo, Timothy D. Harris, and György Buzsáki. Large-scale, high-density (up to 512 channels) recording of local circuits in behaving animals. *Journal of Neurophysiology*, 111(5):1132–1149, 2014. Page 54

R. L. Beurle. Properties of a mass of cells capable of regenerating pulses. *Philosophical Transactions of the Royal Society B*, 240:55–94, 1956. Page 27, Page 29

R.D. Bickford. Electroencephalography. In *Encyclopedia of Neuroscience*. Birkhauser, 1987. Page 15

Benjamin Blankertz, Steven Lemm, Matthias Treder, Stefan Haufe, and Klaus Robert Müller. Single-trial analysis and classification of ERP components - A tutorial. *NeuroImage*, 56(2): 814–825, 2011. ISSN 10538119. doi: 10.1016/j.neuroimage.2010.06.048. Page 50

Ingo Bojak and DTJ Liley. Modeling the effects of anesthesia on the electroencephalogram. *Physical Review E*, 71(4):041902, 2005. Page 49

Tiago Branco and Kevin Staras. The probability of neurotransmitter release: variability and feedback control at single synapses. *Nature Reviews Neuroscience*, 10:373–383, 2009. Page 9, Page 27

Korbinian Brodmann and Laurence J. Garey. *Brodmann's Localisation in the Cerebral Cortex. The Principles of Comparative Localisation in the Cerebral Cortex Based on Cytoarchitectonics*. Springer, 3rd edition, 2006. Page 9

Matthew J. Brookes, Karen J. Mullinger, Claire M. Stevenson, Peter G. Morris, and Richard Bowtell. Simultaneous EEG source localisation and artifact rejection during concurrent fMRI by means of spatial filtering. *NeuroImage*, 40(3):1090–1104, 2008. ISSN 10538119. doi: 10.1016/j.neuroimage.2007.12.030. Page 49

Matthew J. Brookes, Jiri Vrba, Karen J. Mullinger, Gerða Björk Geirsdóttir, Winston X. Yan, Claire M. Stevenson, Richard Bowtell, and Peter G. Morris. Source localisation in concurrent EEG/fMRI: Applications at 7T. *NeuroImage*, 45(2):440–452, 2009. ISSN 10538119. doi: 10.1016/j.neuroimage.2008.10.047. Page 49

Robert Grover Brown and Patrick Y.C. Hwang. *Introduction to Random Signals and Applied Kalman Filtering*. Institute for Nonlinear Science. John Wiley & Sons, 4th edition, 2012. Page 44

Nicolas Brunel and Mark C. W. van Rossum. Lapicque's 1907 paper: from frogs to integrate-and-fire. *Biological Cybernetics*, 97(5-6):337–339, 2007. Page 19, Page 21

CV Buhusi and WH Meck. What makes us tick? Functional and neural mechanisms of interval timing. *Nature Reviews Neuroscience*, 6(10):755–765, 2005. Page 31

A. N. Burkitt. A review of the integrate-and-fire neuron model: I. Homogeneous synaptic input. *Biological Cybernetics*, 95(1):1–19, 2006. ISSN 03401200. doi: 10.1007/s00422-006-0068-6. Page 56

Khalafalla O. Bushara. Neurologic presentation of celiac disease. *Gastroenterology*, 128(4 Suppl 1):S92–S97, 2005. Page 5

Daniel P. Buxhoeveden and Manuel F. Casanova. The minicolumn hypothesis in neuroscience. *Brain*, 125(5):935–951, 2002. Page 10

György Buzsáki, Costas a Anastassiou, and Christof Koch. The origin of extracellular fields and currents–EEG, ECoG, LFP and spikes. *Nature reviews. Neuroscience*, 13(6):407–20, 2012. ISSN 1471-0048. doi: 10.1038/nrn3241. Page 34

Patrizio Campisi and Daria La Rocca. Brain waves for automatic biometric-based user recognition. *IEEE Transactions on Information Forensics and Security*, 9(5):782–800, 2014. ISSN 15566013. doi: 10.1109/TIFS.2014.2308640. Page 50

Jose L. Cantero et al. Functional Integrity of Thalamocortical Circuits Differentiates Normal Aging from Mild Cognitive Impairment. *Human Brain Mapping*, 30:3944–3957, 2009. Page 74

Yuzhen Cao, Kaili Ren, Fei Su, Bin Deng, Xile Wei, and Jiang Wang. Suppression of seizures based on the multi-coupled neural mass model. *Chaos*, 25(10), 2015. ISSN 10541500. doi: 10.1063/1.4931715. Page 49

Richard Caton. The Electric Currents of the Brain. *British Medical Journal*, 2:278, 1875. Page 12

V. Caune, R. Ranta, S. Le Cam, J. Hofmanis, L. Maillard, L. Koessler, and V. Louis-Dorr. Evaluating dipolar source localization feasibility from intracerebral SEEG recordings. *NeuroImage*, 98:118 – 133, 2014. ISSN 1053-8119. doi: http://dx.doi.org/10.1016/j.neuroimage.2014.04.058. Page 49

CDC Statistics for Autism. Data and Statistics: Autism Spectrum Disorder (ASD). https://www.cdc.gov/ncbddd/autism/data.html, 2018. Accessed: 2018-12-24. Page 6

Bruno Cessac and Thierry Viéville. On dynamics of integrate-and-fire neural networks with conductance based synapses. *Frontiers in Computational Neuroscience*, 2(2), 2008. Page 26

Richard P. Chi and Allan W. Snyder. Brain stimulation enables the solution of an inherently difficult problem. *Neuroscience Letters*, 515(2):121–124, 2012. ISSN 03043940. doi: 10.1016/j.neulet.2012.03.012. Page 50

Derek J. Chong, Gregory L. Sahlem, and Carl W. Bazil. Introduction to electroencephalography. In Teri J. Barkoukis and Alon Y. Avidan, editors, *Review of Sleep Medicine*. Butterworth-Heinemann, 2007. Page 15

Philippe Courtier and Olivier Talagrand. Variational Assimilation of Meteorological Observations With the Adjoint Vorticity Equation. II: Numerical Results. *Quarterly Journal of the Royal Meteorological Society*, 113(478):1329–1347, 1987. Page 39

George P. Cressman. An Operational Objective Analysis System. *Monthly Weather Review*, 87 (10):367–374, 1959. Page 36

Olivier David, Lee Harrison, and Karl J. Friston. Modelling event-related responses in the brain. *NeuroImage*, 25(3):756–770, 2005. ISSN 10538119. doi: 10.1016/j.neuroimage.2004.12.030. Page 30

Olivier David, Stefan J. Kiebel, Lee M. Harrison, Jérémie Mattout, James M. Kilner, and Karl J. Friston. Dynamic causal modeling of evoked responses in EEG and MEG. *NeuroImage*, 30 (4):1255–1272, 2006. ISSN 10538119. doi: 10.1016/j.neuroimage.2005.10.045. Page 30

Peter Dayan and Laurence F. Abbott. *Theoretical Neuroscience*. MIT Press, 2001 edition, 2001. Page 32, Page 54

Suzanne M. de la Monte and Jack R. Wands. Alzheimer's Disease Is Type 3 Diabetes—Evidence Reviewed. *Journal of Diabetes Science and Technology*, 2(6):1101–1113, 2008. Page 5

Lorento de Nó. Cerebral cortex: architecture, intracortical connections, motor projections. In J. Fulton, editor, *Physiology of the Nervous System*. Oxford University Press, New York, 1949. Page 10

Gustavo Deco, Viktor K. Jirsa, Peter A. Robinson, Michael Breakspear, and Karl Friston. The Dynamic Brain: From Spiking Neurons to Neural Masses and Cortical Fields. *PLoS Computational Biology*, 4(8):e1000092, 2008. Page 27, Page 32

José Del R. Millán, Pierre W. Ferrez, Ferran Galán, Eileen Lew, and Ricardo Chavarriaga. Non-Invasive Brain-Machine Interaction. *International Journal of Pattern Recognition and Artificial Intelligence*, 22(05):959–972, 2008. ISSN 0218-0014. doi: 10.1142/S0218001408006600. Page 50

Easycap. Easycap Equidistant Layouts. https://www.easycap.de/wordpress/wp-content/uploads/2018/02/Easycap-Equidistant-Layouts.pdf, 2018. Page 119, Page 120

G. Bard Ermentrout and David H. Terman. *Mathematical Foundations of Neuroscience*. Interdisciplinary Applied Mathematics. Springer, 2010. Page 54

Geir Evensen. Sequential data assimilation with a nonlinear quasi-geostrophic model using Monte Carlo methods to forecast error statistics. *Journal of Geophysical Research*, 99(C5): 10143–10162, 1994. Page 38, Page 41, Page 48

Ramsey Faragher. Understanding the Basis of the Kalman Filter Via a Simple and Intuitive Derivation. *IEEE Signal Processing Magazine*, 29(5):128–132, 2012. Page 44

Farzaneh S. Fard, Paul Hollensen, Dietmar Heinke, and Thomas P.Trappenberg. Modeling human target reaching with an adaptive observer implemented with dynamic neural fields. *Neural Networks*, 72:13–30, 2015. Page 30

Miguel A. Faria, Jr. Violence, mental illness, and the brain — A brief history of psychosurgery: Part 1 — From trephination to lobotomy. *Surgical Neurology International*, 4(49), 2013. Page 5

O. Faugeras, J. Touboul, and B. Cessac. A constructive mean-field analysis of multi-population neural networks with random synaptic weights and stochastic inputs. *Frontiers in Computational Neuroscience*, 3(1), 2009. Page 32, Page 33, Page 57

Paul Fearnhead and Hans R. Künsch. Particle Filters and Data Assimilation. *Annual Review of Statistics and Its Application*, 5:421–449, 2018. Page 40

Dean Fergusson, Steve Doucette, Kathleen Cranley Glass, Stan Shapiro, David Healy, Paul Hebert, and Brian Hutton. Association between suicide attempts and selective serotonin reuptake inhibitors: systematic review of randomised controlled trials. *British Medical Journal*, 330, 2005. Page 5

Rhoda L. Fisher and Seymour Fisher. Antidepressants for children. Is scientific support necessary? *The Journal of Nervous and Mental Disease*, 184(2):99–102, 1996. Page 5

Richard FitzHugh. Impulses and Physiological States in Theoretical Models of Nerve Membrane. *Biophysical Journal*, 1(6):445–466, 1961. Page 25

Nicolas Fourcaud-Trocmé, David Hansel, Carl van Vreeswijk, and Nicolas Brunel. How Spike Generation Mechanisms Determine the Neuronal Response to Fluctuating Inputs. *The Journal of Neuroscience*, 23(37):11628–11640, 2003. Page 22

W. J. Freeman. *Mass Action in the Nervous System. Examination of the Neurophysiological Basis of Adaptive Behavior through the EEG.* Academic Press, 1975. Page 28, Page 33

D. R. Freestone, P. Aram, M. Dewar, K. Scerri, D. B. Grayden, and V. Kadirkamanathan. A data-driven framework for neural field modeling. *NeuroImage*, 56(3):1043–1058, 2011a. ISSN 10538119. doi: 10.1016/j.neuroimage.2011.02.027. Page 30, Page 49

D. R. Freestone et al. *Patient-Specific Neural Mass Modeling - Stochastic and Deterministic Methods*, chapter 5, pages 63–82. World Scientific Publishing Co., 2011b. doi: 10.1142/9789814525350_0005. Page 41, Page 73

Dean R. Freestone, Dragan Nesic, Amirhossein Jafarian, Mark J. Cook, and David B. Grayden. A neural mass model of spontaneous burst suppression and epileptic seizures. In *Proceedings of the Annual International Conference of the IEEE Engineering in Medicine and Biology Society, EMBS*, pages 5942–5945, 2013a. ISBN 9781457702167. doi: 10.1109/EMBC.2013.6610905. Page 49

Dean R. Freestone, Philippa J. Karoly, Dragan Nešić, Parham Aram, Mark J. Cook, and David B. Grayden. Estimation of effective connectivity via data-driven neural modeling. *Frontiers in Neuroscience*, 8:383, 2014a. ISSN 1662-453X. doi: 10.3389/fnins.2014.00383. Page 42, Page 81

Dean R Freestone, Philippa J Karoly, Dragan Nešić, Parham Aram, Mark J Cook, and David B Grayden. Estimation of effective connectivity via data-driven neural modeling. *Frontiers in neuroscience*, 8(November):383, 2014b. ISSN 1662-4548. doi: 10.3389/fnins.2014.00383. Page 49

D.R. Freestone, Levin Kuhlmann, M.S. Chong, D. Nesic, David B. Grayden, P. Aram, R. Postoyan, and M. J. Cook. Patient-specific neural mass modeling - stochastic and deterministic methods. *Recent Advances in Predicting and Preventing Epileptic Seizures*, pages 63–82, 2013b. Page 16, Page 49

K.J. Friston, L. Harrison, and W. Penny. Dynamic causal modelling. *NeuroImage*, 19(4): 1273–1302, 2003. Page 30

Lev S. Gandin. *Objective analysis of meteorological fields.* Israel Program for Scientific Translations, English 1965 edition, 1965. Page 38

Jordi Garcia-Ojalvo and José Sancho. *Noise in Spatially Extended Systems.* Institute for Nonlinear Science. Springer, 1999 edition, 1999. Page 115, Page 128

Crispin W. Gardiner. *Handbook of Stochastic Methods for Physics, Chemistry, and the Natural Sciences.* Springer, 2004. Page 115

Carl Friedrich Gauss. *Theoria motus corporum coelestium in sectionibus conicis solem ambientium.* 1809. Page 36, Page 37

Wulfram Gerstner and Werner M. Kistler. *Spiking Neuron Models.* Cambridge University Press, 2002. ISBN 0-521-81384-0. Page 22, Page 32

S. Gillijns, O. Barrero Mendoza, J. Chandrasekar, B. L. R. De Moor, D. S. Bernstein, and A. Ridley. What Is the Ensemble Kalman Filter and How Well Does it Work? In *Proceedings of the 2006 American Control Conference*, pages 4448–4453, 2006. Page 48

Rainer Goebel. Mapping the brain's cortical columns to develop innovative brain-computer interfaces. `https://phys.org/news/2016-03-brain-cortical-columns-brain-computer-interfaces.html`, 2016. Accessed: 2018-10-13. Page 11

Ary L. Goldberger, Luis A. N. Amaral, Leon Glass, Jeffrey M. Hausdorff, Plamen Ch. Ivanov, Roger G. Mark, Joseph E. Mietus, George B. Moody, Chung-Kang Peng, and H. Eugene

Stanley. PhysioBank, PhysioToolkit, and PhysioNet: Components of a New Research Resource for Complex Physiologic Signals. *Circulation*, 101(23):215–220, 2000. Page 92, Page 129

Geoffrey J. Goodhill and Miguel Á. Carreira-Perpiñán. Cortical columns. In *Encyclopedia of Cognitive Science*. Macmillan Publishers Ltd., 2002. Page 10

N. J. Gordon, D. J. Salmond, and A. F. M. Smith. Novel approach to nonlinear/non-Gaussian Bayesian state estimation. In *IEE Proceedings-F*, volume 140, pages 107–113, 1993. Page 40

Jean Gotman. Noninvasive methods for evaluating the localization and propagation of epileptic activity. *Epilepsia*, 44 Suppl 1:21–29, 2003. ISSN 0013-9580. Page 49

Bruce Graham, David Sterratt, Andrew Gillies, and David Willshaw. *Principles of Computational Modelling in Neuroscience*, volume 3. Cambridge University Press, 2011. ISBN 9780521877954. doi: 10.1109/MPUL.2012.2196841. Page 56

J. S. Griffith. A field theory of neural nets: I: Derivation of field equations. *The Bulletin of Mathematical Biophysics*, 25(1):111–120, 1963. Page 27, Page 29

J. S. Griffith. A field theory of neural nets: II: Properties of the field equations. *The Bulletin of Mathematical Biophysics*, 27(2):187–195, 1965. Page 27, Page 29

François Grimbert and Olivier Faugeras. Bifurcation analysis of Jansen's neural mass model. *Neural Computation*, 18(12):3052–3068, 2006. Page 77

E. Guigon, P. Grandguillaume, I. Otto, L. Boutkhil, and Y. Burnod. Neural network models of cortical functions based on the computational properties of the cerebral cortex. *Journal of Physiology-Paris*, 88(5):291–308, 1994. Page 26

Avgis Hadjipapas, Erik Casagrande, Angel Nevado, Gareth R. Barnes, Gary Green, and Ian E. Holliday. Can we observe collective neuronal activity from macroscopic aggregate signals? *NeuroImage*, 44:1290–1303, 2009. Page 33

Espen Hagen, David Dahmen, Maria L. Stavrinou, Henrik Lindén, Tom Tetzlaff, Sacha J. Van Albada, Sonja Grün, Markus Diesmann, and Gaute T. Einevoll. Hybrid scheme for modeling local field potentials from point-neuron networks. *Cerebral Cortex*, 26(12):4461–4496, 2016. ISSN 14602199. doi: 10.1093/cercor/bhw237. Page 55

Franz Hamilton, Tyrus Berry, Nathalia Peixoto, and Timothy Sauer. Real-time tracking of neuronal network structure using data assimilation. *Phys. Rev. E*, 88:052715, Nov 2013. doi: 10.1103/PhysRevE.88.052715. Page 42, Page 48

Franz Hamilton, John Cressman, Nathalia Peixoto, and Timothy Sauer. Reconstructing neural dynamics using data assimilation with multiple models. *EPL (Europhysics Letters)*, 107(6): 68005, 2014. ISSN 0295-5075. doi: 10.1209/0295-5075/107/68005. Page 42, Page 49

Franz Hamilton, Tyrus Berry, and Timothy Sauer. Ensemble Kalman filtering without a model. *Physical Review X*, 6(1), 2016. ISSN 21603308. doi: 10.1103/PhysRevX.6.011021. Page 49

D. Hansel and G. Mato. Existence and Stability of Persistent States in Large Neuronal Networks. *Physical Review Letters*, 86:4175–4178, 2000. Page 22

D. Hansel and G. Mato. Existence and stability of persistent states in large neuronal networks. *Physical Review Letters*, 86(18):4175–4178, 2001. ISSN 00319007. doi: 10.1103/PhysRevLett.86.4175. Page 55

D Hansel, G Mato, and C Meunier. <Hansel1995.pdf>. *Neural Computation*, 337:307–337, 1995. Page 55

Meysam Hashemi, Axel Hutt, and Jamie Sleigh. Anesthetic action on extra-synaptic receptors: effects in neural population models of EEG activity. *Frontiers in Systems Neuroscience*, 8 (232), 2014. Page 16

Stefan Haufe, Ryota Tomioka, Thorsten Dickhaus, Claudia Sannelli, Benjamin Blankertz, Guido Nolte, and Klaus Robert Müller. Large-scale EEG/MEG source localization with spatial flexibility. *NeuroImage*, 54(2):851–859, 2011. ISSN 10538119. doi: 10.1016/j.neuroimage.2010.09.003. Page 49

Martin Havlicek, Alard Roebroeck, Karl Friston, Anna Gardumi, Dimo Ivanov, and Kamil Uludag. Physiologically informed dynamic causal modeling of fMRI data. *NeuroImage*, 122: 355–372, 2015. ISSN 10959572. doi: 10.1016/j.neuroimage.2015.07.078. Page 30

Saskia Helbling, Sundeep Teki, Martina F. Callaghan, William Sedley, Siawoosh Mohammadi, Timothy D. Griffiths, Nikolaus Weiskopf, and Gareth R. Barnes. Structure predicts function: Combining non-invasive electrophysiology with in-vivo histology. *NeuroImage*, 108: 377–385, 2015. ISSN 10959572. doi: 10.1016/j.neuroimage.2014.12.030. Page 50

C. R. Hema, M. P. Paulraj, and Harkirenjit Kaur. Brain signatures: A modality for biometric authentication. In *2008 International Conference on Electronic Design, ICED 2008*, 2008. ISBN 9781424423156. doi: 10.1109/ICED.2008.4786753. Page 50

Leah C. Hibel, Douglas A. Granger, Dante Cicchetti, and Fred Rogosch. Salivary biomarker levels and diurnal variation: associations with medications prescribed to control children's problem behavior. *Child Development*, 78(3):927–937, 2007. Page 5

A. V. Hill. Excitation and Accommodation in Nerve. In *Proceedings of the Royal Society of London. Series B, Biological Sciences*, volume 119, pages 305–355, 1936. Page 21

Bertil Hille. *Ion Channels of Excitable Membranes*. Sinauer Associates, 2001. Page 20

Alan L. Hodgkin and Andrew F. Huxley. A quantitative description of membrane current and its application to conduction and excitation in nerve. *The Journal of Physiology*, 117(4): 500–544, 1952. Page 20, Page 22, Page 32

James E. Hoke and Richard A. Anthes. The Initialization of Numerical Models by a Dynamic-Initialization Technique. *Monthly Weather Review*, 104:1551–1556, 1976. Page 36

Jonathan C. Horton and Daniel L. Adams. The cortical column: a structure without a function. *Philosophical Transactions of the Royal Society B*, 360:837–862, 2005. Page 10

David H. Hubert and Torsten N. Wiesel. Functional architecture of macaque monkey visual cortex. *Proceedings of the Royal Society of London B*, 198(1130):1–59, 1977. Page 10

E. M. Izhikevich and G. M. Edelman. Large-scale model of mammalian thalamocortical systems. *Proceedings of the National Academy of Sciences*, 105(9):3593–3598, 2008. ISSN 0027-8424. doi: 10.1073/pnas.0712231105. Page 55

Eugene M. Izhikevich. *Dynamical Systems in Neuroscience: The Geometry of Excitability and Bursting*. Computational Neuroscience. The MIT Press, 2007. Page 22

Ben H. Jansen and Vincent G. Rit. Electroencephalogram and visual evoked potential generation in a mathematical model of coupled cortical columns. *Biological Cybernetics*, 73(4):357–366, 1995. Page 28, Page 76, Page 78, Page 119, Page 125

Ben H. Jansen, George Zouridakis, and Michael E. Brandt. A neurophysiologically-based mathematical model of flash visual evoked potentials. *Biological Cybernetics*, 68:275–283, 1993. Page 28, Page 119, Page 125

Herbert Jasper and Wilder Penfield. *Epilepsy and the Functional Anatomy of the Human Brain*. Little, Brown, 2nd edition, 1954. Page 16

Herbert H. Jasper. Electrocorticography. In Wilder Penfield and Theodore C. Erickson, editors, *Epilepsy and Cerebral Localization*. Springfield, IL: Charles C. Thomas, 1941. Page 12

Maciej Jedynak, Antonio J. Pons, Jordi Garcia-Ojalvo, and Marc Goodfellow. Temporally correlated fluctuations drive epileptiform dynamics. *NeuroImage*, 146:188–196, 2017. Page 30

Jeffrey Uhlmann. Firs-Hand: The Unscented Transform. `http://ethw.org/First-Hand:The_Unscented_Transform`, 2016. Page 47

Simon J. Julier and Jeffrey K. Uhlmann. Unscented Filtering and Nonlinear Estimation. *Proceedings of the IEEE*, 92(3):401–422, 2004. Page 46, Page 47

Valer Jurcak, Daisuke Tsuzuki, and Ippeita Dan. 10/20, 10/10, and 10/5 systems revisited: Their validity as relative head-surface-based positioning systems. *NeuroImage*, 34(4):1600–1611, 2007. ISSN 10538119. doi: 10.1016/j.neuroimage.2006.09.024. Page 116

Rudolf Emil Kalman. A New Approach to Linear Filtering and Prediction Problems. *Transactions of the ASME–Journal of Basic Engineering*, 82(Series D):35–45, 1960. Page 37, Page 38, Page 46

Eugenia Kalnay. *Atmospheric Modelling, Data Assimilation and Predictability*. Cambridge University Press, 1st edition, 2003. Page 36, Page 39

Eric R. Kandel, James H. Schwartz, and Thomas M. Jessell, editors. *Principles of Neural Science*. McGraw-Hill, 2000. Page 28

Jonathan C Kao, Paul Nuyujukian, Stephen I Ryu, Mark M Churchland, John P Cunningham, and Krishna V Shenoy. Single-trial dynamics of motor cortex and their applications to brain-machine interfaces. *Nature Communications*, 2015. Page 50

Pramod P. Khargonekar and Krishan M. Nagpal. Filtering and Smoothing in an H^{∞} Setting. In *Proceedings of the 28th Conference on Decision and Control*, volume 1, pages 415–420, 1989. Page 41

Stefan J. Kiebel, Marta I. Garrido, Rosalyn J. Moran, and Karl J. Friston. Dynamic causal modelling for EEG and MEG. *Cognitive Neurodynamics*, 2(2):121–136, 2008. ISSN 18714080. doi: 10.1007/s11571-008-9038-0. Page 30

Joe Kilian and Hava T. Siegelmann. The Dynamic Universality of Sigmoidal Neural Networks. *Information and Computation*, 128(1):48–56, 1996. ISSN 08905401. doi: 10.1006/inco.1996.0062. Page 58

R. E. Kistler. A study of data assimilation techniques in an autobarotropic primitive equation channel model. Master's thesis, Department of Meteorology, Pennsylvania State University, 1974. Page 36

Stephen B. Klein and B. Michael Thorne. *Biological Psychology*. Worth Publishers, 2nd edition, 2006. Page 12

G. H. Klem, H. O. Lüders, H. H. Jasper, and C. Elger. The ten-twenty electrode system of the International Federation. *Electroencephalography and clinical neurophysiology. Supplement*, 52:3–6, 1999. Page 12, Page 129

Bruce W. Knight. Dynamics of Encoding in a Population of Neurons. *The Journal of General Physiology*, 59:734–766, 1972a. Page 21

Bruce W. Knight. The Relationship between the Firing Rate of a Single Neuron and the Level of Activity in a Population of Neurons: Experimental Evidence for Resonant Enhancement in the Population Response. *The Journal of General Physiology*, 59:767–778, 1972b. Page 21

Christof Koch. *Biophysics of Computation: Information Processing in Single Neurons*. Oxford University Press, 1999. ISBN 0-19-510491-9. Page 22

Peter J. Koehler and Christopher J. Boes. A history of non-drug treatment in headache, particularly migraine. *Brain*, 133:2489–2500, 2010. Page 11

A. N. Kolmogorov, W. L. Doyle, and Ivan Selin. Interpolation and extrapolation of stationary random sequences. *Bulletin of the Academy of Sciences, USSR series on Mathematics*, 1941. Translation by RAND Corporation, memorandum RM-30090-PR. Page 38

Beatrix Krause, Javier Márquez-Ruiz, and Roi Cohen Kadosh. The effect of transcranial direct current stimulation: a role for cortical excitation/inhibition balance? *Frontiers in human*

neuroscience, 7(September):602, 2013. ISSN 1662-5161. doi: 10.3389/fnhum.2013.00602. Page 50

Morten L Kringelbach, Ned Jenkinson, Sarah L F Owen, and Tipu Z Aziz. Translational principles of deep brain stimulation. *Nature reviews. Neuroscience*, 8(8):623–635, 2007. ISSN 1471-003X (Print); 1471-003X (Linking). doi: 10.1038/nrn2196. Page 50

Levin Kuhlmann, Dean R. Freestone, Jonathan H. Manton, Bjorn Heyse, Hugo E M Vereecke, Tarmo Lipping, Michel M R F Struys, and David T J Liley. Neural mass model-based tracking of anesthetic brain states. *NeuroImage*, 133:438–456, 2016. ISSN 10959572. doi: 10.1016/j.neuroimage.2016.03.039. Page 16, Page 42, Page 49, Page 73

Alexandre Kuhn, Stefan Rotter, and Ad Aertsen. Correlated input spike trains and their effects on the response of the leaky integrate-and-fire neuron. *Neurocomputing*, 44-46:121–126, 2002. ISSN 09252312. doi: 10.1016/S0925-2312(02)00372-7. Page 59

Jeffrey R Lacasse and Jonathan Leo. Serotonin and Depression: A Disconnect between the Advertisements and the Scientific Literature. *PLoS Medicine*, 2(12):e392, 2005. Page 5

Camilo Lamus, Matti S. Hämäläinen, Simona Temereanca, Emery N. Brown, and Patrick L. Purdon. A spatiotemporal dynamic distributed solution to the MEG inverse problem. *NeuroImage*, 63(2):894–909, 2012. ISSN 10538119. doi: 10.1016/j.neuroimage.2011.11.020. Page 49

Milad Lankarany, W.-P. Zhu, and M.N.S. Swamy. Joint estimation of states and parameters of Hodgkin–Huxley neuronal model using Kalman filtering. *Neurocomputing*, 136:289–299, 2014. Page 49

Louis Lapicque. Recherches quantitatives sur l'excitabilité électrique des nerfs traitée comme une polarisation. *Journal de Physiologie et de Pathologie Générale*, 9:620–635, 1907. Page 19

PE Latham, BJ Richmond, PG Nelson, and S. Nirenberg. Intrinsic dynamics in neuronal networks. I. Theory. *Journal of Neurophysiology*, 83(2):808–827, 2000. Page 22

François-Xavier Le Dimet and Olivier Talagrand. Variational algorithms for analysis and assimilation of meteorological observations: theoretical aspects. *Tellus A: Dynamic Meteorology and Oceanography*, 38(2):97–110, 1986. Page 39

Lucy Lee, Karl Friston, and Barry Horwitz. Large-scale neural models and dynamic causal modelling. *NeuroImage*, 30(4):1243–1254, 2006. ISSN 10538119. doi: 10.1016/j.neuroimage.2005.11.007. Page 30

Klaus Lehnertz, Ralph G. Andrzejak, Jochen Arnhold, Thomas Kreuz, Florian Mormann, Christoph Rieke, Guido Widman, and Christian E. Elger. Nonlinear EEG Analysis in Epilepsy:. *Journal of Clinical Neurophysiology*, 18(3):209–222, 2001. ISSN 0736-0258. doi: 10.1097/00004691-200105000-00002. Page 49

Simin Li, Jie Li, and Zheng Li. An improved unscented kalman filter based decoder for cortical brain-machine interfaces. *Frontiers in Neuroscience*, 10(DEC), 2016. ISSN 1662453X. doi: 10.3389/fnins.2016.00587. Page 42

D.T.J. Liley, B.L. Foster, and I. Bojak. Co-operative populations of neurons: Mean field models of mesoscopic brain activity. In N. Le Novère, editor, *Computational Systems Neurobiology*. Springer, Dordrecht, 2012. Page 28

Xian Liu and Qing Gao. Parameter estimation and control for a neural mass model based on the unscented kalman filter. *Phys. Rev. E*, 88:042905, Oct 2013. doi: 10.1103/PhysRevE.88.042905. Page 76, Page 77, Page 119, Page 124

F. H. Lopes da Silva, A. Hoeks, H Smits, and L. H. Zetterberg. Model of brain rhythmic activity. *Kybernetik*, 15(1):27–37, 1974. ISSN 0340-1200. doi: 10.1007/BF00270757. Page 28

Armando López-Cuevas, Bernardino Castillo-Toledo, Laura Medina-Ceja, and Consuelo Ventura-Mejía. State and parameter estimation of a neural mass model from electrophysiological signals during the status epilepticus. *NeuroImage*, 113:374–386, jun 2015. ISSN 10538119. doi: 10.1016/j.neuroimage.2015.02.059. Page 42

Francisco López-Muñoz, Jesús Boya, and Cecilio Alamo. Neuron theory, the cornerstone of neuroscience, on the centenary of the Nobel Prize award to Santiago Ramón y Cajal. *Brain Research Bulletin*, 70:391–405, 2006. Page 8

Andrew C. Lorenc. Analysis methods for numerical weather prediction. *Quarterly Journal of the Royal Meteorological Society*, 112(474):1177–1194, 1986. Page 37, Page 39

Andrew C. Lorenc. The potential of the ensemble Kalman filter for NWP—a comparison with 4D-Var. *Quarterly Journal of the Royal Meteorological Society*, 129(595):3183–3203, 2003. Page 41

Z F Mainen and T J Sejnowski. Reliability of spike timing in neocortical neurons. *Science*, 268 (5216):1503–1506, 1995. ISSN 0036-8075. doi: 10.1126/science.7770778. Page 54

Jaakko Malmivuo and Robert Plonsey. *Bioelectromagnetism. Principles and Applications of Bioelectric and Biomagnetic Fields*. Oxford University Press, 1st edition, 1995. Page 12, Page 92

Lara V. Marcuse, Madeline C. Fields, and Jiyeoun (Jenna) Yoo. *Rowan's Primer of EEG*. Elsevier, 2nd edition, 2016. Page 12, Page 13, Page 14

Peter S. Maybeck. *Stochastic models, estimation, and control*, volume 141 of *Mathematics in Science and Engineering*. Academic Press, Inc., 1979. Page 44

J. W. Middleton, M. J. Chacron, B. Lindner, and A. Longtin. Firing statistics of a neuron model driven by long-range correlated noise. *Physical Review E - Statistical Physics, Plasmas, Fluids, and Related Interdisciplinary Topics*, 68(2):8, 2003. ISSN 1063651X. doi: 10.1103/PhysRevE.68.021920. Page 54

L. Miele, A. Liguori, G. Marrone, M. Biolato, C. Araneo, F.G. Vaccaro, A. Gasbarrini, and A. Grieco. Fatty liver and drugs: the two sides of the same coin. *European Review for Medical and Pharmacological Sciences*, 21(1 Suppl):86–94, 2017. Page 5

Brooke S.G. Molina, Stephen P. Hinshaw, James M. Swanson, L. Eugene Arnold, Benedetto Vitiello, Peter S. Jensen, Jeffery N. Epstein, Betsy Hoza, Lily Hechtman, Howard B. Abikoff, Glen R. Elliott, Laurence L. Greenhill, Jeffrey H. Newcorn, Karen C. Wells, Timothy Wigal, Robert D. Gibbons, Kwan Hur, Patricia R. Houck, and The MTA Cooperative Group. The MTA at 8 Years: Prospective Follow-up of Children Treated for Combined-Type ADHD in a Multisite Study. *Journal of the American Academy of Child and Adolescent Psychiatry*, 48(5):484–500, 2009. Page 5

Thomas J. Moore, Joseph Glenmullen, and Curt D. Furberg. Prescription drugs associated with reports of violence towards others. *PLoS One*, 5(12):e15337, 2010. Page 5

R. J. Moran, K. E. Stephan, T. Seidenbecher, H. C. Pape, R. J. Dolan, and K. J. Friston. Dynamic causal models of steady-state responses. *NeuroImage*, 44(3):796–811, 2009. ISSN 10538119. doi: 10.1016/j.neuroimage.2008.09.048. Page 31

Rosalyn Moran, Dimitris a Pinotsis, and Karl Friston. Neural masses and fields in dynamic causal modeling. *Frontiers in computational neuroscience*, 7(May):57, 2013. ISSN 1662-5188. doi: 10.3389/fncom.2013.00057. Page 30

Carmen Moreno, Gonzalo Laje, Carlos Blanco, Huiping Jiang, Andrew B. Schmidt, and Mark Olfson. National Trends in the Outpatient Diagnosis and Treatment of Bipolar Disorder in Youth. *JAMA Psychiatry*, 64(9):1032–1039, 2007. Page 5

Catherine Morris and Harold Lecar. Voltage oscillations in the barnacle giant muscle fiber. *Biophysical Journal*, 35(1):193–213, 1981. Page 23

J.C. Mosher, R.M. Leahy, and P.S. Lewis. EEG and MEG: forward solutions for inverse methods. *IEEE Transactions on Biomedical Engineering*, 46(3):245–259, 1999. ISSN 00189294. doi: 10.1109/10.748978. Page 34, Page 49

Angelo Mosso. Sulla circolazione del sangue nell cervello dell'uomo. *Atti della Reale Academia dei Lincei*, 3(5), 1880. Page 12

V. Mountcastle. An organizing principle for cerebral function: the unit model and the distributed system. In G. Edelman and V. Mountcastle, editors, *The Mindful Brain*. MIT Press, Cambridge, Mass., 1978. Page 11

Vernon B. Mountcastle. Modality and topographic properties of single neurons of cat's somatic sensory cortex. *Journal of Neurophysiology*, 20:408–434, 1957. Page 10

Vernon B. Mountcastle. The columnar organization of the neocortex. *Brain*, 120:701–722, 1997. Page 11

Matthew J. Moye and Casey O. Diekman. Data Assimilation Methods for Neuronal State and Parameter Estimation. *Journal of Mathematical Neuroscience*, 8(11), 2018. Page 42, Page 49

E.J. Müller, S.J. van Albada, J.W. Kim, and P.A. Robinson. Unified neural field theory of brain dynamics underlying oscillations in Parkinson's disease and generalized epilepsies. *Journal of Theoretical Biology*, 428:132–146, 2017. Page 30

J. Nagumo, S. Arimoto, and S. Yoshizawa. An Active Pulse Transmission Line Simulating Nerve Axon. In *Proceedings of the IRE*, volume 50, 1962. Page 25

Henry A. Nasrallah, Jan Loney, Stephen C. Olson, Mona McCalley-Whitters, John Kramer, and Charles G. Jacoby. Cortical atrophy in young adults with a history of hyperactivity in childhood. *Psychiatry Research*, 17(3):241–246, 1986. Page 5

Timothy S. Nelson, Courtney L. Suhr, Alan Lai, Amy J. Halliday, Dean R. Freestone, Karen J. McLean, Anthony N. Burkitt, and Mark J. Cook. Seizure severity and duration in the cortical stimulation model of experimental epilepsy in rats: A longitudinal study. *Epilepsy Research*, 89(2-3):261–270, 2010. ISSN 09201211. doi: 10.1016/j.eplepsyres.2010.01.010. Page 50

Ngoc Anh Thi Nguyen, Hyung-Jeong Yang, and Sunhee Kim. HOKF: High Order Kalman Filter for Epilepsy Forecasting Modeling. *Biosystems*, 158:57–57, 2017. Page 49

NIMH Statistics for Mental Illness. Nimh: Mental illness. `https://www.nimh.nih.gov/health/statistics/mental-illness.shtml#part_154785`, 2017. Accessed: 2018-12-24. Page 6

Seiji Ogawa, Tso-Ming Lee, Asha S. Nayak, and Paul Glynn. Oxygenation-sensitive contrast in magnetic resonance image of rodent brain at high magnetic fields. *Magnetic Resonance in Medicine*, 14(1):68–78, 1990. Page 12

Mohamed Oubbati, Michael Schanz, and Paul Levi. Neural fields for behavior-based control of mobile robots. In *IFAC Proceedings Volumes*, volume 39, pages 61–66, 2006. Page 30

H. A. Panofsky. Objective Weather-Map Analysis. *Journal of Meteorology*, 6:386–392, 1949. Page 36

Stefano Panzeri, Jakob H. Macke, Joachim Gross, and Christoph Kayser. Neural population coding: combining insights from microscopic and mass signals. *Trends in Cognitive Sciences*, 19(3):162–172, 2015. Page 26, Page 54, Page 55

Margarita Papadopoulou, Gerald Cooray, Richard Rosch, Rosalyn Moran, Daniele Marinazzo, and Karl Friston. Dynamic causal modelling of seizure activity in a rat model. *NeuroImage*, 2016. ISSN 10538119. doi: 10.1016/j.neuroimage.2016.08.062. Page 30

Stephen G. Penny. Mathematical foundations of hybrid data assimilation from a synchronization perspective. *Chaos*, 27(126801), 2017. Page 41

Gertrudis Perea and Alfonso Araque. GLIA modulates synaptic transmission. *Brain Research Reviews*, 63(1–2):93–102, 2010. Page 8, Page 27

Gertrudis Perea, Marta Navarrete, and Alfonso Araque. Tripartite synapses: astrocytes process and control synaptic information. *Trends in Neurosciences*, 32(8):421–431, 2009. Page 8, Page 27

Joel S Perlmutter and Jonathan W Mink. Deep brain stimulation. *Annual review of neuroscience*, 29:229–57, 2006. ISSN 0147-006X. doi: 10.1146/annurev.neuro.29.051605.112824. Page 50

Jessica M. Phillips, Martin Vinck, Stefan Everling, and Thilo Womelsdorf. A long-range fronto-parietal 5- to 10-Hz network predicts "top-down" controlled guidance in a task-switch paradigm. *Cerebral Cortex*, 24(8):1996–2008, 2014. ISSN 14602199. doi: 10.1093/cercor/bht050. Page 50

D. A. Pinotsis, R. J. Moran, and K. J. Friston. Dynamic causal modeling with neural fields. *NeuroImage*, 59(2):1261–1274, 2012. ISSN 10538119. doi: 10.1016/j.neuroimage.2011.08.020. Page 30

D. A. Pinotsis, J. P. Geerts, L. Pinto, T. H. B. FitzGerald, V. Litvak, R. Auksztulewicz, and K. J. Friston. Linking canonical microcircuits and neuronal activity: Dynamic causal modelling of laminar recordings. *NeuroImage*, 146:355–366, 2017. Page 31

D.A. Pinotsis and K.J. Friston. Neural fields, masses and bayesian modelling. In S. Coombes, P. beim Graben, R. Potthast, and J. Wright, editors, *Neural Fields*. Springer, Berlin, 2014. Page 30

P.K.Fung and P.A. Robinson. Neural field theory of calcium dependent plasticity with applications to transcranial magnetic stimulation. *Journal of Theoretical Biology*, 324:72–83, 2013. Page 30

P.K.Fung, A.L. Haber, and P.A. Robinson. Neural field theory of plasticity in the cerebral cortex. *Journal of Theoretical Biology*, 318:44–57, 2013. Page 30

A. J. Pons, Jose L. Cantero, Mercedes Atienza, and Jordi Garcia-Ojalvo. Relating structural and functional anomalous connectivity in the aging brain via neural mass modeling.

NeuroImage, 52(3):848–861, 2010. ISSN 10538119. doi: 10.1016/j.neuroimage.2009.12.105. Page 116

Dale Purves, George J. Augustine, David Fitzpatrick, William C. Hall, Anthony-Samuel LaMantia, James O. McNamara, and S. Mark Williams, editors. *Neuroscience*. Sinauer Associates, 2004. Page 8, Page 21, Page 31

Mikhail I. Rabinovich, Pablo Varona, Allen I. Selverston, and Henry D I Abarbanel. Dynamical principles in neuroscience. *Reviews of Modern Physics*, 78(4), 2006. ISSN 00346861. doi: 10.1103/RevModPhys.78.1213. Page 22, Page 25

Pasko Rakic. Confusing cortical columns. *Proceedings of the National Academy of Sciences*, 105 (34):12099–12100, 2008. Page 10, Page 11

Wilfrid Rall. Branching dendritic trees and motoneuron membrane resistivity. *Experimental Neurology*, 1(5):491–527, 1959. Page 20

Wilfrid Rall. Theory of Physiological Properties of Dendrites. *Annals of the New York Academy of Sciences*, 96:1071–1092, 1962. Page 20

R.G.Abeysuriya and P.A.Robinson. Real-time automated EEG tracking of brain states using neural field theory. *Journal of Neuroscience Methods*, 258:28–45, 2016. Page 30

John E. Richards. Recovering dipole sources from scalp-recorded event-related-potentials using component analysis: principal component analysis and independent component analysis. *International Journal of Psychophysiology*, 54:201–220, 2004. Page 75, Page 78, Page 119

Gerasimos G. Rigatos. Estimation of wave-type dynamics in neurons' membrane with the use of the Derivative-free nonlinear Kalman Filter. *Neurocomputing*, 131:186–299, 2014. Page 49

A.J. Rockel, R.W. Hiorns, and T.P. Powell. The basic uniformity in structure of the neocortex. *Brain*, 103(2):221–244, 1980. Page 11

Serafim Rodrigues, Anton V. Chizhov, Frank Marten, and John R. Terry. Mappings between a macroscopic neural-mass model and a reduced conductance-based model. *Biological Cybernetics*, 102(5):361–371, 2010. Page 32

Michael Roth, Carsten Fritsche, Gustaf Hendeby, and Fredrik Gustafsson. The ensemble Kalman filter and its relations to other nonlinear filters. In *23rd European Signal Processing Conference (EUSIPCO)*, volume 1, pages 1236–1240, 2015. Page 41

Alex Roxin, Nicolas Brunel, and David Hansel. Role of delays in shaping spatiotemporal dynamics of neuronal activity in large networks. *Physical Review Letters*, 94(23), 2005. ISSN 00319007. doi: 10.1103/PhysRevLett.94.238103. Page 55

Alex Roxin, Nicolas Brunel, David Hansel, Gianluigi Mongillo, and C. van Vreeswijk. On the Distribution of Firing Rates in Networks of Cortical Neurons. *Journal of Neuroscience*, 31 (45):16217–16226, 2011. ISSN 0270-6474. doi: 10.1523/JNEUROSCI.1677-11.2011. Page 58

Charles S. Roy and Charles S. Sherrington. On the Regulation of the Blood-Supply of the Brain. *The Journal of Physiology*, 11(1-2):85–108, 1890. Page 12

Sepideh Sadaghiani, Guido Hesselmann, Karl J Friston, and Andreas Kleinschmidt. The relation of ongoing brain activity, evoked neural responses, and cognition. *Frontiers in systems neuroscience*, 4(June):20, 2010. ISSN 1662-5137. doi: 10.3389/fnsys.2010.00020. Page 50

Joshua P. Salmon and Thomas P. Trappenberg. Modeling the integration of expectations in visual search with centre-surround neural fields. *Neural Networks*, 21:1476–1492, 2008. Page 30

Yoshikazu Sasaki. Some Basic Formalisms in Numerical Variational Analysis. *Monthly Weather Review*, 98(12):875–883, 1970. Page 37

S.J. Schiff. *Neural Control Engineering: The Emerging Intersection Between Control Theory and Neuroscience*. Computational neuroscience. MIT Press, 2012. ISBN 9780262015370. Page 6, Page 83

Lori Schuh and Ivo Drury. Intraoperative electrocorticography and direct cortical electrical stimulation. *Seminars in Anesthesia, Perioperative Medicine and Pain*, 16(1):46–55, 1997. Page 16

Bonan Shan, Jiang Wang, Bin Deng, Xile Wei, Haitao Yu, and Huiyan Li. UKF-based closed loop iterative learning control of epileptiform wave in a neural mass model. *Cognitive Neurodynamics*, 9(1):31–40, 2015. ISSN 18714099. doi: 10.1007/s11571-014-9306-0. Page 42

Bonan Shan, Jiang Wang, Bin Deng, Xile Wei, Haitao Yu, Zhen Zhang, and Zhen Li. Particle swarm optimization algorithm based parameters estimation and control of epileptiform spikes in a neural mass model. *Chaos*, 26, 2016. Page 50

Pradeep Shenoy, Kai J. Miller, Jeffrey G. Ojemann, and Rajesh P. N. Rao. Generalized Features for Electrocorticographic BCIs. In *IEEE Transactions on Biomedical Engineering*, volume 55, pages 273–280, 2008. Page 17

T. Shimokawa, A. Rogel, K. Pakdaman, and S. Sato. Stochastic resonance and spike-timing precision in an ensemble of leaky integrate and fire neuron models. *Physical Review E - Statistical Physics, Plasmas, Fluids, and Related Interdisciplinary Topics*, 59(3):3461–3470, 1999. ISSN 1063651X. doi: 10.1103/PhysRevE.59.3461. Page 54

Ali Shoeb. *Application of Machine Learning to Epileptic Seizure Onset Detection and Treatment*. PhD thesis, Massachusetts Institute of Technology, 2009. Page 92, Page 129

Fernando Lopes Da Silva. *EEG: Origin and Measurement*, chapter 5, pages 63–82. World Scientific Publishing Co., 2011. doi: 10.1142/9789814525350_0005. Page 12

Dan Simon. *Optimal State Estimation: Kalman, H Infinity, and Nonlinear Approaches*. Wiley-Interscience, 1st edition, 2006. Page 40

Gerald L. Smith, Stanley F. Schmidt, and Leonard A. McGee. Application of Statistical Filter Theory to the Optimal Estimation of Position and Velocity on Board a Circumlunar Vehicle. Technical report, National Aeronautics and Space Administration, Ames Research Center, 1962. Page 46

Surjo R. Soekadar, Niels Birbaumer, Marc W. Slutzky, and Leonardo G. Cohen. Brain-machine interfaces in neurorehabilitation of stroke. *Neurobiology of Disease*, 83:172–179, 2015. ISSN 1095953X. doi: 10.1016/j.nbd.2014.11.025. Page 50

H. W. Sorenson. Least-squares estimation: from Gauss to Kalman. *IEEE Spectrum*, 7(7):63–68, 1970. Page 43

Roberto C. Sotero, Nelson J. Trujillo-Barreto, Yasser Iturria-Medina, Felix Carbonell, and Juan C. Jimenez. Realistically Coupled Neural Mass Models Can Generate EEG Rhythms. *Neural Computation*, 19(2):478–512, 2007. Page 16

A. Spiegler and V. Jirsa. Systematic approximations of neural fields through networks of neural masses in the virtual brain. *NeuroImage*, 83:704–725, 2013. Page 30

Statistics for Dementia. Dementia statistics. https://www.alz.co.uk/research/statistics, 2015. Accessed: 2018-12-24. Page 6

O. A. Stepanov. Kalman Filtering: Past and Present. An Outlook from Russia. (On the Occasion of the 80th Birthday of Rudolf Emil Kalman). *Gyroscopy and Navigation*, 2(2):99–110, 2011. Page 25, Page 46

K. E. Stephan, W. D. Penny, R. J. Moran, H. E M den Ouden, J. Daunizeau, and K. J. Friston. Ten simple rules for dynamic causal modeling, 2010. ISSN 10538119. Page 30

K. E. Stephan, F. Schlagenhauf, Q. J M Huys, S. Raman, E. A. Aponte, K. H. Brodersen, L. Rigoux, R. J. Moran, J. Daunizeau, R. J. Dolan, K. J. Friston, and A. Heinz. Computational neuroimaging strategies for single patient predictions. *NeuroImage*, 145:180–199, 2015. ISSN 10959572. doi: 10.1016/j.neuroimage.2016.06.038. Page 50

Klaas Enno Stephan and Alard Roebroeck. A short history of causal modeling of fMRI data. *NeuroImage*, 63(2):856–863, 2012. Page 30

David Sterratt, Bruce Graham, Andrew Gillies, and David Willshaw. *Principles of Computational Modelling in Neuroscience*. Cambridge University Press, 2011. ISBN 978-0-521-87795-4. Page 21

Ian H. Stevenson and Konrad P. Kording. How advances in neural recording affect data analysis. *Nature Neuroscience*, 14(2):139–142, 2012. Page 5

Leland Stewart and Perry McCarty. Use of Bayesian belief networks to fuse continuous and discrete information for target recognition, tracking, and situation assessment. In *Proc. SPIE, Signal Processing, Sensor Fusion and Target Recognition*, volume 1699, pages 177–185, 1992. Page 40

Ruslan L. Stratonovich. Optimum nonlinear systems which bring about a separation of a signal with constant parameters from noise. *Radiofizika*, 2(6):892–901, 1959. Page 46

David Sussillo, Sergey D Stavisky, Jonathan C Kao, Stephen I Ryu, and Krishna V Shenoy. Making brain-machine interfaces robust to future neural variability. *Nature Communications*, 2016. Page 50

J. Szentágothai. The neuron network of the cerebral cortex: a functional interpretation. *Proceedings of the Royal Society B*, 201(1144):935–951, 1978. Page 10

Olivier Talagrand and Philippe Courtier. Variational Assimilation of Meteorological Observations With the Adjoint Vorticity Equation. I: Theory. *Quarterly Journal of the Royal Meteorological Society*, 113(478):1311–1328, 1987. Page 39

M. Teplan. Fundamentals of eeg measurement. *Measurement Science Review*, 2(2), 2002. Page 14

Jean-Noéul Thepaut and Philippe Courtier. Four-dimensional variational data assimilation using the adjoint of a multilevel primitive-equation model. *Quarterly Journal of the Royal Meteorological Society*, 117(502):1225–254, 1991. Page 39

Raul Toral and Pere Colet. *Stochastic numerical methods: an introduction for students and scientists*. John Wiley & Sons, 2014. ISBN 3527683127. Page 118

Z. Turi, W. Paulus, and a. Antal. Functional Neuroimaging and Transcranial Electrical Stimulation. *Clinical EEG and Neuroscience*, 43(3):200–208, 2012. ISSN 1550-0594. doi: 10.1177/1550059412444978. Page 50

J. K. Uhlmann. *Simultaneous map building and localization for real time applications*. PhD thesis, Oxford University, 1994. Page 47

István Ulbert, Eric Halgren, Gary Heit, and George Karmos. Multiple microelectrode-recording system for human intracortical applications. *Journal of Neuroscience Methods*, 106(1):69–79, 2001. Page 16

R. van der Merwe and E. A. Wan. The Unscented Kalman Filter for Nonlinear Estimation. In *Adaptive Systems for Signal Processing, Communications, and Control Symposium 2000. AS-SPCC. The IEEE 2000*, pages 153–158, 2000. Page 47, Page 48, Page 126

R. van der Merwe and E. A. Wan. The square-root unscented Kalman filter for state and parameter-estimation. In *2001 IEEE International Conference on Acoustics, Speech, and Signal Processing. Proceedings. (ICASSP '01)*, volume 6, pages 3461–3464, 2001. Page 48, Page 124, Page 125, Page 127

A. van Rotterdam, F. H. Lopes da Silva, J. van den Ende, M. A. Viergever, and A. J. Hermans. A model of the spatial-temporal characteristics of the alpha rhythm. *Bulletin of Mathematical Biology*, 44(2):283–305, 1982. Page 28

C. E. Vargas-Irwin, G. Shakhnarovich, P. Yadollahpour, J. M. K. Mislow, M. J. Black, and J. P. Donoghue. Decoding Complete Reach and Grasp Actions from Local Primary Motor Cortex Populations. *Journal of Neuroscience*, 30(29):9659–9669, 2010. ISSN 0270-6474. doi: 10.1523/JNEUROSCI.5443-09.2010. Page 54

Eva Verhellen and Paul Boon. EEG source localization of the epileptogenic focus in patients with refractory temporal lobe epilepsy, dipole modelling revisited. *Acta neurologica Belgica*, 107(3):71–77, 2007. ISSN 0300-9009. Page 49

Timothy Wagner, Antoni Valero-Cabre, and Alvaro Pascual-Leone. Noninvasive human brain stimulation. *Annual Review of Biomedical Engineering*, 9(1):527–565, 2007. ISSN 1523-9829. doi: 10.1146/annurev.bioeng.9.061206.133100. Page 50

Zhiguo Wang, Wouter Kruijne, and Jan Theeuwes. Lateral interactions in the superior colliculus produce saccade deviation in a neural field model. *Vision Research*, 62:66–74, 2012. Page 30

Andrew White, Philip A. Williams, Jennifer L. Hellier, Suzanne Clark, F. Edward Dudek, and Kevin J. Staley. EEG spike activity precedes epilepsy after kainate-induced status epilepticus. *Epilepsia*, 51(3):371–383, 2010. Page 15

Kevin Whittingstall, Gerhard Stroink, Larry Gates, JF Connolly, and Allen Finley. Effects of dipole position, orientation and noise on the accuracy of EEG source localization. *BioMedical Engineering OnLine*, 2(1):14, 2003. ISSN 1475-925X. doi: 10.1186/1475-925X-2-14. Page 49

Norbert Wiener. *Extrapolation, Interpolation, and Smoothing of Stationary Time Series, with Engineering Applications*. MIT Press, Cambridge, MA, 1949 edition, 1949. Page 38

Sobanawartiny Wijeakumar, Joseph P. Ambrose, John P. Spencer, and Rodica Curtu. Model-based functional neuroimaging using dynamic neural fields: An integrative cognitive neuroscience approach. *Journal of Mathematical Psychology*, 76:212–235, 2017. Page 30

H. R. Wilson and J. D. Cowan. Excitatory and inhibitory interactions in localized populations of model neurons. *Biophysical Journal*, 12:1–24, 1972. Page 28

J.J. Wright and D.T.J. Liley. Dynamics of the brain at global and microscopic scales: Neural networks and the EEG. *Behavioral and Brain Sciences*, 19:285–320, 1996. Page 26

Guifeng Xu, Lane Strathearn, Buyun Liu, Binrang Yang, and Wei Bao. Twenty-Year Trends in Diagnosed Attention-Deficit/Hyperactivity Disorder Among US Children and Adolescents, 1997-2016. *JAMA Network Open*, 1(4):e181471, 2018. Page 6

Shuangming Yang, Bin Deng, Jiang Wang, Huiyan Li, Chen Liu, Chris Fietkiewicz, and Kenneth A Loparo. Efficient implementation of a real-time estimation system for thalamocortical hidden Parkinsonian properties. *Scientific Reports*, 2017. Page 50

Yongseok Yoo. On predicting epileptic seizures from intracranial electroencephalography. *Biomedical Engineering Letters*, pages 1–5, 2017. ISSN 2093-985X. doi: 10.1007/s13534-017-0008-5. Page 50

Rafael Yuste. From the neuron doctrine to neural networks. *Nature Reviews Neuroscience*, 16 (8):487–497, 2015. ISSN 1471-003X. doi: 10.1038/nrn3962. Page 5, Page 20, Page 54

Bas-Jan Zandt, Sid Visser, Michel J.A.M. van Putten, and Bennie ten Haken. A neural mass model based on single cell dynamics to model pathophysiology. *Journal of Computational Neuroscience*, 37(3):549–568, 2014. Page 33, Page 58, Page 59, Page 70

Z Zhang. A fast method to compute surface potentials generated by dipoles within multilayer anisotropic spheres. *Physics in medicine and biology*, 40(3):335–349, 1995. ISSN 0031-9155. doi: 10.1088/0031-9155/40/3/001. Page 34, Page 49

Catharina Zich, Stefan Debener, Cornelia Kranczioch, Martin G. Bleichner, Ingmar Gutberlet, and Maarten De Vos. Real-time EEG feedback during simultaneous EEG-fMRI identifies the cortical signature of motor imagery. *NeuroImage*, 114:438–447, 2015. ISSN 10959572. doi: 10.1016/j.neuroimage.2015.04.020. Page 50

Julie Magno Zito, Daniel J. Safer, Susan dosReis, James F. Gardner, Myde Boles, and Frances Lynch. Trends in the Prescribing of Psychotropic Medications to Preschoolers. *JAMA*, 283 (8):1025–1030, 2000. Page 5